BONNER METEOROLOGISCHE ABHANDLUNGEN

Heft 85 (2018) (ISSN 0006-7156)
Herausgeber: Andreas Hense

Rüdiger Hewer

STOCHASTIC PHYSICAL MODELS FOR WIND FIELDS AND PRECIPITATION EXTREMES

BONNER METEOROLOGISCHE ABHANDLUNGEN

Heft 85 (2018) (ISSN 0006-7156)
Herausgeber: Andreas Hense

Rüdiger Hewer

STOCHASTIC PHYSICAL MODELS FOR WIND FIELDS AND PRECIPITATION EXTREMES

Stochastic physical models for wind fields and precipitation extremes

Dissertation
zur
Erlangung des Doktorgrades (Dr. rer. nat.)
der
Mathematisch-Naturwissenschaftlichen Fakultät
der
Rheinischen Friedrich-Wilhelms-Universität Bonn

vorgelegt von
M.Sc. Rüdiger Hewer
aus
Mannheim

Bonn, Februar, 2018

Diese Arbeit ist die ungekürzte Fassung einer der Mathematisch-Naturwissenschaftlichen Fakultät der Rheinischen Friedrich-Wilhelms-Universität Bonn im Jahr 2018 vorgelegten Dissertation von Rüdiger Hewer aus Mannheim.

This paper is the unabridged version of a dissertation thesis submitted by Rüdiger Hewer born in Mannheim to the Faculty of Mathematical and Natural Sciences of the Rheinische Friedrich-Wilhelms-Universität Bonn in 2018.

Anschrift des Verfassers: Address of the author:

Rüdiger Hewer
Meteorologisches Institut der
Universität Bonn
Auf dem Hügel 20
D-53121 Bonn

1. Gutachter: PD. Dr. Petra Friederichs, Rheinische Friedrich-Wilhelms-Universität Bonn
2. Gutachter: Prof. Dr. Andreas Hense, Rheinische Friedrich-Wilhelms-Universität Bonn

Tag der Promotion: 18. Juni 2018

Abstract

A major goal of this thesis is to introduce stochastic, physically consistent models for precipitation extremes based on the moisture budget. The moisture budget describes the moisture flux convergence and is essential for the generation of precipitation and in particular extreme precipitation. The introduced models are used to extensively study to which extent the budget equation can account for characteristics of precipitation extremes. An important question in this respect is under which conditions the budget equation generates a heavy-tailed behavior. A further point is to understand whether the spatial structure of the humidity transport is essential in generating precipitation extremes. It is demonstrated that the humidity budget equation does not allow for the emergence of heavy-tailed precipitation distributions from light-tailed distribution for wind and humidity. At the same time finite sample approximations of the models suggest that asymptotic properties may be of very limited practical relevance. The models considered here show a remarkable stability to the correlation of wind and humidity. We prove the convergence of a precipitation model to its max-stable limit, which yields asymptotic spatial independence of precipitation extremes. Further, there is no prominent difference between precipitation extremes in purely rotational or purely divergent flow. The budget equation reveals a strong sensitivity to the marginal distributions of wind and humidity and further assumptions, which shows the need for well-established distributional assumptions for these variables.

In order to model moisture flux convergence spatially consistent a multivariate Gaussian random field formulation is introduced. It represents the differential relations of a wind field and related variables such as the streamfunction, velocity potential, vorticity, and divergence. The covariance model of the Gaussian random field is based on a flexible bivariate Matérn covariance function for the streamfunction and velocity potential. It allows for different variances in the potentials, nonzero correlations between them, anisotropy, and a flexible smoothness parameter. The joint covariance function of the related variables is derived analytically. Further, it is shown that a consistent model with nonzero correlations between the potentials and positive definite covariance function is possible, rebutting a claim of Obukhov (1954). The statistical model is fitted to forecasts of the horizontal wind fields of a mesoscale numerical weather prediction system. Parameter uncertainty is assessed by a parametric bootstrap method. The estimates reveal only physically negligible correlations between the potentials. The covariance model provides opportunity for a wealth of applications in data assimilation.

Contents

1 Introduction

The amount of typical extreme precipitation substantially exceeds the moisture that is stored locally in a column of the atmosphere (Trenberth et al., 2003). Hence, a necessary condition for such events is sufficient moisture supply. Conversely, if a large quantity of humidity is transported to a specific location, the Clausius-Clapeyron threshold is exceeded and precipitation emerges. Thus humidity transport is essential in generating heavy precipitation (Trenberth, 1999; Trenberth et al., 2003). The transport of humidity is given by the following budget-equation

$$\int_0^H \frac{\partial}{\partial t} q + \nabla \cdot (Uq)\, dz = E - P, \tag{1}$$

where H is the upper boundary of the moisture containing layer of the troposphere, q is the absolute humidity, U the horizontal wind field, E the evaporation and P precipitation. In this thesis stochastic and physically consistent models for precipitation extremes based on the moisture budget are introduced. Using these models we will extensively study to which extent the budget equation can account for characteristics of precipitation extremes. We address the following questions.

> Under which conditions generates the moisture budget (1) a heavy-tailed P? Which terms in (1) are essential for the generation of extremes?

The stochastic models for extreme precipitation are introduced and studied in Chapter 3.

Perhaps the most demanding task for a stochastic model based on the budget equation (1) is to find a stochastic process that models the moisture flux convergence spatially consistent. We base our model on the right hand side of $\nabla \cdot (Uq) = U \cdot \nabla q + q \nabla \cdot U$ and introduce in Chapter 2 a stochastic process that describes the wind field U its divergence $\nabla \cdot U$ and further related variables such as streamfunction, velocity potential and vorticity. The variables are connected via the Helmholtz decomposition. In dimension two it states that any wind field U can be uniquely decomposed given appropriate boundary conditions into a rotational and divergent component. For the potentials streamfunction ψ and velocity potential χ we have $U = \nabla \times \psi + \nabla \chi$. Divergence is given by $\nabla \cdot U = \Delta \chi$ and vorticity by $\nabla \times U = \Delta \psi$, where Δ is the 2-dimensional Laplace operator. Here, we address the following questions.

> Is there a stochastic process able to represent the differential relations between the variables of the Helmholtz decomposition, which is suffi-

ciently flexible to be a useful approximation for realistic wind fields? Can such a process model the correlations of streamfunction and velocity potential?

Our approach models the differential relations of the Helmholtz relation exactly and its consistency makes it an intrinsically valuable geostatistical approach. It has various potential applications in data assimilation as it allows one to perform an update step preserving the physical balance. Generating physically consistent initial conditions is a major goal in data assimilation (Daley, 1991; Gottwald, 2014; Laloyaux et al., 2016) and the lack of such initial conditions resulted in the failure of the first numerical weather prediction systems (Daley, 1991). In a case study we fit the process to the output of a numerical weather prediction system, assess their uncertainty and discuss utility and limitations of the model. Chapter 2 as well as parts of the abstract have been published with slight modifications in Hewer et al. (2017).

The models discussed here are *physical* in the sense that they adopt characteristic physical relations that link various meteorological variables. In this sense we use the word *physical* in this thesis. The models are not *dynamical* as they do not represent a closed system, whose temporal development is self-contained.

The two chapters of this thesis are connected in two ways. First, the stochastic methods introduced in Chapter 2 are indispensable in formulating and simulating the precipitation models of Chapter 3. The physical consistency of the wind field model is necessary to obtain a physically consistent model for the precipitation fields. Secondly and more generally, both approaches are statistical models that are based on physical reasoning.

From a statistical point of view such methods are valuable as they provide a method to reduce the number of independent variables in a system. For example, in Chapter 2 a covariance model for streamfunction and velocity potential suffices to derive the covariance of the wind field, vorticity and divergence. The information that is contained in the physical relations allows one to reduce the estimation uncertainty, as more data is available to estimate the same number of parameters. Further, physical relations can be used to infer stochastic properties. The distribution of precipitation can be inferred from the distributions of wind and humidity field. For example, Wilson and Toumi (2005) modeled precipitation as a product of three Gaussian variables based on physical reasoning.

From a meteorological point of view such methods are attractive as they can be used to understand which physical terms and relations can explain observed stochastic properties like heavy tails or spatial structure. Further, such physically

motivated models are particularly interesting if observational data are rare or suffer from systematic errors. For example there are few observations of vertical velocity in the atmosphere such that physical understanding of the influence of its distribution is particularly important. Theoretical insight into the distribution of extreme precipitation events may be particularly needed as there are few very long time series and their homogeneity may be questioned (Venema et al., 2012). Wilson and Toumi (2005) argue that physically-motivated models are stable under climatic change and may thus be used to assess its consequences. Extrapolation methods from extreme value theory (EVT) rely on the appropriateness of asymptotic relations, yet the appropriateness is questioned by e.g. Wilson and Toumi (2005) and Veneziano et al. (2009). In such a situation a physically based distribution for precipitation may give useful preasymptotic approximations. Relying on more precise characterization of the underlying process these methods allow for finite-sample improvements of the extrapolation methods.

Recent improvements in data assimilation have led to substantial progress in predictive skill of weather forecasts (Bauer et al., 2015). The present study performs basic research, which could lead to improvements in data assimilation and therefore may provide added value to numerical weather prediction (NWP). Similarly, this thesis improves our understanding of the generation of extreme precipitation events and could lead to more realistic extrapolation and representation of extreme events. Due to the fundamental risks that our society faces with respect to precipitation and flooding (MunichRe, 2017) such methods are valuable to both society and economy.

2 A Matérn based multivariate Gaussian random process for a consistent model of the horizontal wind components and related variables

2.1 Introduction

An appropriate representation of the covariance structure in spatial models of meteorological variables is essential when analyzing (Gandin, 1963; Kalnay, 2003) meteorological data using data assimilation (Hollingsworth and Lönnberg, 1986; Evensen, 1994; Bonavita et al., 2012; Pu et al., 2016). Assuming Gaussian statistics this requires an appropriate representation of the background error covariance matrix. Further, spatial stochastic models for meteorological variables should respect physical relationships.

One of the first approaches to include physical consistency via differential relations between variables can be found in Kolmogorov (1941). Thiébaux (1977) introduced a covariance model for wind fields assuming geostrophic balance, thereby incorporating anisotropy error covariance structure of the geopotential height. Daley (1985) derived a covariance model for the horizontal wind components assuming a Gaussian covariance model for the velocity potential and the streamfunction, where he derived the differential relations between the potentials and the wind field. The covariance model proposed by Daley (1985) is rather flexible as it allows for geostrophic coupling, nonzero correlation of streamfunction and velocity potential, and differing scales for the two potentials. Daley (1985) also considered geopotential height as an additional model variable. However, the resulting covariance function for the wind fields is not positive definite for many parameter combinations. Hollingsworth and Lönnberg (1986) adapted Daley's method and formulated a covariance function for the potentials using cylindrical harmonics. They show that on the synoptic scale the correlation between the potentials is small, such that Daley (1991) reformulated his model for zero correlations. These approaches (Thiébaux, 1977; Hollingsworth and Lönnberg, 1986; Daley, 1985) as well as our model differ from current data assimilation methods, as they provide an explicit, parametric and analytic covariance model for the background error. So-called *control variable transform* methods (Bannister, 2008) describe the background error matrix in an implicit non-parametric way via its square root [1] using latent variables which model the physical variables. Sample based methods like the ensemble Kalman filter (Evensen, 1994) describe the error statistics based on

[1] e.g. Cholesky decomposition

estimates obtained from an ensemble.

The data assimilation literature (e.g. Thiébaux, 1977; Hollingsworth and Lönnberg, 1986; Daley, 1985) typically uses the stochastic models in order to describe the covariance matrix of the background error, which is the difference of a forecast and the true field. Similar methods have also been used in order to describe the full turbulent field (Frehlich et al., 2001). There has also been considerable interest in describing the statistics of the velocity field directly or via its spectrum (Bühler et al., 2014; Lindborg, 2015; Bierdel et al., 2016).

While Thiébaux (1977), Hollingsworth and Lönnberg (1986) and Daley (1985) include physical relations via differentiation of the covariance function, finite difference operators are used in Bayesian hierarchical models. For example, Royle et al. (1999) modeled the geostrophic relation of pressure and wind field.

In this chapter, we propose a multivariate Gaussian random field (GRF) formulation for six atmospheric variables in a horizontal two-dimensional Cartesian space. Assuming a bivariate Matérn covariance for streamfunction ψ and velocity potential χ, we derive the covariance structure of the horizontal wind components $\vec{U} = (u, v)^T$ as well as vorticity $\nabla \times \vec{U} := -\frac{\partial}{\partial e_2} u + \frac{\partial}{\partial e_1} v$ and divergence $\nabla \cdot \vec{U}$. All of these quantities are connected via the Helmholtz decomposition, which states that for any given wind field $\vec{U}$ there exists a streamfunction ψ and velocity potential χ, such that $\vec{U} = \nabla \times \psi + \nabla \chi$, where $\nabla \times \psi := \big(-\frac{\partial}{\partial e_2} \psi, \frac{\partial}{\partial e_1} \psi \big)^T$. In dimension two and with appropriate boundary conditions this decomposition is unique. Curl and divergence of the wind field are given as $\nabla \times \vec{U} = \Delta \psi$ and $\nabla \cdot \vec{U} = \Delta \chi$, respectively, where Δ is the 2-dimensional Laplace operator.

Our multivariate GRF formulation is novel for several reasons. While e.g. Daley (1985) only used the potentials to derive the covariance function of the wind fields, our model is formulated for all related variables, including a formulation for the potential functions and the wind field, as well as vorticity and divergence. Secondly, our model provides a formulation for anisotropy in the wind field and the related potentials. Further, we allow for nonzero correlations between the rotational and divergent wind component, which might be particularly relevant for atmospheric fields on sub-geostrophic scales. We show that the scale parameters considered by Daley (1985) are inconsistent with nonzero correlations between streamfunction and velocity potential, as they do not lead to a positive definite model. An exact derivation of the condition under which the covariance function of Daley's model is positive definite is given in Appendix A. Further our model is a counter example to a theorem of Obukhov (1954), which claims that there is no isotropic wind field with nonzero correlation of the rotational and non-rotational component of the

wind field. More details to Obukhov's claim are given in Appendix B.

The covariance function of our multivariate GRF will be incorporated into an upcoming version of the spatial statistics R package RandomFields (Schlather et al., 2016). This opens the possibility for a wealth of applications in spatial statistics, including the conditional simulation of streamfunction and velocity potential given an observed wind field, a consistent formulation of the covariance structure for both the potential and the horizontal wind components to be used in data assimilation, or stochastic interpolation (Kriging) of each of the involved variables given the others. Kriging is the process of computing the conditional expectation of a certain variable given others. It is typically used to interpolate fields.

To exemplify the multivariate GRF we estimated its parameters for atmospheric fields of the ensemble-NWP, COSMO-DE-EPS (Gebhardt et al., 2011), provided by the German meteorological service (DWD). COSMO-DE is a high-resolution forecast system, that provides forecasts on the atmospheric mesoscale (Baldauf et al., 2011). Estimation is realized using the maximum likelihood method, while uncertainty in the parameter estimation is assessed by parametric bootstrap (Efron and Tibshirani, 1994). We also discuss the meteorological relevance of the parameters.

The remainder of the chapter is organized as follows. In Section 2.2 we introduce the multivariate GRF, and demonstrate how the physical relations and anisotropy are included in the model formulation. Section 2.3 introduces the COSMO-DE-EPS data. Section 2.4 is devoted to the parameter estimation and the assessment of the uncertainties, while Section 2.5 presents and interprets the results of the estimation. We conclude in Section 2.6 and discuss potential applications, limits and extensions of our multivariate GRF.

2.2 Theory

An important aspect of our multivariate GRF is the inclusion of the differential relations between the atmospheric variables. Under weak regularity assumptions the derivative of a Gaussian process is again a Gaussian process (Adler and Taylor, 2007). Hence, the assumption of Gaussianity of the streamfunction and the velocity potential implies Gaussianity of all the considered variables. A zero-mean Gaussian process is uniquely characterized by the covariance function, we only need to study the joint covariance of a random field and its derivatives. A Gaussian process $\left(X_s, s \in \mathbb{R}^d\right)$ is a continuously indexed stochastic process. For each finite number of locations $(s_i, i = 1, \ldots, n)$ the variables $(X_{s_i}, i = 1, \ldots, n)$ have a multivariate Gaussian distribution.

Let $X_s, s \in \mathbb{R}$, be a stochastic process with finite second moments, and assume

that the covariance function $C(s,t) = \mathrm{Cov}\left(X_s, X_t\right)$ is twice continuously differentiable, then the covariance model of the process and its mean-square derivative is given by

$$\mathrm{Cov}\left(\begin{pmatrix} X_s \\ d_s X_s \end{pmatrix}, \begin{pmatrix} X_t \\ d_t X_t \end{pmatrix}\right) = \begin{pmatrix} \mathrm{Cov}\left(X_s, X_t\right) & d_t\mathrm{Cov}\left(X_s, X_t\right) \\ d_s\mathrm{Cov}\left(X_s, X_t\right) & d_s d_t\mathrm{Cov}\left(X_s, X_t\right) \end{pmatrix}, \qquad (2)$$

where $s, t \in \mathbb{R}$ (Ritter, 2000). Using the linearity in the arguments the validity of this equation can be roughly seen by

$$\begin{aligned} \mathrm{Cov}\left(X_s, d_t X_t\right) &= \lim_{\Delta \to 0} \mathrm{Cov}\left(X_s, \frac{X_t - X_{t+\Delta}}{\Delta}\right) \\ &= \lim_{\Delta \to 0} \frac{\mathrm{Cov}\left(X_s, X_t\right) - \mathrm{Cov}\left(X_s, X_{t+\Delta}\right)}{\Delta} \\ &= d_t\mathrm{Cov}\left(X_s, X_t\right). \end{aligned}$$

One key advantage of this approach is that the bivariate covariance in (2) allows us to model the dependence between the process and its derivative. In order to provide a better theoretical basis for this idea, we consider the following definition.

Definition. A stochastic process $X_t, t \in \mathbb{R}^d$ is mean square differentiable at $t \in \mathbb{R}^d$ in direction $e_i, i = 1, \ldots, d$, if there exists a random variable $X_t^{(i)}$ with $\mathbb{E}\left(X_t^{(i)}\right)^2 < \infty$ such that,

$$\mathbb{E}\left(\left(\frac{X_t - X_{t+\Delta e_i}}{\Delta}\right) - X_t^{(i)}\right)^2 \to 0 \quad \text{as} \quad \Delta \to 0,$$

where e_i denotes the unit vector in the $i-th$ coordinate direction. In this case, we use the following notation $\frac{\partial}{\partial e_i} X_t = X_t^{(i)}$.

A stochastic process is mean square differentiable if its covariance function is twice continuously differentiable (Ritter, 2000). However, this condition is neither sufficient nor necessary for the differentiability of the sample paths. For Gaussian processes the following conditions on the derivatives of the process guarantees continuity of the sample paths. The paths of a Gaussian process are continuous, if there exist $0 < C < \infty$ and $\alpha, \eta > 0$ such that

$$\mathbb{E}\left|\frac{\partial}{\partial s} X_s - \frac{\partial}{\partial t} X_t\right|^2 \leq \frac{C}{\left|\ln|s-t|\right|^{1+\alpha}},$$

for all $|s-t| < \eta$, see Theorem 1.4.1. in Adler and Taylor (2007).

In our case, the covariance function describes the dependence of the horizontal wind components u_s and v_s, streamfunction ψ, velocity potential χ, and the Laplacian of the potentials (i.e. vorticity $\zeta = \Delta\psi$ and divergence $D = \Delta\chi$) at locations $s, t \in \mathbb{R}^2$,

$$C(s,t)$$
$$= \mathrm{Cov}\Big(\big(\ \psi_s,\ \chi_s,\ u_s,\ v_s,\ \Delta\psi_s,\ \Delta\chi_s\ \big)^T, \big(\ \psi_t,\ \chi_t,\ u_t,\ v_t,\ \Delta\psi_t,\ \Delta\chi_t\ \big)^T\Big). \quad (3)$$

The covariance function $C(s,t)$ is well-defined, if

$$C_{\psi,\chi}(s,t) = \mathrm{Cov}\left(\big(\ \psi_s\ \chi_s\ \big)^T, \big(\ \psi_t\ \chi_t\ \big)^T\right)$$

is four times continuously differentiable. Four times differentiability of the covariance function is equivalent to the process being twice mean square differentiable, see Lemma 14 in Ritter (2000).

In the remainder of the chapter we will consider stationary processes, which means that $C(s,t)$ depends only on the lag vector $h = t - s$. We will adopt a commonly used notation for stationary processes, $C(h) := C(0,h)$. Our next step is to review two notions of isotropy that exist for multivariate processes. Following Schlather et al. (2015) a vector of scalar quantities is called isotropic if the covariance function C fulfills

$$C(Qh) = C(h) \qquad h \in \mathbb{R}^d, \quad (4)$$

for all rotation matrices Q and $h = t - s$. A matrix Q is a rotation matrix if QQ^T equals the d-dimensional identity matrix and $\det(Q) = 1$. Under the assumption of stationarity (4) is equivalent to the more typically used notion of isotropy $C(h) = C(\|h\|)$. Bi- (multi-) variate variables consisting of scalar quantities such as streamfunction, velocity potential or the Laplacian thereof fulfill (4). A multivariate process is *vector isotropic* if its covariance functions fulfills

$$C(h) = Q^T C(Qh) Q \quad \text{for all } h \in \mathbb{R}^d. \quad (5)$$

This relation shows that $\mathbb{E}\left(X_0 X_h^T\right) = \mathbb{E}\left(Q^T X_0 \left(Q^T X_{Qh}\right)^T\right)$, which means that the covariance is preserved if the lag vector h and the random vector are rotated simultaneously.

In the remainder of the chapter we consider isotropic processes, hence $C_{\psi,\chi}(Qh) = C_{\psi,\chi}(h)$ for all rotation matrices Q. Using the notation,

$$A = \begin{pmatrix} r_1 \cos\theta & r_1 \sin\theta \\ -r_2 \sin\theta & r_2 \cos\theta \end{pmatrix}, \quad (6)$$

we set $C_{\psi,\chi,A}(h) = C_{\psi,\chi}(Ah)$.

The effect of the anisotropy matrix A on the covariance function of the vector components, namely the rotational part $\nabla \times \psi$ and the divergent part $\nabla\chi$, is nontrivial. The divergent part satisfies

$$\mathrm{Cov}\left(\nabla\chi\left(As\right),\nabla\chi\left(At\right)\right)=A^{T}\mathrm{Cov}\left(\left(\nabla\chi\right)\left(As\right),\left(\nabla\chi\right)\left(At\right)\right)A. \tag{7}$$

The rotational part fulfills a more complex formula

$$\begin{aligned}&\mathrm{Cov}\left(\nabla\times\psi\left(As\right),\nabla\times\psi\left(At\right)\right) \\ &=RA^{T}R^{T}\mathrm{Cov}\left(\left(\nabla\times\psi\right)\left(As\right),\left(\nabla\times\psi\right)\left(At\right)\right)RAR^{T},\end{aligned} \tag{8}$$

where

$$R=\begin{pmatrix}0 & -1\\ 1 & 0\end{pmatrix}.$$

If A is simply a rotation matrix (i.e. $r_1 = r_2 = 1$), then $RAR^T = A$, which implies that both the divergent and the rotational part are vector-isotropic. For the Laplacians we obtain the following transformation

$$\begin{aligned}\mathrm{Cov}\left(\Delta\chi\left(As\right),\Delta\chi\left(At\right)\right)=r_1^4\mathrm{Cov}\left(\partial_{e_1}^2\chi\Big|_{As},\partial_{e_1}^2\chi\Big|_{At}\right)+r_2^4\mathrm{Cov}\left(\partial_{e_2}^2\chi\Big|_{As},\partial_{e_2}^2\chi\Big|_{At}\right)\\ +2r_1^2r_2^2\mathrm{Cov}\left(\partial_{e_1}^2\chi\Big|_{As},\partial_{e_2}^2\chi\Big|_{At}\right).\end{aligned} \tag{9}$$

In the appendix we provide the formulae for all entries of the covariance matrix (3) in the isotropic case. Equations (7) – (9) are useful since they are the easiest way to compute the covariance in the anisotropic case from the covariance in the isotropic case. They have been derived using the chain rule and the linearity of the covariance function in both arguments.

Our GRF is a counter example to a theorem of Obukhov (1954), which claims that the rotational and divergent component of isotropic vector fields are necessarily uncorrelated, which is equivalent to streamfunction and velocity potential being uncorrelated. Obukhov considers an invalid expression for the covariance of a rotational field and deduces from this expression that it is necessarily uncorrelated to a gradient field. We present the detailed argument in the Appendix B.

In the remainder of the chapter we will exemplify the full process in the case that the potential functions have the following bivariate structure.

$$C_{\psi,\chi}\left(s,t\right)=\begin{pmatrix}\sigma_\psi^2 & \rho\sigma_\psi\sigma_\chi\\ \rho\sigma_\psi\sigma_\chi & \sigma_\chi^2\end{pmatrix}M\left(\left\|A\left(t-s\right)\right\|_2,\nu\right), \tag{10}$$

where $M\left(\cdot,\nu\right)$ denotes the Matérn correlation function with smoothness parameter ν, and $\|t-s\|_2$ the L^2 norm. Goulard and Voltz (1992) consider a more general model and prove its positive definiteness, implying the positive definiteness of our model (10). Figure 2.1 represents a realization of the full stochastic process, with parameters chosen in order illustrate the flexibility of the model. The rotational wind component is larger than the divergent wind component with a ratio

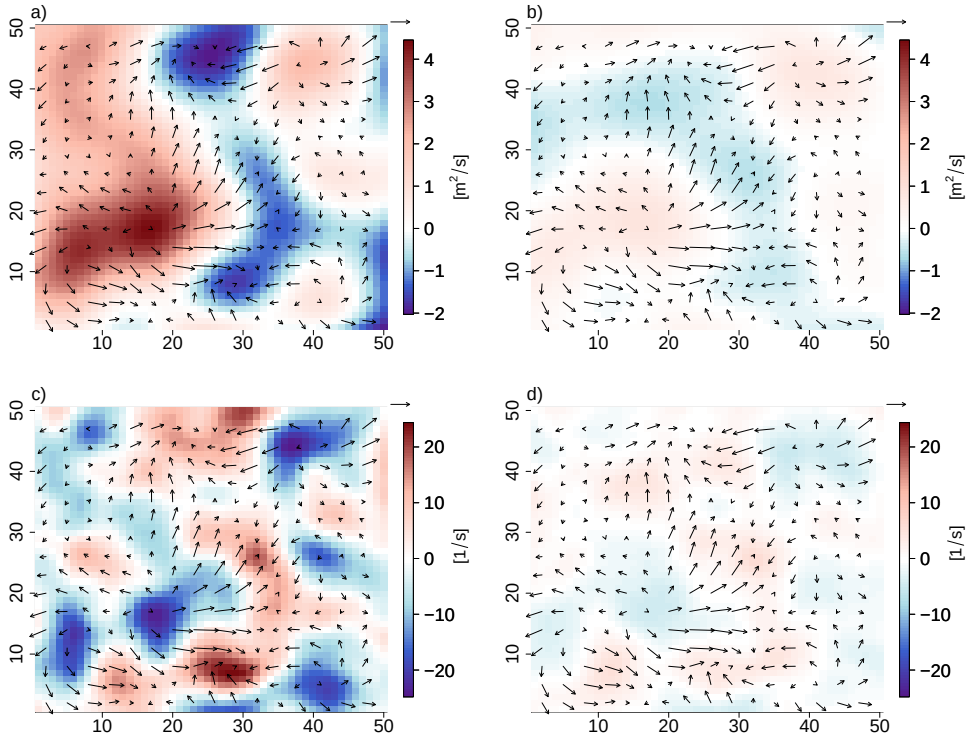

Figure 2.1: Isotropic realization of the multivariate GRF on a 50×50 grid with unit grid point distance and parameters $\nu = 5$, $\sigma_\chi/\sigma_\psi = 0.3$, $\rho = 0.7$, $r_1 = r_2 = 0.25$. In color are shown a) streamfunction, b) velocity potential, c) vorticity, and d) divergence. The arrows represent the associated wind fields in m/s. The arrow in the right upper corner is a standard arrow of 0.5 m/s. The x/y-axis indicate distance measured in grid points.

of $\sigma_\chi/\sigma_\psi = 0.3$. The two potential functions are strongly correlated with a correlation coefficient of $\rho = 0.7$. The coherence of the variables can be very well spotted, although the simulation of the process is inherently stochastic. The smoothness is set to $\nu = 5$, which implies that not only the potentials but also vorticity and divergence are continuously differentiable. We will see later in Section 2.4, that realistic mesoscale wind fields have a smoothness parameter close to 1.25. This suggests that the vorticity and divergence fields are discontinuous.

2.3 Data

The horizontal wind fields are taken from the NWP model COSMO-DE, namely the wind fields at model level 20 (i.e. at approximately 7 km height). COSMO-DE is the operational version of the non-hydrostatic limited-area NWP model consortium of Small-scale Modeling (COSMO) operated by DWD (Baldauf et al., 2011). It provides forecasts over Germany and surrounding countries on a 2.8 km horizontal grid and 50 vertical levels. At this grid size deep convection is permitted by the dynamics and COSMO-DE is able to generate deep convection without an explicit parameterization thereof. Thus COSMO-DE particularly aims at the prediction of mesoscale convective precipitation with a forecast horizon of up to one day. The ensemble prediction system (COSMO-DE-EPS) uses COSMO-DE with different lateral boundary conditions (LBC), perturbed initial conditions and slightly modified parameterizations. The four LBC are generated by the Global Forecast Systems of NCEP, the Global Model of DWD, the Integrated Forecast System of ECMWF and the Global Spectral Model of the Meteorological Agency of Japan. For details on the setup of COSMO-DE-EPS the reader is referred to Gebhardt et al. (2011), Peralta et al. (2012), and references therein.

In our application we concentrate on a COSMO-DE forecast for 12 UTC on 5 June 2011 initialized on 00 UTC. COSMO-DE-EPS provides 20 forecasts of horizontal wind fields on a grid with 461×421 grid points. Five ensemble members are forced with identical LBC, respectively. They only differ due to perturbed initial conditions and four different parameterizations. Thus differences between the members with identical LBC are mainly due to small-scale internal dynamics. These differences are the differences obtained from subtracting two fields which have been generated using the same lateral boundary conditions. All combinations of fields with different model physics and identical lateral boundary conditions generate a set of 40 different fields of differences. The differences are referred to as inner-LBC anomalies.

To illustrate the data, Figure 2.2 displays a field of inner-LBC anomalies of the zonal wind component. The fields exhibits small scale anomalies with amplitudes that vary over the model region while the spatial structure seems relatively homogeneous. Thus, the data violate the assumption of stationarity. In order to model the instationarity of the variance we estimate the spatial kinetic energy $\widehat{g}$ by applying a kernel smoother to the kinetic energy field. In analogy to the field of electric susceptibility $(1 + \chi_e)$, which models the spatial varying potential polarization of the dielectric medium (Jackson, 1962), we apply the following transformation to the data

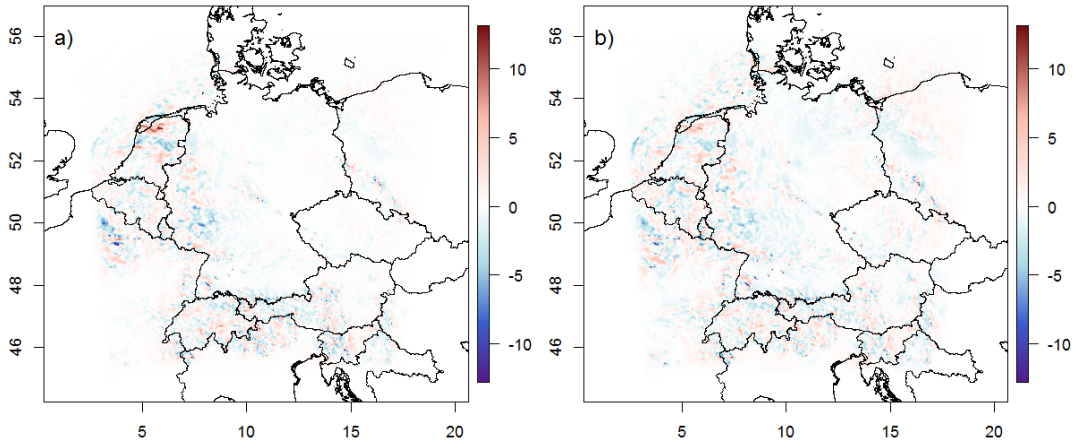

Figure 2.2: Zonal wind component at 12 UTC on 5 June 2011. a) Shows the inner-LBC anomalies, b) the transformed inner-LBC anomalies. The colors represent wind speed in m/s. The x/y- axis are in longitude and latitude.

$$\widetilde{U}_s = \frac{U_s}{c + \widehat{g}_s},$$

where $c \in \mathbb{R}_+$. Such a transformation, if applied to the full field $\left(\widetilde{\chi}, \widetilde{\psi}, \widetilde{U}, \widetilde{D}, \widetilde{\zeta}\right) = (\chi, \psi, U, D, \zeta)/(c+\widehat{g})$, violates the differential relations that hold between the variables, though they are still valid approximately. For example for a non-rotational field we have

$$\nabla\left(\frac{\chi}{c+\widehat{g}}\right) = \frac{\nabla\chi}{c+\widehat{g}} + \varepsilon. \tag{11}$$

The smoother the transformation the smaller the approximation error

$$\varepsilon = -\frac{\chi\nabla\left(c+\widehat{g}\right)}{\left(c+\widehat{g}\right)^2}.$$

Due to the constant $c > 0$ the transformation (11) does not resolve the full instationarity of the data. Still we find that this transformation is superior to the more natural transformation $\widetilde{U} = U/\widehat{g}$, as the approximation error for the potential functions is strongly reduced by the introduction of $c > 0$. We observe a trade-off between the differential relations being hardly violated and on the other side Gaussian marginal distribution and constant variance in space by a rougher function $\widehat{g}$ and values of c close to zero. We chose $c = 1/3$ and a kernel such that the transformation kurtosis of the data is reduced from 24 to 16, while we have to accept

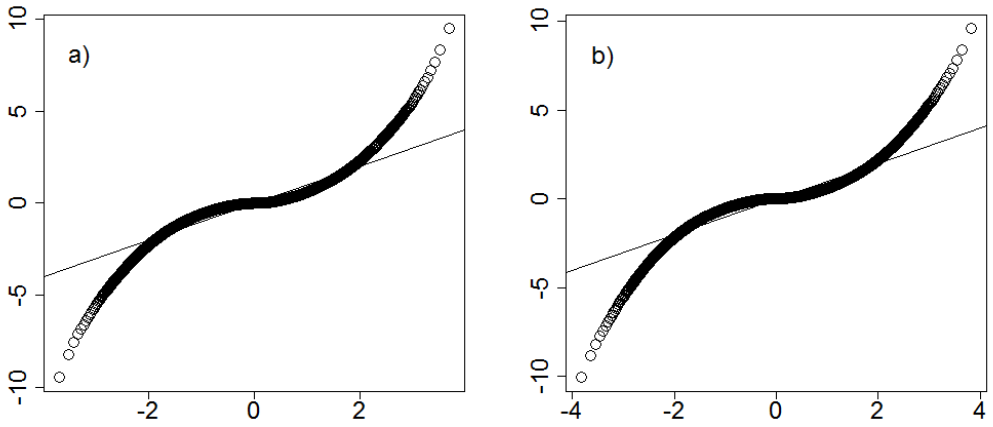

Figure 2.3: Quantile-Quantile plot of (a) the zonal, and (b) the meridional wind component of transformed inner-LBC anomalies versus a standard normal distribution. The linear lines indicate perfect accordance with the marginal distributions, both graphs depict clear deviation from the normal distribution.

an error of the potential fields close to 15 percent. The error is measured by comparing the potential that satisfies $\nabla\widetilde{\chi} = U/(c + \widehat{g})$ and the potential that satisfies $\nabla\chi = U$ and is normalized by $c + \widehat{g}$ (the same is done for the rotational part). For a Pareto optimal solution to this trade-off see Appendix D. Figure 2.2 shows that the instationarity of the original fields is mitigated by the transformation. Figure 2.3 shows the marginal distribution of the transformed inner-LBC anomalies for the zonal and the meridional wind component. Both distributions deviate from the assumption of Gaussian marginals, although Gaussianity is a common assumption for wind fields in the meteorological literature (Frehlich et al., 2001). The kurtosis amounts to about 16 instead of 3, which results in heavier extreme values than expected under the assumption of Gaussianity.

2.4 Parameter estimation

We start by parameter estimation of the bivariate GRF model for the transformed inner-LBC anomalies of the horizontal wind fields described in Section 2.3. Since the computation of the Gaussian likelihood would require the inversion of a quadratic matrix with $2 \times 461 \times 421$ rows, a standard maximum likelihood approach is unfeasible. We thus use a composite likelihood (CL) approach to approximate the true likelihood function. An overview of the CL approach is given in Varin et al.

(2011). Here, we apply a special version of the CL approach known as pairwise likelihood (Cox and Reid, 2004). For a *bivariate* field this likelihood is a product of 4-dimensional likelihoods. We calculate the log likelihood of the CL as

$$l^c(\theta) = \sum_{s \in \mathbb{G}} \sum_{h \in N} \log\left(L\left(u_s, v_s, u_{s+h}, v_{s+h} | \, \theta\right)\right),$$

where θ denotes the parameter vector, and $\mathbb{G}$ denotes the set of all grid points. The set N controls for which separations h the likelihood is computed. The set N has to be determined relative to the given problem. If feasible it should include all lags h for which there is non-negligible dependence and some for which there is negligible dependence, in order to estimate the range. One way of determining this is to inspect the empirical covariance estimate. We chose N to be a regular 41×41 grid with step size one, which is centered in the origin. The choice is justified by the low uncertainties observed in the parametric bootstrap samples presented below.

The unknown parameters are the variances of the potentials σ^2_ψ and σ^2_χ, their correlation ρ, the smoothness parameter ν, and the scale parameters r_1, r_2, and the angle θ of the anisotropy.

To reduce the number of parameters, we use the correlation function instead of the covariance function, which only depends on the ratio and not on the magnitude of the variances of streamfunction and velocity potential (Daley, 1991). This is possible as we can estimate the variance of the zonal and meridional wind with very low uncertainty due to the large size of the considered grid. The CL was maximized using the built-in function optim of R Core Team (2015). In order to show the independence of the optimization technique of the initial values it was started 50 times with varying initial parameters. This reveals that there is a single global maximum of the likelihood function.

Parameter uncertainty such as the Fisher information are not available for our problem. We thus resort to a parametric bootstrap (Efron and Tibshirani, 1994) to assess the uncertainty of the parameter estimates. We simulated the multivariate GRF using circulant embedding (Wood and Chan, 1994) to obtain independent realizations of the fitted process. Re-estimating the parameters for a sample of 100 independent realizations provides the uncertainty of the parameter estimates given that the estimated model is true. The simulation of the data was made possible by the implementation of the considered covariance model in an upcoming version of the spatial statistics package RandomFields (Schlather et al., 2016). The parametric bootstrap describes the estimation uncertainty based on the assumption that the model is sufficiently close to the data. It cannot assess the uncertainty related to the modeling error. As the considered data deviates from Gaussian distribution

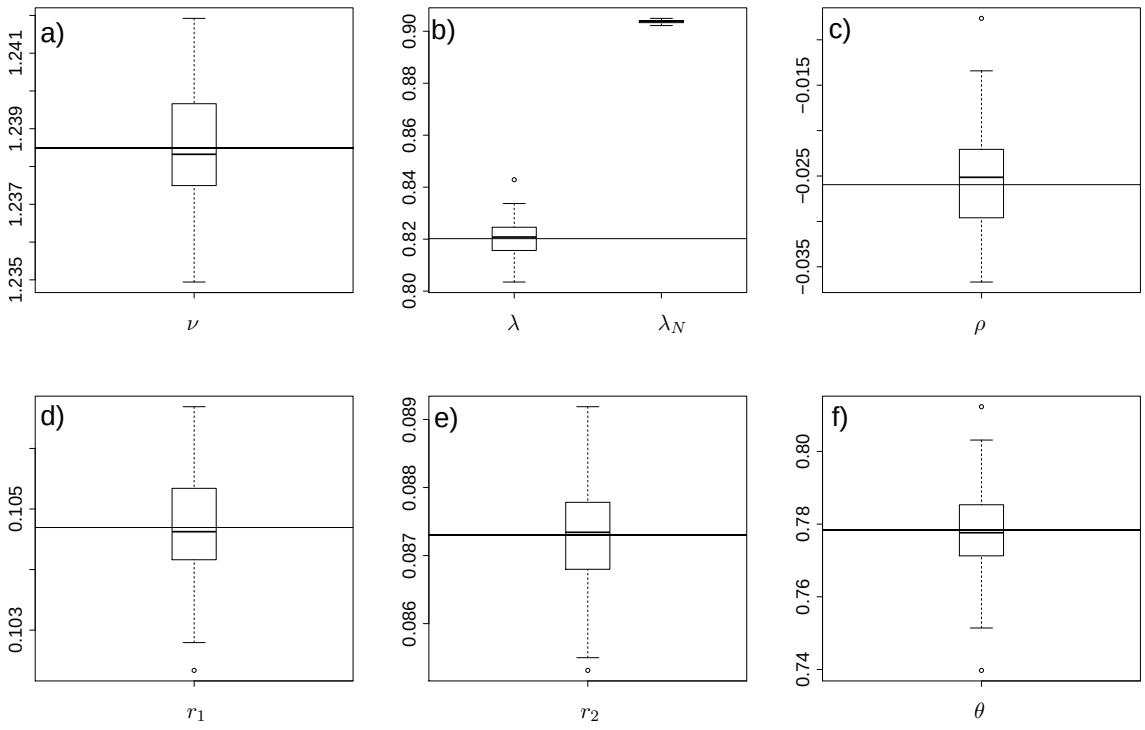

Figure 2.4: Box-whisker plots representing the parametric bootstrap estimates for the inner-LBC wind anomalies. The horizontal lines indicate the maximum-likelihood estimates: a) shows the smoothness parameter ν, the left box-whisker in b) represents the maximum-likelihood estimates (λ), and the right box-whisker the numerically derived estimates (λ_N) of the ratio $\lambda = \sigma_\chi/\sigma_\psi$. c) shows the correlation ρ, d) the scale parameters r_1 e) the scale parameter r_2, and f) the angle of the anisotropy matrix θ.

and is only approximately stationary this error is presumably not negligible.

2.5 Results

Figure 2.4 shows the estimates of the parameters of the multivariate GRF and the respective distribution of the parametric bootstrap estimates as a boxplot. The ratio of divergent and rotational wind is estimated to about $\sigma_\chi/\sigma_\psi \approx 0.82$. This indicates, that both wind components are of the same order of magnitude. A geostrophic balance would require a ratio of order $\sigma_\chi/\sigma_\psi = 0.1$, with a significant

dominance of the rotational wind component. This is not the case in COSMO-DE, which is well consistent with the mesoscale dynamics, which are highly non-geostrophic. The results are also consistent with Bierdel (2012)[2]. Her spectral analysis of the horizontal wind fields of COSMO-DE-EPS revealed a slightly stronger rotational than divergent component.

Figure 2.4b compares the statistical estimate for $\lambda = \sigma_\chi/\sigma_\psi$ to a numeric estimate, which equals the ratio of the L^2-norms of curl and divergence of the wind field calculated with finite difference approximations and which is denoted by λ_N. Both estimators have been computed on data simulated by our model (10). The comparison made for the two estimators has the limitation of the parametric bootstrap described in Section 2.4. The uncertainty related to the modeling error cannot be quantified by it. Yet the performance on data simulated by our model can be assessed. Although the statistical estimate has a higher variance it clearly outperforms the numeric estimate due to the relatively large bias of the latter on data simulated from our model. Our model can be used to generate data with known parameters on this data the performance of estimators can be assessed.

The correlation between streamfunction and velocity potential ρ is almost zero $\approx -2.5\times10^{-2}$. Similar results have been described for larger scales (Hollingsworth and Lönnberg, 1986) and have often been assumed in the literature (Daley, 1991). The smoothness parameter ν is close to 1.24. This corresponds non continuous fields of vorticity and divergence. A quasi realistic model for vorticity are the point vortices where vorticity is concentrated on a single point, or given as a delta function in space (Aref, 2007). This relatively low value of ν is not due to noise in the data. We have included tentatively a noise parameter in the estimation but it was set to zero and similar values as in Figure 2.4 were obtained. As a measure for the anisotropy we consider the ratio of the scale parameters r_1/r_2. This ratio is significant larger than 1 for both data sets, which suggests that the data is anisotropic. The estimated parameters are very much in accordance with our expectations, as they describe a non-geostrophic and anisotropic wind field. The most important result is that the independence of streamfunction and velocity potential in the case of the 5 June 2011 is valid on the mesoscale. Similar results were already known for larger scales (Hollingsworth and Lönnberg, 1986). In addition, our parametric bootstrap reveals that this covariance model can be estimated with a very high precision if the distribution of the data is close to the model. Under the same condition we have shown that our estimate of the ratio of divergence and vorticity is superior to

[2]Personal communication: Lotte Beata Bierdel (2012): Mesoskalige Turbulenz in dem konvektionsauflösenden Wettervorhersagemodell COSMO-DE-EPS. Masterarbeit in Meteorologie. Meteorologisches Institut der Friedrich-Wilhelms-Universität Bonn. 159p.

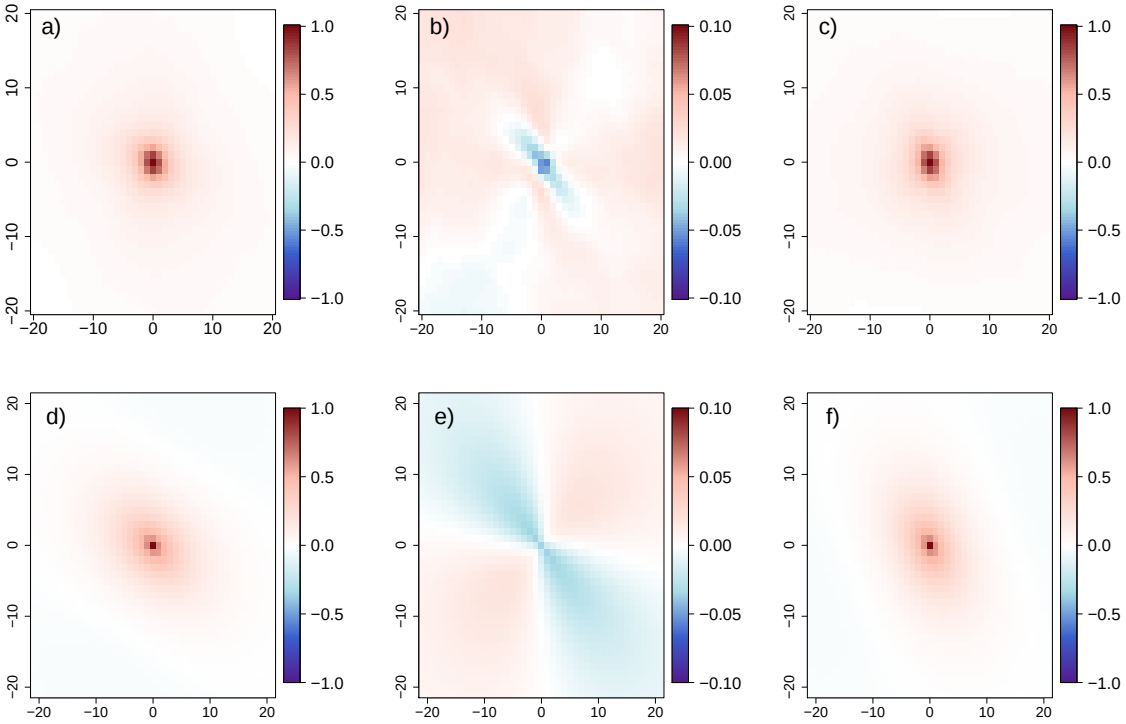

Figure 2.5: Empirical correlation (above) and estimated correlation (below) for the inner-LBC anomalies. a) (u,u) empirical correlation; b) (u,v) empirical correlation; c) (v,v) empirical correlation; d) (u,u) estimated correlation; e) (u,v) estimated correlation; f) (v,v) estimated correlation.

a numeric estimate.

Figure 2.5 shows the empirical estimate of the correlation structure of the data and the correlation obtained for the maximum likelihood estimation. Again the scale and the orientation of the correlation is very well matched. The (u, u) and (v, v) auto correlation component is matched relatively well. The (u, v) correlation component has a deviation from the data as there are regions of positive correlation, which is not present in the empirical correlation estimate.

The implementation of our covariance model in an upcoming version of the R package RandomFields (Schlather et al., 2016) allows for the simulation of large field with a size of the order of (800×800) grid points. This is made feasible by using circulant embedding introduced by Wood and Chan (1994). Circulant embedding is a powerful simulation technique, which to the best of our knowledge,

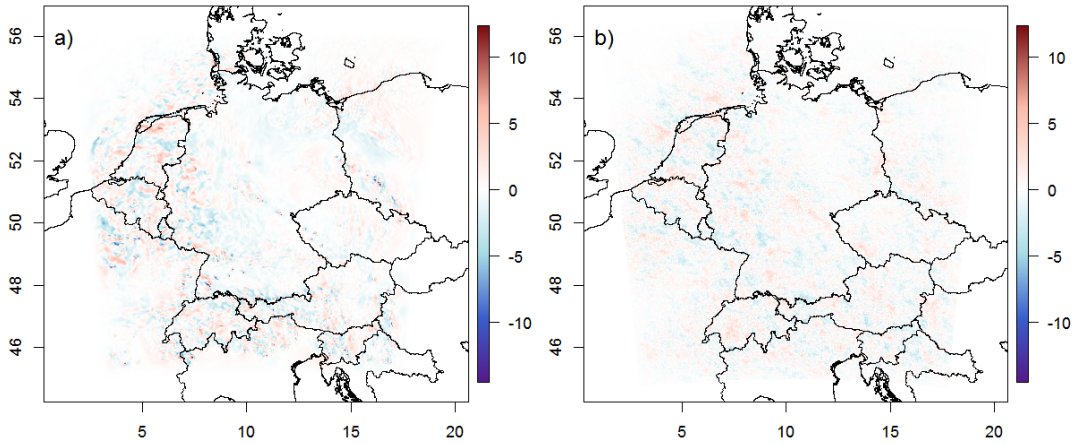

Figure 2.6: a) Same as Figure 2.2b). b) Zonal wind component of a realization of the fitted GRF. The x/y- axis are in longitude and latitude.

has not been used for the simulation of wind fields yet. Figure 2.6 shows the zonal wind anomalies from Figure 2.2 together with a realization of the fitted multivariate GRF, which has been scaled with the spatial variance that has not been resolved by the transformation (11). It shows that the orientation as well as the spatial scale of the zonal wind fields match very well. The multivariate GRF shows less extreme values and less values very close to zero, due to the assumption of Gaussianity. However, visual accordance is quite well, such that we conclude that the multivariate GRF formulation represents a useful stationary, multivariate Gaussian random fields approximation of mesoscale wind anomalies.

2.6 Conclusions

In this chapter we introduce a multivariate GRF which jointly models streamfunction, velocity potential, the 2-dimensional wind field, vorticity and divergence. Its flexibility allows for different variances of the potential functions, anisotropy and a flexible smoothness parameter. Further, the model is able to represent nonzero correlation of the divergent and non-divergent wind component. All parameters of the proposed covariance model have direct meteorological interpretation, such that they provide meteorological insight into the dynamics of the atmosphere. Further, the model allows us to easily implement meteorological balances such as non-divergence or geostrophy.

We have reviewed the theory that guarantees the existence of derivatives of stochastic processes, developed a complex covariance model for various atmospheric

variables and studied its transformation subject to anisotropy. Our multivariate GRF is a counter example to a theorem of Obukhov (1954), which claims that the rotational and divergent components of an isotropic vector field are necessarily uncorrelated.

We have developed an estimation technique and shown its performance for wind anomalies of a mesoscale ensemble prediction system (COSMO-DE-EPS). A parametric bootstrap method provides estimates of the uncertainty implicit in our estimation technique. We thus provide estimates for the ratio of variances of the rotational and divergent wind component without numerical approximations. Numeric estimates suffer from a truncation error, which arises due to the numerical scheme that computes the derivatives of the wind field.

The multivariate GRF formulation may be particularly useful for global atmospheric models with a spectral representation of the horizontal fields, such as the ECHAM climate model (Roeckner et al., 2003). Spectral models solve the prognostic equations for the potentials instead of the horizontal wind components, whereas the observations are given as horizontal wind vectors. Our multivariate GRF formulation provides a consistent formulation of the covariance structure for both the potential and the horizontal wind components. A stochastic formulation of the potentials may also be relevant for the assimilation of measurements of the vertical velocity (Bühl et al., 2015), which provide proxies for the horizontal divergence of the field. Our covariance function represents the divergence within a stochastic model, which is needed to assimilate the observations.

The proposed covariance model can be used to interpolate observed wind fields and to compute the associated derivative fields. This is feasible either by conditional simulation or Kriging. Numerical methods have been used for interpolation (Schaefer and Doswell III, 1979) and the computation of derivatives of vector fields (Caracena, 1987; Doswell III and Caracena, 1988). While numeric methods become significantly more complex for scattered observations, the multivariate GRF formulation provides an accessible way for both problems which additionally provides information about the uncertainty.

The fields obtained by computing the expectation of velocity potential and streamfunction given a certain wind field can be shown to solve the differential equations of the Helmholtz equation. In this sense our covariance model can be used via Kriging to solve the Helmholtz equation. As stochastic models describe the uncertainty of all of the variables these methods even allow stochastic error bands to be computed for the solution of the partial differential equations.

Another potential application is the stochastic simulation of the transport of

tracer variables such as aerosols or humidity in the atmosphere. Stochastic models that describe gradient fields and their divergence have been considered in the literature (Scheuerer and Schlather, 2012). However, to the best of our knowledge no stochastic model has been formulated to jointly model spatial wind fields and its divergence. Both variables are needed to describe the transport adequately.

Our methods show that both physical coherence and geostrophic constraints can be easily implemented into a covariance model. Further, we have illustrated that the model parameters can be estimated with very small uncertainty on data simulated by our model.

Acknowledgments:
Rüdiger Hewer was funded by Volkswagen Stiftung within the project "Mesoscale Weather Extremes: Theory, Spatial Modeling and Prediction (WEX-MOP)." Data used in this study are kindly provided by DWD. We thank Chris Snyder and an anonymous reviewer for the thoughtful comments, which improved our paper substantially. We are especially grateful to the reviewer for the idea to transform the data such that our model assumptions are more appropriate. We thank Sebastian Buschow for help in preparing the data.

3 Precipitation extremes in stochastic models based on the moisture budget

In this chapter we introduce stochastic, physically consistent models for precipitation extremes based on the moisture budget equation (1). Using these models we will extensively study to which extent the budget equation can account for characteristics of precipitation extremes. In Section 3.1 we introduce basic concepts of EVT for both univariate and multivariate random variables and stochastic processes and study under which conditions products of random variables are heavy-tailed. In Section 3.2 an overview of the literature related to precipitation extremes is given. Section 3.3 reviews the physically motivated stochastic model of Wilson and Toumi (2005) and introduces three models for precipitation fields. The precipitation models proposed in this section are based on the stochastic process for wind and related variables introduced in Section 2.2. In Section 3.4 we investigate both asymptotic extremal properties of the models and their extremal behavior for finite sample size. Section 3.5 discusses and reviews the main results of our approach to model precipitation fields.

3.1 Extreme value theory

3.1.1 Univariate extreme value theory

EVT has been developed to estimate the probability of extreme events. It has been used in many scientific fields like hydrology (Coles and Tawn, 1996), meteorology (Lenderink and Van Meijgaard, 2008), climate science (Katz, 1999) and geology (Knopoff and Kagan, 1977) and applications like insurance and finance (Embrechts et al., 1999). Due to a remarkable simplicity of the tail behavior it is possible in many situations to extrapolate into the tail of the distribution function. This means that based on a sample of a distribution it is possible to give meaningful estimates of the probability of non-observed extreme quantiles.

There are two basic approaches to describe the behavior of extreme events. The first approach is to describe the distribution of the maximum of a sample,

$$P\left(\max\left(X_1,\ldots,X_n\right)\leq c\right)=F^n\left(c\right)\overset{i.D.}{\to}G(c)\quad\left(n\to\infty\right),\tag{12}$$

where $X_i\overset{iid}{\sim}F$, F is a distribution function and G is a distribution yet to be determined. The second approach introduces distributions H that describe a random variable conditional on exceeding a certain threshold,

$$P\left(X\leq c+T|X>T\right)\overset{i.D.}{\to}H(c)\quad\left(T\to\infty\right).\tag{13}$$

The two approaches exhibit largely similar results as will be shown below. Following De Haan and Ferreira (2006), we start with the first one. Let $x^\star = \sup_x (F(x) < 1)$, then $F^n(x) \to 0$ whenever $x < x^\star$ and $F^n(x) = 1$ if $x \geq x^\star$. This means that the maximum over n realizations tends to the upper endpoint of the distribution as $n \to \infty$. In order to obtain more precise results we have to transform $\max(X_1, \ldots, X_n)$ such that a non-degenerate limit in (12) occurs. A distribution is called degenerate if its probability is localized in a single point. Hence, we are searching for limits of the kind

$$F^n(a_n x + b_n) \overset{i.D.}{\to} G(x) \quad (n \to \infty), \tag{14}$$

with a non-degenerate distribution function G. Such functions G play a vital role in EVT. We cite the following definition from De Haan and Ferreira (2006).

Definition 1. A non-degenerate distribution function G that fufills (14) for a distribution function F and sequences $a_n, b_n \in \mathbb{R}, a_n > 0$ is called generalized extreme value distribution (GEV).

There is a remarkably simple characterization of the class of GEV. Again we cite the following theorem from De Haan and Ferreira (2006) which was originally proved by Fisher and Tippett (1928) and Gnedenko (1943).

Theorem 2. The class of GEV is given by $G_\gamma(ax + b)$ with $a \in \mathbb{R}_+, b \in \mathbb{R}$,

$$G_\gamma(x) = \exp\left(-(1 + \gamma x)^{-1/\gamma}\right) \qquad 1 + \gamma x > 0,$$

with $\gamma \in \mathbb{R}$. The limit for $\gamma \to 0$ is

$$G_0(x) = \exp(-\exp(-x)).$$

Proof. See Theorem 1.1.3 in De Haan and Ferreira (2006). □

The distribution G_o is known as the Gumbel distribution and the parameter γ as shape parameter. For positive shape parameter the distribution G_γ is called Fréchet distribution and for negative-shape Weibull distribution. The theorem shows that up to affine transformations the class of extreme-value distributions consists of a single parameter family. We introduce a further important concept from Embrechts et al. (1997).

Definition 3. A distribution function F for which there are sequences $a_n \in \mathbb{R}_+, b_n \in \mathbb{R}$ such that

$$(F(a_n x + b_n))^n = F(x) \quad \text{for all } n,$$

is called max-stable.

The above equation shows that the maximum over n realizations of a max-stable distribution F has up to an affine transformation distribution function F. The class of non-degenerate max-stable distribution is identical to the GEV (Theorem 3.2.2 of Embrechts et al., 1997). If for a certain distribution function F there are sequences $a_n, b_n \in \mathbb{R}, a_n > 0$ such that

$$F^n\left(a_n x + b_n\right) \overset{i.D.}{\to} G_\gamma\left(x\right) \quad (n \to \infty),$$

we say that F lies in the max-domain of attraction of G_γ or $F \in D\left(G_\gamma\right)$. We will call a distribution heavy-tailed if it is in the max-domain of attraction of the Fréchet distribution. A distribution function in the max-domain of attraction of the Weibull or the Gumbel distribution will be called light-tailed. This is a typical but not generally adopted use of the notions light and heavy-tailed. The following theorem presents a simple condition implying that a distribution function lies in the max-domain of attraction of a GEV. For simplicity the theorem is slightly more restrictive than Theorem 1.1.8 in De Haan and Ferreira (2006).

Theorem 4. Let F be a distribution function and $x^\star = \sup_x \{x | F(x) < 1\}$. Assume that F is a twice continuously differentiable and invertible distribution function. Further assume that the density f is strictly positive in a left-open interval containing $x^\star$. If

$$\lim_{t \uparrow x^\star} \left(\frac{1-F}{f}\right)'(t) = \gamma$$

or

$$\lim_{x \uparrow x\star} \frac{\left(1-F(t)\right) f'(t)}{f(t)^2} = -\gamma - 1,$$

then

$$\lim_{n \to \infty} \left(F(a_n x + b_n)\right)^n = G_\gamma\left(x\right),$$

where $b_n = F^{-1}\left(1 - 1/n\right)$ and $a_n = 1/\left(n f(b_n)\right)$.

Proof. See Theorem 1.1.8 in De Haan and Ferreira (2006). □

In order to illustrate this result we derive the extreme value behavior of an exponentially distributed random variable.

Example 5. The distribution function of an exponentially distributed random variable is $F(x) = 1 - \exp(-x/\lambda)$, $\lambda \in \mathbb{R}_+$. This function is invertible with inverse $F^{-1}(x) = -\lambda \ln(-x + 1)$ and is a smooth function. The density $f(x) =$

$\exp(-x/\lambda)/\lambda$ is strictly positive on the real axis and has the right endpoint $x^\star = \infty$. Further we have

$$\frac{(1-F(t))\,f'(t)}{f(t)^2} = \frac{-\exp(-x/\lambda)\exp(-x/\lambda)/\lambda^2}{(\exp(-x/\lambda)/\lambda)^2} = -1$$

and hence $\gamma = 0$. The exponential distribution is in the domain of attraction of the Gumbel distribution and

$$\lim_{n\to\infty} P\left(\frac{\max(X_1,\ldots,X_n) - b_n}{a_n} \leq x\right) = \lim_{n\to\infty} (F(a_n x + b_n))^n = \exp(-\exp(-x)),$$

where $b_n = -\lambda \ln(1/n) = \lambda \ln n$ and $a_n = 1/(nf(b_n)) = \lambda$.

Similar to the central limit theorem describing the sample mean, this theorem describes the limit distribution of the sample maxima. The sequences a_n, b_n transform the maximum such that a non-degenerate limit distribution is obtained. The maximum of a sample of length 10 is already very close to the Gumbel limit. Example 5 shows that the maximum of a sample of length n of an exponential distribution is of order $\mathcal{O}(\ln n)$. For other distributions like the normal distribution it is well-known that the convergence of the maximum to the Gumbel limit is very slow and therefore hardly applicable. The following theorem is implied by Theorem 1.1.6 in De Haan and Ferreira (2006).

Theorem 6. For $\gamma \in \mathbb{R}$ the following statements are equivalent.
(i) There exist sequences $a_n \in \mathbb{R}_+, b_n \in \mathbb{R}$ such that

$$\lim_{n\to\infty} F^n(a_n x + b_n) = G_\gamma(x) = \exp\left(-(1+\gamma x)^{-1/\gamma}\right),$$

for all x fulfilling $(1+\gamma x) > 0$.
(ii) There is a positive function h such that we have,

$$\lim_{t\to x^\star} \frac{1-F(t+xh(t))}{1-F(t)} = (1+\gamma x)^{-1/\gamma}, \tag{15}$$

where $x^\star := \sup_x \{x | F(x) < 1\}$.

Proof. See Theorem 1.1.6 in De Haan and Ferreira (2006). □

The theorem provides a connection between the two fundamental distributions (12) and (13). The first statement is the classical convergence of the maximum of a sample to an extreme value distribution. The second statement is related to the probability of exceeding a certain threshold $t + xh(t)$. This connection can be made much more explicit. Let Y be a random variable with distribution function F. If $x > 0$, we can deduce as $h(t) > 0$,

$$\frac{1-F\left(t+xh(t)\right)}{1-F(t)}=\frac{P\left(Y>t+xh(t)\right)}{P\left(Y>t\right)}=P\left(\frac{Y-t}{h(t)}>x\middle|\,Y>t\right).$$

This shows that essentially equation (15) describes the tail behavior of F. Theorem 6 establishes an equivalence of the limit behavior of the maximum of a sample and the tail of the distribution. Further, this theorem motivates the definition of the generalized Pareto distribution (GPD) as the limit distribution of exceedances.

Definition 7. The GPD with shape parameter γ is given by

$$F_\gamma(x)=\begin{cases}1-(1+\gamma x)^{-1/\gamma} & \gamma>0,\ x>0\\ 1-\exp\left(-x\right) & \gamma=0,\ x>0\\ 1-(1+\gamma x)^{-1/\gamma} & \gamma<0,\ 0<x<1/|\gamma|.\end{cases}$$

Similarly to the GEV, the GPD has three different regimes. For $\gamma>0$ we observe a polynomial decay of the inverse probability of exceedances. This behavior is associated with heavy tails. For $\gamma=0$ the decay is exponential and the distribution is light-tailed. For $\gamma<0$ the distribution has finite support and the probability of exceedances decays polynomially.

Since the GPD describes the tail of the distribution, it is reasonable to estimate the parameter γ from the largest values in a sample. If $\gamma>-1/2$ the maximum likelihood estimate $\widehat{\gamma}_n$ is asymptotically normally distributed (De Haan and Ferreira, 2006). The convergence rate is $\gamma-\widehat{\gamma}_n=\mathcal{O}\left(\frac{1}{\sqrt{n}}\right)$ (De Haan and Ferreira, 2006), where $\widehat{\gamma}_n$ is the maximum-likelihood estimate from a sample of length n. The limitation $\gamma>-1/2$ is no restriction in our context as most studies describing precipitation extremes propose either $\gamma=0$ or $\gamma>0$. This result is essential for this study as we will use estimates of the shape parameter in order to describe the extremal behavior of precipitation distributions (Sections 3.4.3).

3.1.2 Multivariate extreme value theory

Multivariate EVT is a tool to describe the dependence structure of multiple extreme events. Although there is no unique reasonable definition of a multivariate extreme, the theory was mainly developed for the componentwise maximum of a vector.

$$\bigvee_{i=1}^{n}X_i:=\left(\bigvee_{i=1}^{n}X_{i,1},\ldots,\bigvee_{i=1}^{n}X_{i,d}\right),$$

where $\bigvee_{i=1}^{n}X_{i,1}:=\max\left(X_{1,1},\ldots,X_{n,1}\right)$ and $X_1,\ldots,X_n$ is a sample of multivariate random variable. This setting may seem artificial and hard to interpret, as the componentwise maximum of a sample is typically not a member of the sample. Yet the theory developed for this setting can be used to solve many applied

problems (De Haan and Ferreira, 2006). Similar to the univariate setting a non-degenerate function G is called d-variate extreme value distribution, if there exists a distribution function F and sequences $a_{n,i} > 0, b_{n,i}, n \in \mathbb{N}, i = 1, \ldots, d$ such that

$$\lim_{n\to\infty} F^n(a_{n,1}x_1 + b_{n,1}, \ldots, a_{n,d}x_d + b_{n,d}) = G(x) \quad x \in \mathbb{R}^d.$$

The marginal of such distributions are the univariate extreme value distributions. A $d-$variate distribution function G is called max-stable if for every $n \in \mathbb{N},\ i = 1, \ldots, d$ there are constants $a_{n,i} > 0, b_{n,i} \in \mathbb{R}$ such that

$$G^n(a_{n,1}x_1 + b_{n,1}, \ldots, a_{n,d}x_1 + b_{n,d}) = G(x) \quad x \in \mathbb{R}^d.$$

The univariate marginals of max-stable distributions are max-stable and the class of non-degenerate max-stable processes coincides with the class of generalized extreme value distriubtions (De Haan and Ferreira, 2006).

To illustrate characteristics of the multivariate setting we present extremal properties of the multivariate Gaussian distribution. The componentwise maximum over Gaussian vectors consists of asymptotically independent [3] entries whenever the variables have correlation $|\rho| < 1$ (Sibuya, 1960). In order to obtain asymptotic relations that are applicable for settings of highly dependent Gaussian variables, Hüsler and Reiss (1989) introduced a triangular array consisting of d-variate vectors $X_{n,i}$ where $i \leq n$ and $n \in \mathbb{N}$. In the bivariate case $d = 2$ the vectors consist of two standard normal Gaussian vectors with correlation p_n. Hüsler and Reiss (1989) show that if

$$(1 - p_n) \ln n \to \lambda^2 \in [0, \infty] \tag{16}$$

the maximum converges to a limit

$$\bigvee_{i=1}^{n} \frac{X_{n,i} - b_n}{b_n} \overset{i.D.}{\to} M_\lambda,$$

where $b_n = \sqrt{2 \ln n}$ and M_λ is a Hüsler-Reiss process. It is a bivariate extreme value distribution with distribution function

$$H_\lambda(x, y) = \exp\left[-\Phi\left(\lambda + \frac{x - y}{2\lambda}\right)\exp(-y) - \Phi\left(\lambda + \frac{y - x}{2\lambda}\right)\exp(-x)\right].$$

The distribution function converges to the limit expressions

$$\lim_{\lambda\to 0} H_\lambda(x, y) = \exp\left(-\exp\left(\min(x, y)\right)\right),$$
$$\lim_{\lambda\to\infty} H_\lambda(x, y) = G_0(x)G_0(y).$$

[3] Let X_n, Y_n be two sequences of random variables. They are called asymptotic independent, if $(X_n, Y_n) \overset{i.D.}{\to} (X, Y)$ $(n \to \infty)$ and X and Y are independent.

The case $\lambda = 0$ models perfect correlation of the Gaussian variables and $\lambda = \infty$ complete independence. The multivariate case is similar to the bivariate, yet quite technical. For example, the multivariate limit distribution cannot be analytically evaluated.

3.1.3 Extreme value theory for stochastic processes

We now give a short overview of EVT for stochastic processes. Typically one considers random processes from the set of continuous functions on the interval $[0,1]$ ($\mathcal{C}[0,1]$). Similar to the multivariate setting the maximum of random functions is taken pointwise. If for *iid* continuous random functions X_i there exist sequences of continuous functions $a_n(t) \in \mathbb{R}_+, b_n(t) \in \mathbb{R}$

$$\bigvee_{i=1}^{n} \frac{X_i(t) - b_n(t)}{a_n(t)} \overset{i.D.}{\to} \eta(t) \quad (n \to \infty), \tag{17}$$

with non-degenerate η, then η is called extreme value process (De Haan and Ferreira, 2006). Convergence in distribution in functional spaces is defined similarly to other spaces. Let $X, X_n \in \mathcal{C}(D)$, $n \in \mathbb{N}$ be random continuous function on a set $D \subset \mathbb{R}^d$. Let F, F_n be the associated distribution functions. We say $X_n \overset{i.D.}{\to} X$ if for any measurable function $g \in \mathcal{C}[0,1]$ we have $\int g dF_n \to \int g dF \, (n \to \infty)$.

The class of non-degenerate max-stable processes coincides with the class of generalized extreme value processes. Similar to the multivariate case it is possible to standardize the marginal distribution to the Fréchet case. Before we introduce a spectral theorem for extreme value processes we need the definition of a Poisson point process.

Definition 8. Let $\mathcal{M}_p\left(\mathbb{R}^d\right)$ be the set of positive measures on $\mathbb{R}^d$, that have values in $\mathbb{N}_0 \bigcup \{\infty\}$. A point process is a random process with values in $\mathcal{M}_p\left(\mathbb{R}^d\right)$. Let ν be a measure on $\left(\mathbb{R}^d, \mathcal{A}\right)$, where $\mathcal{A}$ is σ-algebra[4] on $\mathbb{R}^d$. If there is a point process Φ fulfilling

(i) for $B \in \mathcal{A} \quad P(\Phi(B) = n) = \dfrac{\lambda^n}{n!} \exp(-\lambda) \quad$ where $\lambda = \nu(B)$

(ii) for disjoint sets $B_1, \ldots, B_m \in \mathcal{A} \quad$ the variables $\Phi(B_1), \ldots, \Phi(B_m)$ are independent,

Φ is called Poisson point process with intensity measure ν ($\Phi \sim \mathrm{PPP}(\nu)$).

De Haan (1984) shows that a wide class of continuous extreme value processes can be constructed via a so-called spectral decomposition. Let Y_t be an extreme

[4]For a definition of σ-algebra see Elstrodt (1997).

value process that fulfills $Y_{t_n} \xrightarrow{P} Y_t$ for any sequence $t_n \to t$. Then there exists a measure ν on $[0,1]$ and functions $f_t(\cdot)$ that fulfill

$$\int_0^1 f_t(\omega)\nu\left(d\omega\right) = 1,$$

such that

$$Y_t \sim \bigvee_{i=1}^{\infty} z_i f_t(x_i),$$

where $\sum_{i=1}^{\infty} \delta_{(z_i,x_i)} \sim \text{PPP}\left(dz/z^2 \times \nu\right)$, where $\delta_{(z,x)}$ is the Dirac function with mass in (z,x). A similar representation called mixed-moving maxima has been used to simulate extreme value processes (Oesting et al., 2012). The theorem shows that extreme value processes can be constructed as the maximum over an infinite number of functions with random intensity.

A further important class of extreme value processes is the Brown-Resnick class (Brown and Resnick, 1977). They occur as the limit process of the normalized maximum over Gaussian processes (Kabluchko et al., 2009). Further they are the continuous generalization of the Hüsler-Reiss distribution. They are constructed in the following way.

Theorem 9. Let $W_i(t), t \in \mathbb{R}^d$ be an *iid* Gaussian process with stationary increments, which means that the distribution of $\left(W_i\left(t+h\right) - W_i\left(t\right)\right)$ is independent of t. Let

$$Z_t = \bigvee_{i=1}^{\infty} u_i \exp\left(W_i\left(t\right) - \frac{\text{Var}\left(W_i(t)\right)}{2}\right), \tag{18}$$

where $\sum_{i=1}^{\infty} \delta_{u_i} \sim \text{PPP}\left(du/u^2\right)$, where δ_u is the Dirac function with mass in u. Then Z_t is a max-stable process with Fréchet marginals, whose distribution depends only on the variogram given by $\gamma\left(h\right) := \mathbb{E}\left(W_1(0) - W_1(h)\right)^2$.

Proof. The theorem can be obtained by applying $\exp\left(\cdot\right)$ to both sides of Theorem 2 in Kabluchko et al. (2009). □

The stochastic process $\left(Z_t, t \in \mathbb{R}^d\right)$ is then called Brown-Resnick process associated to the variogram $\gamma\left(h\right)$. The theorem gives a very simple construction principle for extreme value processes, as the spatial function in (18) are generated by Gaussian processes.

3.1.4 Asymptotic properties of products of random variables

The transport equation (1) consists of products of random variables. This motivates the following consideration on asymptotic properties of products. We will show that for a large class of distributions products of light-tailed distributions cannot be heavy-tailed. Further we will study the shape parameter of products of heavy-tailed distributions.

If a distribution F is in the domain of attraction of a GEV G_γ and if $\gamma \leq 0$ then $\mathbb{E}_F\left\{|X|^\alpha \mathbb{1}\left(X > x\right)\right\}$ is finite for any $\alpha \in \mathbb{R}_+, x < \sup\left(x|F(x) < 1\right)$ (De Haan and Ferreira, 2006). In the Fréchet case, there is also a clear relation between extreme value index and the above expression. Namely, if $\gamma > 0$ and $x \in \mathbb{R}$, then (De Haan and Ferreira, 2006)

$$\mathbb{E}_F\left\{|X|^\alpha \mathbb{1}\left(X > x\right)\right\} \quad \begin{cases} < \infty & \alpha < 1/\gamma \\ = \infty & \alpha > 1/\gamma. \end{cases} \tag{19}$$

We now introduce the class of distribution functions $\mathcal{F}$ for which the expression $\mathbb{E}_F\left\{|X|^\alpha \mathbb{1}\left(X > x\right)\right\}$ is finite if and only if $\mathbb{E}X^\alpha$ is finite. It is clear that the positive distributions and the symmetric distributions lie in $\mathcal{F}$. The absolute value of any distribution function lies in $\mathcal{F}$. Further, any distribution whose upper tail behavior is more extreme than the lower lies in $\mathcal{F}$. Hence, $\mathcal{F}$ includes most functions of practical relevance. We now use this class of distributions to characterize the shape parameter of products of random variables.

For a product of two *iid* random variables X, Y with distribution function F (not necessarily $F \in \mathcal{F}$) we obtain the following expressions for the moments

$$\mathbb{E}\left(XY\right)^n = \mathbb{E}X^n\mathbb{E}Y^n = \left(\mathbb{E}X^n\right)^2, \tag{20}$$

while for full dependence $X = Y$ we obtain

$$\mathbb{E}\left(XY\right)^n = \mathbb{E}X^{2n}. \tag{21}$$

If $F \in \mathcal{F}$ and F is in the domain of attraction of the Weibull or Gumbel distribution, all moments exist for F. From the above relations we see that also all moments of X^2 and XY exist. Hence, if the product is in the domain of attraction of any extreme value distribution, it is not in the Fréchet domain. This is an important result showing that products of light-tailed random variables cannot be heavy-tailed if the multiplicands lie in $\mathcal{F}$. This holds irrespective of their correlation and is especially true for the n-th power X^n of a random variable. This result can easily be extended to non-identically distributed multiplicands X and Y. It is clear that that all moments of the product XY exist. Hence, it is not heavy-tailed.

For heavy-tailed distributions we see from (20) that products of *iid* random variables XY have the squared moments of one of the multiplicands. If the multiplicands lie in $\mathcal{F}$ and the product in the max-domain of attraction of a GEV, the relation (19) shows that, it has the same shape parameter as the multiplicand. Hence products of independent heavy-tailed distribution cannot enhance the asymptotic extremal behavior. Again, this can be extended to non-identically distributed products XY. As it is clear that either X_1X_2 or Y_1Y_2 has a more extreme behavior than the original products for $X_1, X_2 \sim X$ independent and $Y_1, Y_2 \sim Y$ independent, the above considerations can be applied.

For squares of variables we have a different situation. Equation (21) shows that the moments of the products are higher moments of the multiplicand. If $X \sim F$, $F \in \mathcal{F}$, F is in domain of attraction of G_γ and X^2 is in domain of attraction of any extreme value distribution, then $X^2 \in D\left(G_{2\gamma}\right)$.

Koutsoyiannis (2004) argues that a heavy-tailed behavior of precipitation could emerge from the interplay of seasonal and non-seasonal variability. Koutsoyiannis (2004) models precipitation as $P = X/Y$, where X, Y are independent Gamma distributions. Here, X represents the non-seasonal variability of precipitation and $1/Y$ the seasonal variability. Koutsoyiannis (2004) shows that P is heavy-tailed. The example is misleading as already the inverse of a gamma distributed variable is heavy-tailed and therefore the seasonality itself is assumed to be heavy-tailed. Since X and $1/Y$ are positive they are in the class $\mathcal{F}$ and if their product is heavy-tailed, then one of the distributions must be heavy-tailed. Otherwise all moments of X/Y would exist. Further X is light-tailed (Beirlant et al., 2004), such that $1/Y$ must be heavy-tailed. In the more typical use of the scale parameter as a multiplier to the random variable our results of this section show that heavy tails cannot be generated for a large class of functions from light-tailed random variables who have scale parameter with light-tails.

3.2 Literature of precipitation extremes

A major issue in the literature related to precipitation extremes is the desire to understand the effect of climate change on the intensity and frequency of extreme precipitation (Groisman et al., 1999; Trenberth et al., 2003; Wilson and Toumi, 2005; Singleton and Toumi, 2013). An important relation is the Clausius-Clapeyron equation describing an increase in the humidity holding capacity by 7% per $1°C$ increase of temperature (Trenberth et al., 2003). It is therefore a widely expressed view that precipitation will increase as suggested by that rate (Trenberth et al., 2003; Singleton and Toumi, 2013), although this may be overly simplistic (Haerter

et al., 2010). Idealized simulations of storms show a precipitation increase consistent with Clausius-Clapeyron scaling on time scales longer than one hour (Singleton and Toumi, 2013). An even stronger increase of precipitation for shorter time periods in such simulations is connected to increases of vertical velocity with temperature (Singleton and Toumi, 2013). Studies using global climate models to investigate the relation between temperature increase and precipitation report a scaling weaker than suggested by the Clausius Clapeyron relation (Allen and Ingram, 2002; Pall et al., 2007), since on large scales precipitation is constrained by divergence of energy flux and not by moisture supply (Allen and Ingram, 2002).

It is claimed that a temperature increase leads to an increase of the frequency of heavy precipitation events (Trenberth et al., 2003). This prediction is consistent with studies claiming that temperature variability is a generator of precipitation extremes and high temperatures can be linked to extreme precipitation events (Haerter et al., 2010).

Singleton and Toumi (2013) show that for heavy precipitation events precipitation efficiency in the simulations is close to 100 %. Precipitation efficiency is the ratio of precipitated water to the total water present in a column of the atmosphere. This result is remarkable since there is no physical process that removes the total humidity from the atmosphere (Trenberth et al., 2003) and Ferrier et al. (1996) report values of precipitation efficiency close to 30%.

Observational data are used to study the change of precipitation due to climate change (Lenderink and Van Meijgaard, 2008; Liu et al., 2009) and in particular using EVT the distribution of precipitation extremes (Li et al., 2005). Here, the use of EVT is of tremendous importance due to the great uncertainty associated with rare extreme events and their potentially heavy-tailed behavior.

A further major problem is the appropriate description of the distribution of precipitation. The variety of distributions used to fit precipitation is so vast that it is described as a "battle of distributions" (Serinaldi and Kilsby, 2014). With respect to extreme precipitation the most important question is whether precipitation extremes are distributed following a heavy-tailed or light-tailed distribution. Knowledge about the tail-behavior is essential for the extrapolation of probability distributions, e.g. it is used to compute the return value of non-observed extreme events, which is of crucial importance to hydrology, insurance industry and architecture. While some studies use light-tailed distributions e.g. *mixed exponential* (Woolhiser and Roldan, 1982), *gamma* (Groisman et al., 1999), more recent studies favor distributions with heavy tail e.g. *quotient of gamma distributions* (Koutsoyiannis, 2004), *GPD with positive shape* (Serinaldi and Kilsby, 2014).

For some distribution functions the convergence of the maximum of a sample is so slow that it is not of practical relevance (Wilson and Toumi, 2005). For example Wilson and Toumi (2005) uses the *stretched exponential distribution* and Biondini (1976) the *log-normal* distribution for precipitation extremes. Both distributions are asymptotically light-tailed, but for finite sample they are well-approximated by heavy-tailed distributions. The slow convergence to the asymptotic behavior makes standard extrapolation of the distribution function problematic and has increased the interest in finite sample properties of the shape parameter of the GEV or GPD (e.g. Koutsoyiannis, 2004; Serinaldi and Kilsby, 2014). Further, the potential non-validity of standard extrapolation methods motivates the use of precipitation distributions justified by physical reasoning (Wilson and Toumi, 2005).

Serinaldi and Kilsby (2014) estimate the GPD for daily precipitation measurements on a data set containing records of 40 year length. While the shape parameter has a slight tendency for very high thresholds towards negative values, it attains for lower thresholds a positive shape parameter. This could be partly explained by the inclusion of non-extreme values, but is mainly interpreted as a small sample bias of the maximum likelihood estimator. Given a fixed threshold (98 percentile) Serinaldi and Kilsby (2014) use a data set containing time series of up to 110 years to study the effect of sample size on the estimates of the shape parameter. For very small sample size the maximum likelihood estimates of the shape parameter tend to slightly negative values and increase to positive shape parameter for larger sample size. They reproduce the small sample bias of the shape estimator by a Monte Carlo experiment using a GPD distribution with a normally distributed shape parameter with positive mean. From this the authors conclude, that the considered data is consistent with a distribution of the shape parameter that varies slowly in time and attains typically positive values. The study proposes a very elegant explanation for the dispute in the literature on whether precipitation is a heavy-tailed phenomenon.

Koutsoyiannis (2004) argues that the popularity of the Gumbel distribution is explained by the fact that for small samples of a Fréchet distribution the hypothesis of a Gumbel distribution cannot be significantly rejected. Koutsoyiannis (2004) describes the bias of moment estimator and maximum likelihood estimator for various sample sizes under the assumption of a Fréchet distribution for heavy precipitation. It is argued that the climate variability or seasonality could be a potential reason for the heavy-tail of extreme precipitation, since a varying scale parameter of a Gamma distribution is shown to generate such a behavior. In Section 3.1.4 we have shown that this argument is misleading, as the scaling parameter is already

heavy-tailed in this case.

Of particular interest to this work is Wilson and Toumi (2005), since they model the budget equation of humidity in a stochastic way in order to infer the distribution of extreme precipitation. The distribution obtained by Wilson and Toumi (2005) is asymptotically light-tailed, but for typical sample sizes used in hydrology or the atmospheric sciences it is better approximated by a heavy-tailed distribution. The authors identify the variability of precipitation efficiency as an important contribution to the extreme distribution of precipitation, while Singleton and Toumi (2013) claim that precipitation efficiency is 100% when extreme precipitation is observed. We describe the Wilson and Toumi (2005) model in more detail in Section 3.3.1.

Another issue of interest is the distribution of precipitation subject to temporal or spatial aggregation (Koutsoyiannis et al., 1998; Coles and Tawn, 1996; Haerter et al., 2010) and the related question whether precipitation shows a universal scaling behavior (Tessier et al., 1993; Hense and Friederichs, 2006). Haerter et al. (2010) studied the distribution of precipitation as a function of temperature and temporal aggregation. For short duration (5min) the extreme precipitation distribution is well-approximated by a power law, which would indicate a scale-free behavior (Haerter et al., 2010). For longer duration exponential decay is observed. The comparison of various averaging periods allows to extrapolate the value to estimate an instantaneous precipitation rate. Koutsoyiannis et al. (1998) investigated the relation of intensity, duration and frequency of precipitation events (IDF). These relations are important for the estimation of the distribution of extreme precipitation amounts and are therefore of interest to the design of buildings. For various potential distributions of precipitation Koutsoyiannis et al. (1998) derived the associated IDF curves.

Coles and Tawn (1996) used a different and more flexible approach to model spatial dependence of precipitation extremes. Using EVT they describe both the marginal distribution and spatial dependency of precipitation extremes. Similar to IDF curves this approach is used to infer the distribution of the averaged precipitation amount in space (Coles and Tawn, 1996). Max-stable processes have been used to describe and simulate spatial precipitation extremes (Gomes et al., 2016) and to provide a class of processes that allow a continuous description of precipitation extremes in space.

Multiplicative and multifractal models are a particularly interesting class of models. Motivated by the scale-free properties of turbulence (Tessier et al., 1993) and their interaction with precipitation these models describe precipitation as the product of a number of random variables, where the number increases with spa-

tial resolution (Tessier et al., 1993; Over and Gupta, 1996). These models have been used to construct IDF curves and to predict precipitation (Langousis and Veneziano, 2007). Based on such models, Veneziano et al. (2009) put into question the validity of asymptotic approximations made in EVT modeling precipitation extremes. This is consistent with Wilson and Toumi (2005) who show that the product of Gaussian variables are approximated unsatisfactorily by their light-tailed limit.

Similar to Wilson and Toumi (2005)'s approach and the above mentioned fractal models there is a literature trying to explain the extremal behavior of precipitation or other atmospheric variables by physically motivated models. Sardeshmukh and Sura (2009) derived a linear stochastic model, which includes correlated and multiplicative noise, from non-linear dynamical systems. These models exhibit heavy tails and explain an observed relation of skewness and kurtosis. Interestingly, they are not unrelated to ARCH-processes (Engle, 1982), which is a highly-useful class for the modeling of financial time series. These processes generate heavy tails (Kesten, 1973) by temporal spikes of the variance known as heteroscedasticity. To the best of our knowledge, it is not known if atmospheric process are heteroscedastic and whether the intermittent behavior of atmospheric motions triggers heavy tails or heteroscedasticity.

3.3 Stochastic models for precipitation extremes

3.3.1 The Wilson and Toumi (2005) model

Wilson and Toumi (2005) propose a probability distribution for precipitation extremes based on the dynamics of moisture transport. The atmosphere is modeled in two layers, where the lower layer contains the moisture and where moisture convergence is exclusively present (Reed and Recker, 1971). Wilson and Toumi (2005) consider the following integral as humidity budget equation. The precipitation rate $\widetilde{R}$ is given by

$$\widetilde{R} = -\int_0^{z_m} \overline{\nabla \cdot (q\rho U)} dz = \int_0^{z_m} \overline{\frac{\partial (q\rho w)}{\partial z}} dz = \overline{(q\rho w)}_{z_m}, \tag{22}$$

where the overbar denotes temporal averaging, q specific humidity, ρ specific density, U the horizontal wind field and w the vertical wind speed, z_m the height of the top of the moist layer. This equation was derived in Stevens and Lindzen (1978) under the assumption of vertically constant q and the anelastic continuity equation $\nabla \cdot (\rho U) = 0$, where U is the 3-dimensional wind field. For more general conditions implying (22) see Stevens and Lindzen (1978). In (22) it is assumed that the complete moisture that ascends at the top of the moist layer is precipitated. Wilson

and Toumi (2005) consider the possibility of temporal storage of moisture in the dry layer and therefore introduce the precipitation efficiency κ. In this model it describes the percentage of moisture, that is precipitated, from the total water ascending at the top of the moist layer. The product of vertical wind and the density equals the mass flux $m = \rho w$. Using the precipitation efficiency κ, Wilson and Toumi (2005) obtain the following model for the precipitation rate R

$$R = \overline{(\kappa m q)}_{z_m}. \tag{23}$$

Motivated by this physical derivation, Wilson and Toumi (2005) model the precipitation rate R as the product of three independent Gaussian variables. The product of three Gaussian variables lies in the domain of attraction of the Gumbel distribution and is hence light-tailed (Wilson and Toumi, 2005). This means that the maximum of a sample of the distribution of product of three Gaussian variables will converge up to affine transformation to a Gumbel distribution. Yet this convergence is very slow (Furrer and Katz, 2008) and for data length typically available in meteorology it is no satisfactory approximation. A maximum from a finite sample of a product of three Gaussian variables is well approximated by a Fréchet distribution, it *appears* to be heavy-tailed. The distribution of R in (23) can be very well approximated by the stretched exponential distribution (Wilson and Toumi, 2005)

$$P\left(R < x\right) = 1 - \exp\left(-\left(\frac{x}{R_0}\right)^c\right), \tag{24}$$

where R_0 is a scale parameter and the shape parameter $c = 2/3$. Wilson and Toumi (2005) show that equation (24) is consistent with observational data. The authors argue that the precipitation observations are inconsistent with the probability distribution of the product of two Gaussian variables, which suggests that the precipitation efficiency is essential in explaining the characteristics of heavy precipitation.

3.3.2 Derivation of a simplified moisture budget

Similar to Wilson and Toumi (2005) we introduce a model for precipitation extremes based on the budget equation for humidity. It follows a passive tracer transport equation

$$\int_0^H \frac{\partial}{\partial t} q + \nabla \cdot (Uq)\, dz = E - \widetilde{P}, \tag{25}$$

where H is the upper boundary of the moisture containing layer of the troposphere, q is the absolute humidity, U the horizontal wind vector, E the evaporation and $\widetilde{P}$ precipitation.

Wilson and Toumi (2005) suggest that multiplication of random variables intensifies the preasymptotic extremal behavior, such that it is plausible to assume that the term $\frac{\partial}{\partial t}q$ is less important than the other terms in (25), we thus neglect it.

We use $\nabla \cdot (Uq) = q\nabla \cdot U + U \cdot \nabla q$, since this will allow to use the methods of Chapter 2 later on. Decomposing the variables U and ∇q in its vertical mean $\overline{U}, \overline{\nabla q}$ and a vertical anomaly $U', (\nabla q)'$ we see that

$$\int_0^H U \cdot \nabla q dz = H\overline{U} \cdot \overline{\nabla q} + \int_0^H U' \cdot (\nabla q)' \, dz.$$

Up to integration the term imposed by the vertical anomaly is similar to the vertically constant term. If the vertical anomaly $U' (\nabla q)'$ fulfills sufficiently fast strong mixing the anomaly term is well approximated by a Gaussian variable (Rosenblatt, 1956) and has thus negligible influence on the extremal behavior. A similar consideration applies for $q\nabla \cdot U$. Neglecting the terms induced by the vertical anomalies of $U, \nabla \cdot U, q, \nabla q$ and the factor H we obtain a simplified two-dimensional budget equation

$$\widetilde{P} = E - U \cdot \nabla q - q\nabla \cdot U.$$

In the following we will call $q\nabla \cdot U$ divergence term and $U \cdot \nabla q$ advection term. Before we introduce stochastic processes that model the terms of the simplified budget equation, we discuss thresholding due to the Clausius-Clapeyron threshold and precipitation efficiency. The Clausius-Clapeyron relation describes saturation water vapor as a function of temperature and pressure. A good approximation is an increase by 7% per degree Celsius. A parcel of moist air exceeding the saturation water vapor pressure generates cloud water proportional to the excess of the threshold. Thus the Clausius-Clapeyron relation imposes a thresholding of the humidity field. Thus the actual precipitation rate is given by

$$P = \left(\widetilde{P} - T\right)_+ = \left(-U \cdot \nabla q - q\nabla \cdot U + E - T\right)_+, \tag{26}$$

where $(x)_+ = \max(0, x)$ and T is the Clausius-Clapeyron threshold.

Precipitation efficiency is the ratio of precipitated water and the total water in a column of the atmosphere. Precipitation efficiency is accounted for in Wilson and Toumi (2005) by a multiplier to the excess humidity, as explained in detail in Section 3.3.1. The parameterization of the transition of cloud droplets to precipitation droplets of Kessler (1969) suggests that the precipitation droplets are proportional to cloud droplets subject to a further thresholding. On the contrary the parameterization in Seifert and Beheng (2001) suggests a quadratic increase

of precipitation droplets with humidity exceeding the Clausius-Clapeyron threshold and therefore an increase of precipitation efficiency in extreme events. While the first parametrization could be modeled by increasing the Clausius-Clapeyron thresholding in (26), the second would suggest to square P. As the physical validity of the parameterizations is not clear especially for extreme events we model the precipitation droplets as proportional to cloud droplets, which is consistent with Kessler (1969).

3.3.3 Stochastic models for precipitation fields

Based on Section 3.3.2 we introduce here a stochastic models for precipitation fields. Generalizing Wilson and Toumi (2005) we introduce a model that describes the spatial distribution of precipitation. Further, our models allow for correlation of various terms included in the budget equation and we do not exclusively rely on the assumption of marginal Gaussianity of the included terms.

We use a zero-mean Gaussian process $\left((\psi_s, \chi_s, q_s)\,, s \in \mathbb{R}^2\right)$ with covariance function

$$\begin{aligned} &\operatorname{Cov}\left(\begin{pmatrix} \psi_s, & \chi_s, & q_s \end{pmatrix}^T, \begin{pmatrix} \psi_t, & \chi_t, & q_t \end{pmatrix}^T\right) \\ &= \begin{pmatrix} \sigma_\psi^2 & \rho_{\psi,\chi}\sigma_\psi\sigma_\chi & \rho_{\psi,q}\sigma_\psi\sigma_q \\ \rho_{\psi,\chi}\sigma_\psi\sigma_\chi & \sigma_\chi^2 & \rho_{\chi,q}\sigma_\chi\sigma_q \\ \rho_{\psi,q}\sigma_\psi\sigma_q & \rho_{\chi,q}\sigma_\chi\sigma_q & \sigma_q^2 \end{pmatrix} M\left(\|b(t-s)\|_2, \nu\right), \end{aligned} \tag{27}$$

where $M(\cdot|\nu)$ is the Matérn covariance function with smoothness parameter ν, $\sigma_\psi^2, \sigma_\chi^2, \sigma_q^2$ the variances and correlations $\rho_{\psi,\chi}, \rho_{\psi,q}, \rho_{\chi,q}$ of ψ, χ and q, $b \in \mathbb{R}_+$ the scale-parameter and $s, t \in \mathbb{R}^2$ two arbitrary locations. Using $U_s = \nabla \times \psi_s + \nabla\chi_s$ and $\nabla \cdot U_s = \Delta\chi_s$ we model $\left((q_s, \nabla q_s, U_s, \nabla \cdot U_s)\,, s \in \mathbb{R}^2\right)$ as a zero-mean Gaussian process with covariance function

$$C(s,t) = \mathbb{E}\left[(q_s, \nabla q_s, -\nabla \times \psi_s + \nabla\chi_s, \Delta\chi_s)^T\,(q_t, \nabla q_t, -\nabla \times \psi_t + \nabla\chi_t, \Delta\chi_t)\right]. \tag{28}$$

In Chapter 2 (in particular Section 2.2) we extensively study such processes and show how to derive (28) from (27). Although $q_s, \nabla q_s$ is not included in Chapter 2 it is straightforward to generalize. Hence we obtain from (25) spatial precipitation fields

$$P_s = \left(-U_s \cdot \nabla q_s - q_s \nabla \cdot U_s + E - T\right)_+ \quad s \in \mathbb{R}^2. \tag{29}$$

In the following we will call model (29) Gaussian model (GM).

We consider two further variations of our model that can be easily derived from GM. The distribution of q is multivariate log-normal such that the gradient field of

humidity has the following simple property, $\nabla q = \nabla \exp(\widetilde{q}) = \exp(\widetilde{q})\nabla\widetilde{q} = q\nabla\widetilde{q}$, where $\widetilde{q}$ is a latent Gaussian process. Let the process $\left((\widetilde{q}_s, \nabla\widetilde{q}_s, U_s, \nabla \cdot U_s), s \in \mathbb{R}^2\right)$ be a zero-mean Gaussian process with covariance function (28). For this model we obtain the following stochastic process

$$P_s = \left(-\exp(\widetilde{q}_s)\nabla\widetilde{q}_s \cdot U_s - \exp(\widetilde{q}_s)\nabla \cdot U_s + E - T\right)_+ \quad s \in \mathbb{R}^2. \tag{30}$$

The model will be called log-normal model (LNM). A further variant of GM can be obtained by assuming that χ and ψ follow a multivariate Student-t distribution. A multivariate Student-t field with $d \in \mathbb{N}$ degrees of freedom is obtained by a Gaussian field that is divided by the variable $\sqrt{\chi_d^2/d}$, where χ_d^2 is a χ^2 distribution with d degrees of freedom. As the denominator of the Student-t field is constant we obtain a very simple formula for the derivatives of such processes: $\nabla\psi = \nabla\left(\frac{\widetilde{\psi}}{\sqrt{\chi_d^2/d}}\right) = \frac{\nabla\widetilde{\psi}}{\sqrt{\chi_d^2/d}}$, where $\widetilde{\psi}$ is a Gaussian process. The spatial derivative of a Student-t process is Student-t distributed with the same degrees of freedom. Using a zero-mean Gaussian process $\left((q_s, \nabla q_s, U_s, \nabla \cdot U_s), s \in \mathbb{R}^2\right)$ with covariance function (28) we obtain the following model

$$P_s = \left(\frac{-U_s \cdot \nabla q_s - q_s \nabla \cdot U_s}{\sqrt{\chi_d^2/d}} + E - T\right)_+ \quad s \in \mathbb{R}^2, \tag{31}$$

which will be called Student-t model (StM) in the following.

In the following sections we will study the extremal behavior of these models. We will discuss the asymptotic properties of the processes, but more often we will be interested in the preasymptotic extremal behavior. A well-known way to describe the preasymptotic shape is to find parameter γ_n such that G_{γ_n} is close to the distribution of M_n (Embrechts et al., 1997). For many distributions the sequence γ_n converges slowly to the true asymptotic shape. Hence, either theoretical estimates or maximum-likelihood estimates of a sample will be used to describe the preasymptotic behavior of distributions. A similar way would be to fit a GPD to the values of a sample exceeding a threshold T. Here, T quantifies the transition from the preasymptotic to the asymptotic regime, similar to n in the first approach.

Except when noted otherwise all results in the following sections have been obtained for the following parameters in (27). $\sigma_\psi = \sigma_\chi = \sigma_q = 1, \rho_{\psi,\chi} = \rho_{\psi,q} = \rho_{\chi,q} = 0, \nu = 2.5$ and $b = 1$ and for StM $d = 6$. The threshold T in (29)-(31) has been set to the 0.7-quantile of the humidity distribution.

3.4 Results

3.4.1 Kinematic properties of the moisture budget

We start by deriving conditions, which imply that the advection and divergence term in GM, LNM and StM are uncorrelated. The covariance function (27) is stationary and isotropic. This implies, for example, that there is a function f such that $f(\|t-s\|) = \mathrm{Cov}(q_s, \chi_t)$, where $\|\cdot\|$ is a norm. Hence, the covariance is symmetric to zero. Further the covariance is four times differentiable whenever $\nu > 2$. The symmetry and differentiability implies that $\mathrm{Cov}(q_s, \nabla\chi_s) = 0$. Similarly we can derive $\mathrm{Cov}(q_s, U_s) = \mathrm{Cov}(\Delta\chi_s, U_s) = \mathrm{Cov}(\nabla q_s, q_s) = \mathrm{Cov}(\nabla q_s, \Delta\chi_s) = 0$. This shows that in GM the advection term and divergence term are independent. In LNM they are uncorrelated. In StM they are uncorrelated whenever the correlation exists, which is equivalent to $d > 2$.

For some of the parameters in (27) we can analytically deduce the influence on the extremal behavior of P_s. If the fields χ, ψ and q are scaled by the same factor $b \in \mathbb{R}_+$ like $\widetilde{X}_s = X_{bs}$, the advection term and the divergence term are scaled by b^2 and the marginal distribution of the transport of humidity in the model (29)-(31) is simply scaled by b^2. Since the terms E and T are independent of that scaling, the marginal distribution of P_s is slightly changed. But as these parameters have very simple deterministic additive structure the extremal properties of P_s are unaffected. Further, the scale parameter has the obvious influence on the spatial structure of P_s.

If the variance of q is multiplied $\widetilde{\sigma}_q^2 = a\sigma_q^2$ and the terms $\widetilde{\sigma}_\chi^2 = \sigma_\chi^2/a$ and $\widetilde{\sigma}_\psi^2 = \sigma_\psi^2/a$ for $a \in \mathbb{R}_+$, the distribution of P_s in models (29)-(31) is obviously unaffected. Multiplication of the variance of q by a has the same influence on the marginal distribution of P_s as a multiplication of the scale by $\sqrt{a}$.

3.4.2 Asymptotic shape and preasymptotic extremal behavior

We start by deriving relations for the asymptotic extremal behavior for GM, LNM and StM. By the methods of Section 3.1.4 it is clear, that all moments of P in GM and LNM exist and that this implies the following statement. If $P \in D(G_\gamma)$, then $\gamma \leq 0$ and P is hence light-tailed.

Using the methods of Section 3.1.4 we see that the α moment of StM is finite whenever $\alpha < 1/d$, where d is the degrees of freedom. Hence, if $P \in D(G_\gamma)$, then $\gamma = 1/d$.

Further we study the preasymptotic extremal behavior for GM, LNM and StM. Gomes and De Haan (1999) show that for a wide class of distribution functions

preasymptotic approximations for the shape parameter for $M_n = \max(X_1, \ldots, X_n)$ are provided by

$$\gamma_n = -\frac{(1 - F(x_n))\, f'(x)}{f(x_n)^2} - 1, \tag{32}$$

where $x_n = F^{-1}\left(1 - \frac{1}{n}\right)$. This means G_{γ_n} is close to the distributions of M_n (for details be refereed to Gomes and De Haan (1999)). A good intuition of this result may be obtained from Theorem 4. The asymptotic expression of this theorem is evaluated for finite values to obtain γ_n.

We will apply this preasymptotic relation to the model of Wilson and Toumi (2005), GM, LNM and StM. The fundamental probability distribution for precipitation extremes derived in Wilson and Toumi (2005) is the stretched-exponential distribution

$$P(P > r) = \exp\left(-r^c\right),$$

where $c = 2/3$. Using (34) Furrer and Katz (2008) obtain for the stretched-exponential distribution

$$\gamma_n = \frac{1 - c}{c \ln n}. \tag{33}$$

Figure 3.1 shows the behavior of preasymptotic values of γ_n for various distributions. For the stretched-exponential distribution with $c = 2/3$ it reduces very slowly and the asymptotic shape is not relevant. In the following sections we will show that the marginal distribution of the GM is close to the product of two Gaussian variables. This distribution is approximatively close to the stretched exponential distribution with $c = 1$ (Frisch and Sornette, 1997). The approximation of Furrer and Katz (2008) suggests that this distribution is not only asymptotically but also for finite-sample light-tailed. In Section 3.4.3 we will see that we obtain a slightly positive shape parameter when computing maximum-likelihood estimates of a GPD with a sample of GM.

The marginal distribution of the LNM has slightly larger preasymptotic shape parameter than the log-normal distribution. For the log-normal distribution it is possible to derive similar preasymptotic estimates of the shape parameter. Setting $x_n = F^{-1}(1 - 1/n) \sim \exp\left(\Phi^{-1}\left(1 - \frac{1}{n}\right)\right)$ to the typical size of a maximum over n realizations we obtain

$$\gamma(x_n) = -\frac{(1 - F(x_n))\, f'(x)}{f(x_n)^2} - 1 = \frac{(1 - \Phi(\ln x_n))\,(\ln x_n + 1)}{\varphi(\ln x_n)} - 1. \tag{34}$$

Figure 3.1 shows that the shape parameter for the log-normal distribution reduces even slower than in the stretched-exponential case. For example, we obtain $\gamma\left(x_{1000}\right) \approx 0.2$.

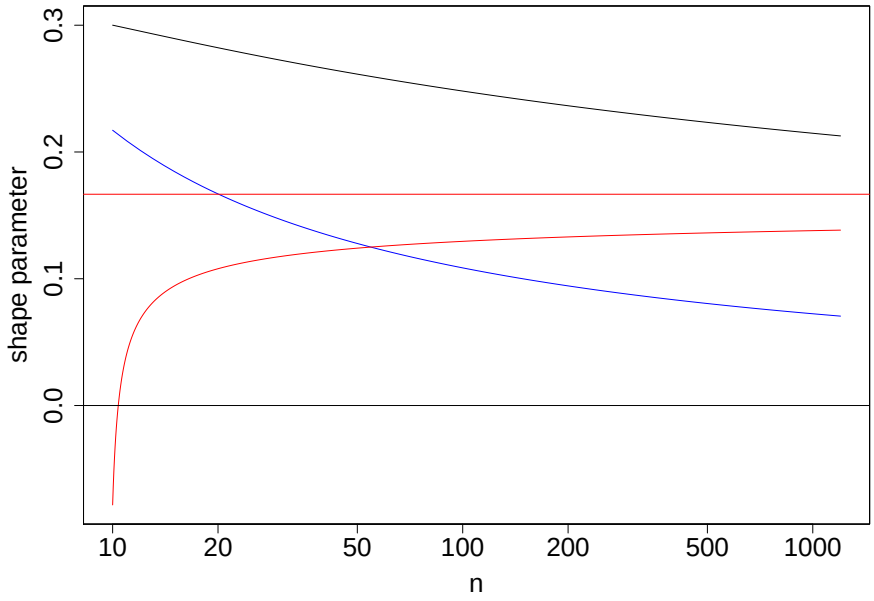

Figure 3.1: Analytic approximation for the shape parameter for the maximum over n realizations of a sample. The stretched-exponential distribution with $c = 2/3$ equation (33)(blue line), the log-normal distribution equation (34) (black line) and the Student-t distribution with $d = 6$ degrees of freedom equation (35) (red line) are shown. The horizontal black line indicates the asymptotic shape parameter of the stretched-exponential and log-normal distributions and the horizontal red line the asymptotic shape of the Student-t distribution.

The asymptotic shape of the StM is similar to a Student-t random variable, since the Student-t variable is heavy-tailed and the other Gaussian variables are light-tailed. The shape parameter of a Student-t random variable is $\gamma = 1/d$ (De Haan and Ferreira, 2006). For $d = 1$ the shape is maximal $\gamma = 1$, and for $d \to \infty$ it converges to zero, and the StM is identical to the GM. For a Student-t variable with d degrees of freedom we obtain setting $x_n = F^{-1}(1 - 1/n)$, where F is the corresponding CDF

$$\gamma(x_n) = -\frac{(1 - F(x_n))\, f'(x_n)}{f(x_n)^2} - 1 = \frac{-x_n\,(1 + 1/d)}{n\left(1 + \frac{x_n^2}{d}\right)^{-(d-1)/2}} \frac{\sqrt{d\pi}\Gamma\,(d/2)}{\Gamma\,((d+1)/2)} - 1, \quad (35)$$

where Γ is the Gamma function. Figure 3.1 shows that $\gamma\,(x_n)$ increases monotonically and relatively fast to its limit $\gamma = 1/6$. Even for a maximum over 1000 realizations the shape of the log-normal distribution is higher than the one of a Student-t, although the former is light-tailed and the latter heavy-tailed. Careful

Table 1: Asymptotic domain of attraction and preasymptotic extremal behavior of the models GM, LNM, StM with d degrees of freedom and Wilson and Toumi (2005). The claims in italics rely on the assumption that the model is in a domain of attraction of a GEV.

	GM	LNM	StM	Wilson and Toumi (2005)
Preasymptotic	light-tailed	heavy-tailed	heavy-tailed	heavy-tailed
Asymptotic	*light-tailed*	*light-tailed*	*heavy-tailed with* $\gamma = 1/d$	light-tailed

checking whether asymptotic approximations are valid is essential for the extrapolation of distribution functions.

For a better overview the asymptotic and preasymptotic extremal behavior of the model in Wilson and Toumi (2005), GM, LNM and StM are summarized in Table 1.

3.4.3 Correlation parameter

In this section we investigate the effect of the correlation parameters $\rho_{\chi,\psi}, \rho_{\chi,q}, \rho_{\chi,q}$ of (27) on the shape of the tail of P_s in models (29)-(31). We will call the parameters $\rho_{\chi,\psi}, \rho_{\chi,q}, \rho_{\chi,q}$ correlations although they are not necessarily identical to the correlation for LNM and the StM. For example, if $\rho_{\chi,q} = 1$ we have for LNM $\mathrm{Cor}(\chi_s, q_s) = \mathrm{Cor}(X, \exp(X)) \approx 0.76$, where X is a standard normal random variable.

The term in $U \cdot \nabla q + q\Delta\chi$ in (26) is given by

$$\frac{\partial}{\partial e_1} q \left(-\frac{\partial}{\partial e_2}\psi + \frac{\partial}{\partial e_1}\chi \right) + \frac{\partial}{\partial e_2} q \left(\frac{\partial}{\partial e_1}\psi + \frac{\partial}{\partial e_2}\chi \right) + q\Delta\chi. \tag{36}$$

For nonzero correlations $\rho_{q,\chi}$ the divergence term and the terms $\frac{\partial}{\partial e_i} q \frac{\partial}{\partial e_i}\chi$ for $i = 1, 2$ are products of correlated variables for the models (29)-(31). In a preasymptotic sense, extreme values of one of the variable are more likely to appear if the other variable is extreme. Yet, asymptotically they are independent whenever $|\rho_{\chi,q}| < 1$ in the Gaussian case (Sibuya, 1960). Since the terms $\frac{\partial}{\partial e_i} q_s$, $\frac{\partial}{\partial e_j}\psi_s$ for $i \neq j$ in (36) are uncorrelated for any value of the parameter $\rho_{\psi,q}$, this parameter has no direct influence on the products in (36). However, it induces a correlation of the two summands of the advection term (36).

Figure 3.2 shows maximum-likelihood estimates of the GPD shape parameter fitted to the upper 5% of a sample of 10^4 precipitation events. For Figure 3.2 a)

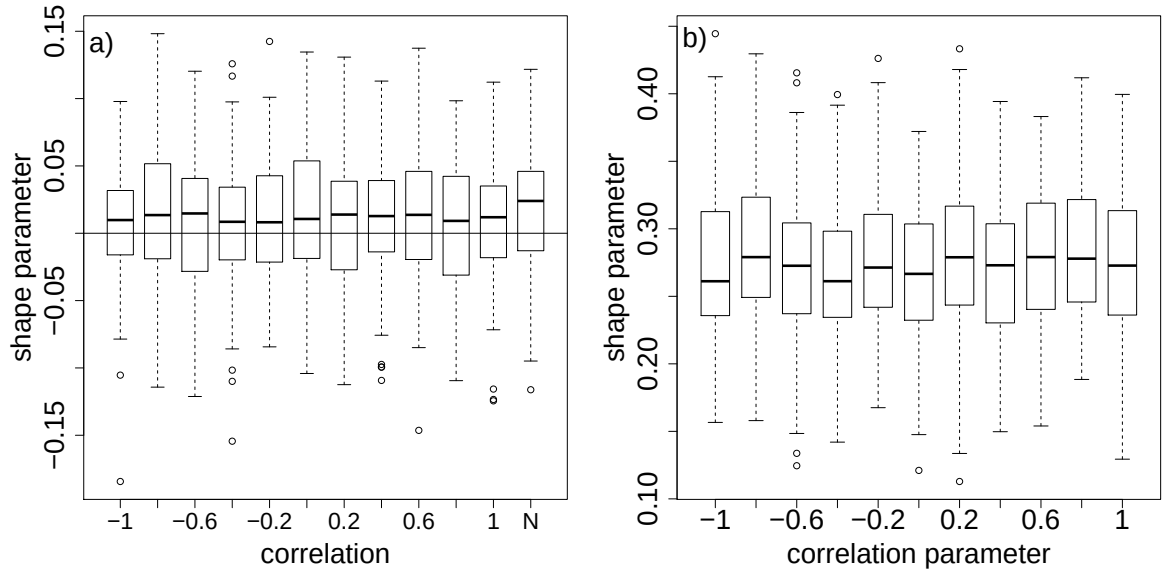

Figure 3.2: 100 replicates of maximum-likelihood estimates of the shape parameter GPD for a sample of $n = 10^4$ precipitation events obtained by considering the upper 5% of the data. a) The samples have been obtained by the GM for varying parameter $\rho_{\chi,q}$. For the very right box (N) the samples have been generated as product of two independent standard normal Gaussian variables. b) Shows LNM for varying parameter $\rho_{\chi,q}$.

the samples have been simulated as a product of two independent standard normal variables or with GM for varying values of $\rho_{\chi,q}$. For all distributions we observe similar distributions of the shape parameter. Hence, the correlation parameter has no significant influence on the maximum-likelihood estimates of a GPD and has thus no substantial influence on the shape of precipitation extremes in the GM. This result is consistent with the asymptotic properties of a product of two Gaussian variables. If the correlation equals one, the product of two Gaussian variables has a χ^2_1 distribution, which has shape parameter $\gamma = 0$ (Beirlant et al., 2004). For independent Gaussian variables the product has also shape parameter $\gamma = 0$ (Wilson and Toumi, 2005).

For varying correlation parameter $\rho_{\psi,q}$ we estimated the shape parameter from the upper 5% of the marginal distribution of the Gaussian. We observed no influence of the parameter (not shown). Similar results were obtained for the correlation parameter $\rho_{\chi,\psi}$ (not shown).

In order to understand the behavior of GM, we investigate the behavior of products of two random variables as a function of their correlation. Figure 3.3 a) shows

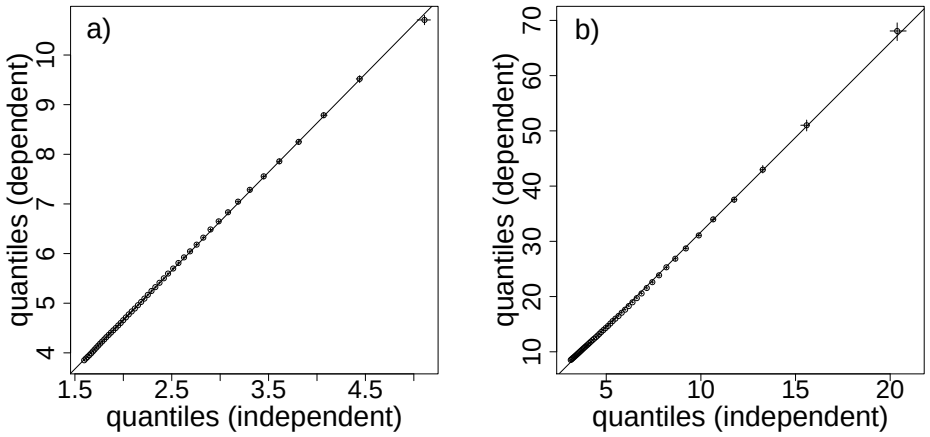

Figure 3.3: Tail-quantiles $q = 0.95 + i/1000$ for $i = 0, \ldots, 49$ of products of independent against products of perfectly correlated variables. The solid line is a regression line and the crosses show bootstrapped 0.95 confidence intervals. a) product of two Gaussian, b) product of Gaussian and log-normal.

quantiles from the upper 5% tail estimated from a sample of length $n = 10^6$ for a product of independent Gaussian variables and for a product of Gaussian variables with correlation 1. The uncertainty was assessed by a bootstrap and is negligible. The linear behavior indicated by the regression line shows a good accordance in tail behavior. The asymptotic equivalence of the two distributions is a good approximation for the upper 5% of the data. Similar properties can be seen from estimating the shape parameter from the upper 5% of a sample from a product of two Gaussian variables with varying correlation, which is shown in Figure 3.4a). There is no influence of the correlation to the extremal behavior of the process. This explains why the GM is insensitive to changes in the correlation of the quantities ψ, χ and q.

Figure 3.2 b) shows maximum-likelihood estimates of the GPD shape parameter fitted to the tail of LNM. This model has an preasymptotic extremal behavior clearly different from GM. The median of the estimated shape parameter lies between 0.2 and 0.3 and differs markedly from the true asymptotic value of $\gamma = 0$. The distribution of the shape parameter is insensitive to the correlation parameter $\rho_{\chi,q}$.

For the product of a Gaussian and a log-normal variable we see slight deviations in the quantile plot in Figure 3.3 b). This is reflected in Figure 3.4 b), where GPD shape parameter for the tail of $X \exp(Y)$ is estimated for varying correlation of the Gaussian variables X and Y. The shape parameter differs markedly from the

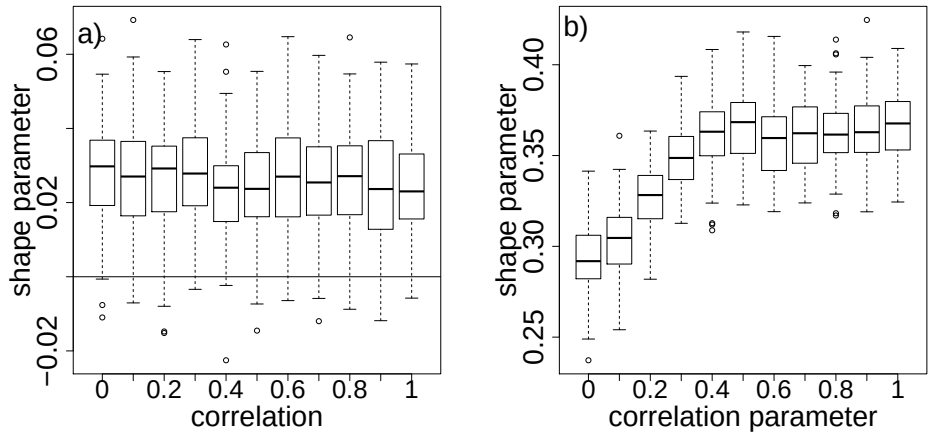

Figure 3.4: Maximum-likelihood estimates of the shape parameter of a GPD obtained from the upper 5% from a sample of length $n = 10^5$. The samples have been generated by a product of variables with varying correlation parameter. The samples are a) product of Gaussian variables, b) product of Gaussian and log-normal variable. The horizontal line in a) indicates the true asymptotic shape parameter.

asymptotic shape parameter $\gamma = 0$ (Beirlant et al., 2004). For $\mathrm{Cor}\,(X, \exp(Y)) = 0$ the median of the shape parameter is slightly below 0.3. If the correlation parameter is increased to 0.5, the shape parameter increases to ≈ 0.37. A further raise of the correlation parameter shows no influence. The differences of the shape parameter may seem negligible, but an examination of the return values shows they are not. For zero mean and unit variance a 50 year return value for the independent product has an approximate return value of 10 years for the perfectly correlated product.

In Figure 3.2b) we saw that the correlation parameter has no influence on the GPD shape parameter estimated for P in LNM, although Figure 3.4 shows that in principle correlation for products of normal and log-normal variables could influence the shape. A plausible explanation for the irrelevance of the correlation parameter is that the advection term in (30) consists of the product of three variables, while the divergence term consists of two variables only. The main generator of extremes is therefore the advection term. As argued in Section 3.4.1 the latent humidity field $\widetilde{q}_s$ is independent from the wind field U_s and $\nabla\widetilde{q}_s$ for all $s \in \mathbb{R}^2$ in any isotropic and stationary covariance model. Hence, the correlation parameter $\rho_{\chi,q}$ has no influence on the dependence structure of $\exp(\widetilde{q}_s), \nabla\widetilde{q}_s$ and $\exp(\widetilde{q}_s), U_s$. This explains why this parameter has no influence on the preasymptotic extremal behavior of LNM. Similar arguments are valid for the correlations $\rho_{\chi,\psi}$ and $\rho_{\psi,\chi}$ in LNM.

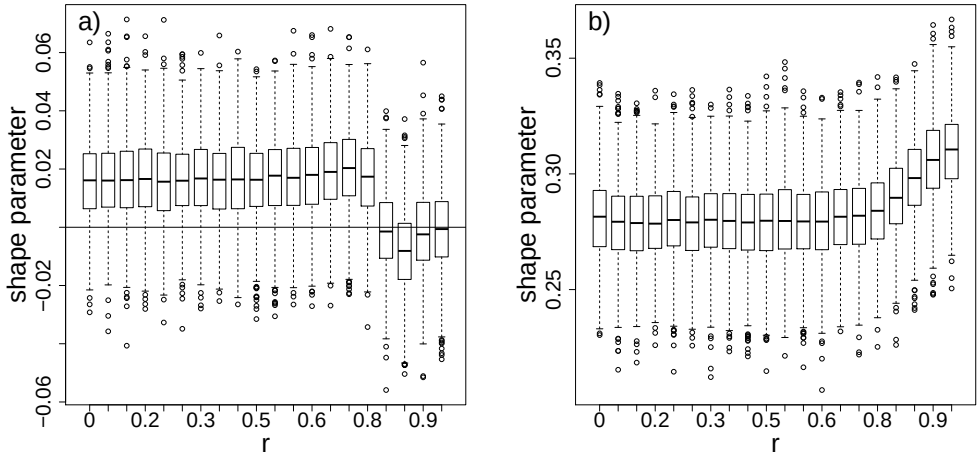

Figure 3.5: 1000 maximum-likelihood estimates of the shape parameter of a GPD obtained from the upper 5% of a sample of length 10^5. a) The data is simulated from the GM. b) The data is generated by the LNM. For both plots the parameter σ_ψ is proportional to r and σ_χ to $(1-r)$.

So far we have not discussed the StM. It is obtained from GM by scaling the moisture flux convergence with an independent scale variable. Hence, it is also insensitive to changes of the correlation parameters $\rho_{\chi,q}, \rho_{\psi,\chi}, \rho_{\psi,q}$.

3.4.4 Precipitation extremes in rotational and divergent flow

Changing the ratio of the variances of streamfunction and velocity potential has very little influence on the distribution of precipitation in the GM. This distribution is very close to the product of two normal distributions. In a qq-plot with sufficiently high sample size there is no visible deviation of the two distributions both for purely rotational and purely divergent flow (not shown). Both rotational and divergent flow generate the same type of extremes in the GM.

Figure 3.5 depicts the behavior of the shape parameter of a GPD estimated from a sample of length $n = 10^5$ subject to changes of the ratio of the divergent and rotational wind components. The variance of the rotational wind component is proportional to r and the divergent component is proportional to $1-r$. In Figure 3.5 a) the shape parameter estimates have been obtained from the upper 5% of the data generated from GM. We observe a slightly higher shape parameter for divergent flow and a reduction for non-divergent flow. The reduction is not monotone and has a minimum close to $r = 0.85$. An explanation for the non-monotone reduction of the shape parameter is that the divergence term in the transport equation (29) has a

higher variance for the considered parameters. The variance of the divergence term is proportional to σ_χ. A similar behavior of the shape parameter can be generated by the following model.

$$P = rX_1X_2 + 5(1-r)X_3X_4,$$

where $X_i, i = 1, \ldots, 4$ are standard normal independent variables. For the value $r \approx 0.85$ we obtain smaller shape parameters than for all others. For this value both summands have similar variance and mitigate each other. Intuitively this can be understood by the central limit theorem. Informally it states that sums of independent random variables are closer to the normal distribution than the summands.

For the LNM we see in Figure 3.5b) a slight increase in the shape parameter for purely rotational flow. The advection term consists of the product of three parameters and has therefore a more extreme finite sample behavior than the divergence term in equation (30). If $r \to 1$ the divergence term becomes negligible and the extremal behavior is no longer mitigated by it. This is similar to the behavior of sums of independent random variables. The sums converge, under appropriate conditions, to normal distributions due to the central limit theorem and are hence asymptotically light-tailed.

3.4.5 Spatial distribution of precipitation extremes

In order to study the spatial structure of the fields we set $b = 1/40$ in (27) and consider fields of size 500×500 with unit grid point distance. Figure 3.6a),c) depict a realization of P in GM and LNM. There are large areas with no precipitation and clusters of precipitation. The clusters vary strongly in intensity, while the size of the clusters is relatively homogeneous. The intensity of the clusters does not seem to have an influence on the size of the clusters. Therefore, we observe regions with very high gradient of the precipitation intensity, as for example close to the intense cluster in the upper left corner of Figure 3.6a). The range of precipitation intensity is much larger in LNM. Both precipitation fields exhibit very rough properties. As $\nu = 2.5$ in (27) neither the divergence field $\nabla \cdot U$ nor the precipitation field is differentiable for both GM and LNM. Although the clustering of precipitation events is a realistic feature, the fields differ from observed precipitation fields. Often precipitation is associated with fronts producing clusters in a line and and orientation that deviates from the isotropy of our models. Further, orographic effects cannot be modeled in our approach, which is another factor that leads to non-stationarity of real precipitation fields.

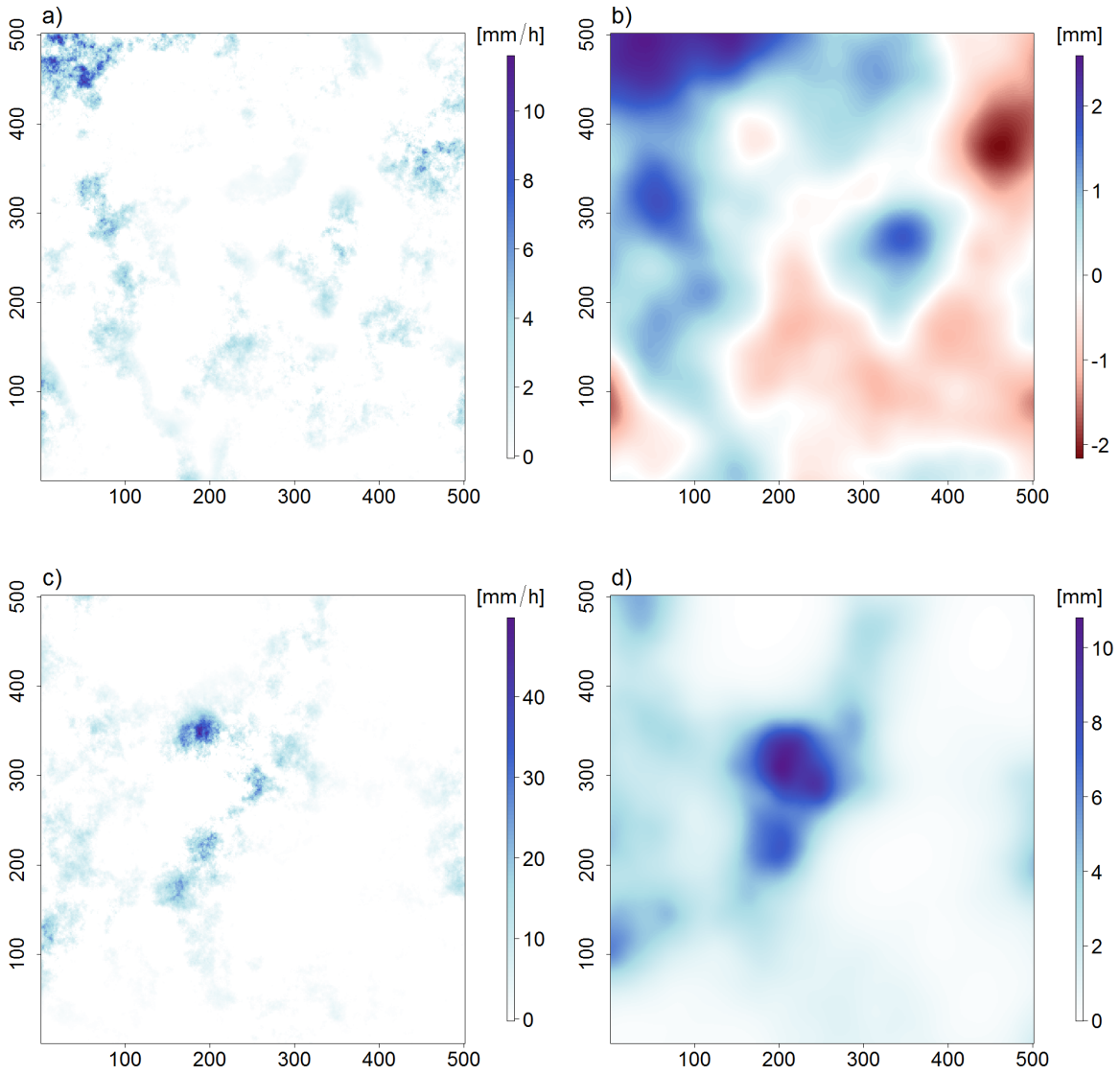

Figure 3.6: a) A precipitation field on a 500×500 grid, obtained from GM. Up to scale in z-direction the StM has the same distribution. b) The associated humidity field q_s from the GM. c) Precipitation field obtained from the log-normal model and d) associated humidity field.

Figure 3.6b),d) shows the associated humidity field q_s. The humidity field is smoother than the precipitation field and has a large spatial scale. Surprisingly, a large proportion of the precipitation cells of the GM are located in a region where the humidity field attains low values. Since the humidity field is a zero-mean Gaussian process, a large proportion of the field is negative. Obviously, this is an unrealistic feature of the model. Still, such fields could be a good approximation for model

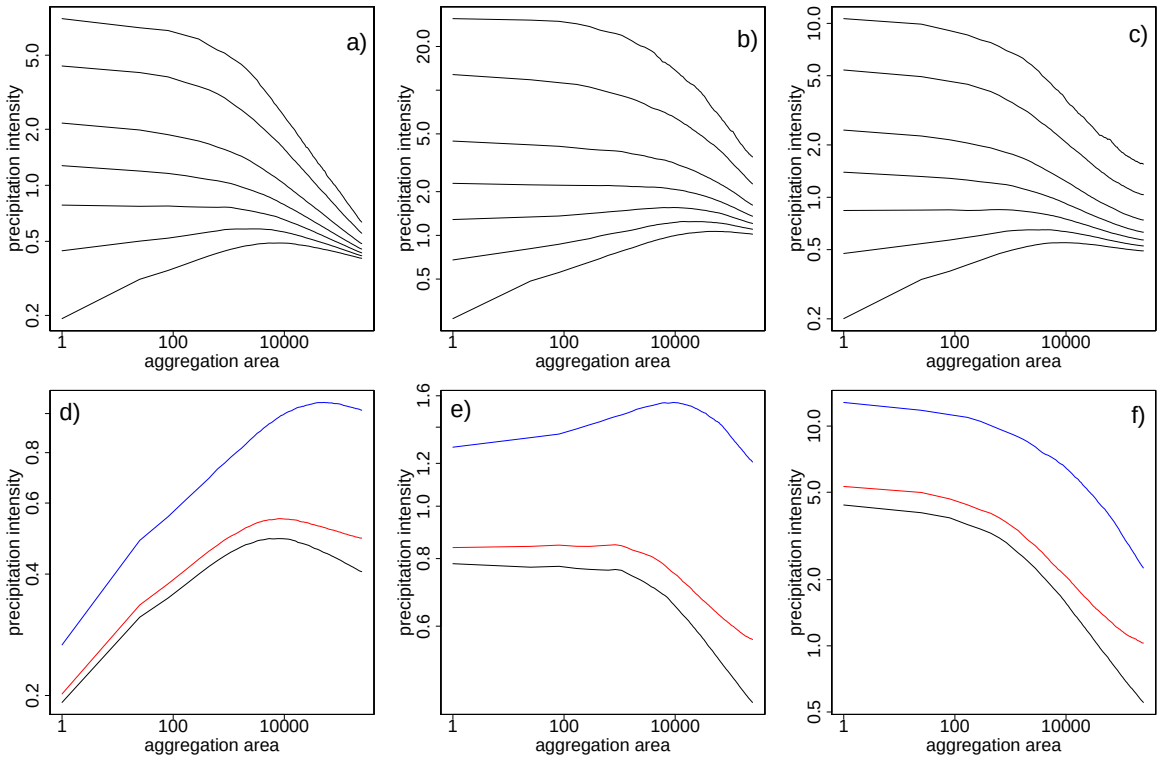

Figure 3.7: Log-log plot of quantiles of precipitation intensity subject to spatial averaging of GM, LNM and StM. The x-axis shows the aggregation area, the y-axis the precipitation intensity. In a),b) and c) the curves correspond to the $0.999, 0.99, 0.95, 0.9, 0.85, 0.8$ and $0.75-$ quantiles, which have been estimated from a sample of length $n = 10^5$. Plot a) is for the GM, b) LNM and c) StM. In d),e) and f) a certain quantile of GM (black), LNM (blue) and StM (red) is shown. In d) the 0.75, e) 0.85 and f) 0.99 quantile is depicted.

minus observation fields.

The precipitation and humidity fields in StM have the same spatial structure as in GM. Basically StM is obtained from GM by multiplication of a spatially constant variable, such that the spatial structure of StM is similar to GM.

The marginal distribution of precipitation extremes is highly dependent on temporal and spatial aggregation. It is therefore not meaningful to speak of precipitation extremes in an absolute sense. Rather, any precipitation intensity should be deemed rare or common with respect to a temporal aggregation period or spatial aggregation area for which it is valid. This is illustrated in Figure 3.7a) which shows the quantiles of precipitation fields of GM subject to spatial averaging. Due to spatial averaging the values of the upper quantiles (0.999-0.85) of precipitation

are strongly reduced. For a single location the 0.999-quantile of precipitation intensity is roughly twice as large as the same quantile for the spatial average over 14^2 grid points. While lower quantiles like the 0.85 quantile show small variation due to spatial averaging, the 0.75 quantile is increased by averaging. Figure 3.7b),c) show analogous results for LNM and StM. Figure 3.7 c),d),e) compare the $0.75, 0.85$ and 0.99 quantile of GM, LNM and StM. GM and StM yield a largely parallel behavior. Only for very large aggregation areas the quantiles of StM reduce slightly slower. Generally the quantiles of LNM are higher and for the 0.75 and 0.99 quantile show stronger variation. Particularly interesting is that we observe due to spatial dependence a non-monotonic reduction of the 0.75 and 0.85 quantile.

In order generate Figure 3.7 and all further Figures in this section we generated $n = 10^5$ realizations of GM, LNM and StM on a 125×125 grid with 4 grid point distance. This is the same area as in Figure 3.6, yet with a rougher resolution.

The reduction of the intensities shown in Figure 3.7 for the GM is due to the reduction of variance by the spatial averaging, since distant precipitation intensities are uncorrelated. A further reason is the change of the marginal distribution due to spatial averaging. For increasing aggregation areas the distribution of precipitation tends to a normal distribution, due to the central limit theorem.

Figure 3.8 shows the histograms of precipitation events from the GM (29) for a single point in space and the average of 125^2 points in space. For better comparison both distributions have been normalized to zero mean and unit variance. The spatial averaging leads to a less skewed distribution and the distribution of the averaged values is closer to a normal distribution, although they clearly differ from a normal distribution.

Figure 3.9a) shows the GPD shape parameter estimated from the tail of GM as a function of spatial averaging. It is highly sensitive and reduces considerably with spatial aggregation. Even though all distributions lie in the domain of attraction of the Gumbel distribution, there is substantial variation of the extreme value estimates for finite sample size. The average of the whole field has a shape parameter $\gamma \approx -0.1$, which is close to the preasymptotic extremal behavior of a normal distribution.

The shape parameter of LNM, which is shown in Figure 3.9b), reduces also rapidly with spatial aggregation over small areas. For larger aggregation areas this tendency reduces considerably. Interestingly, for the complete aggregation area of size 500^2 the shape is still very far from the shape, that would be expected from a normal distribution. Even though Figure 3.6c) suggests that there are lot of degrees of freedom in the field.

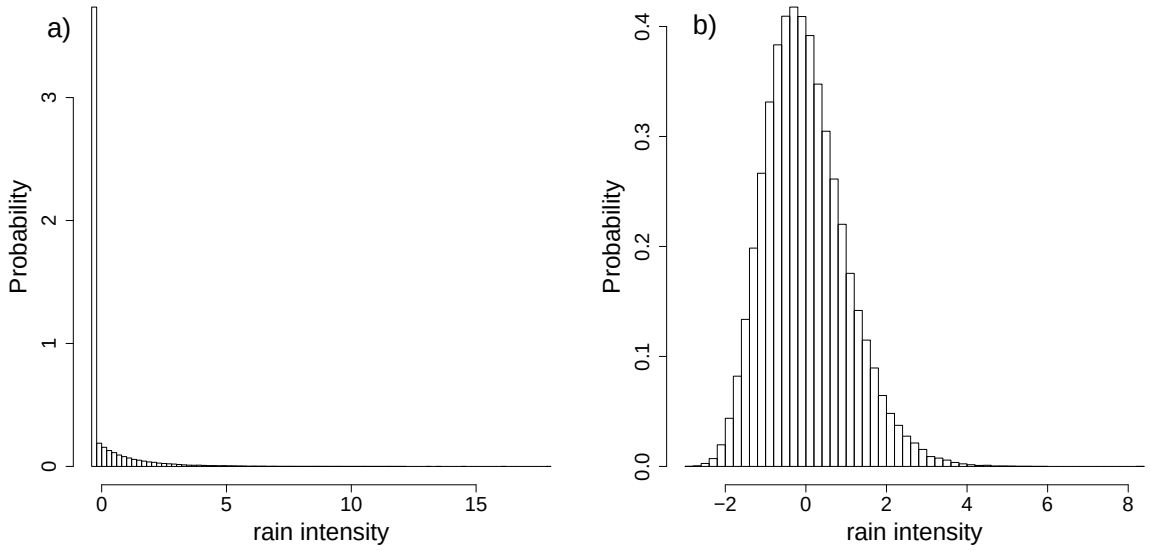

Figure 3.8: Distribution of precipitation intensity normalized to zero mean and unit variance for a) precipitation intensity at one location and b) averaged over area of size 500^2 for the process (29) (GM).

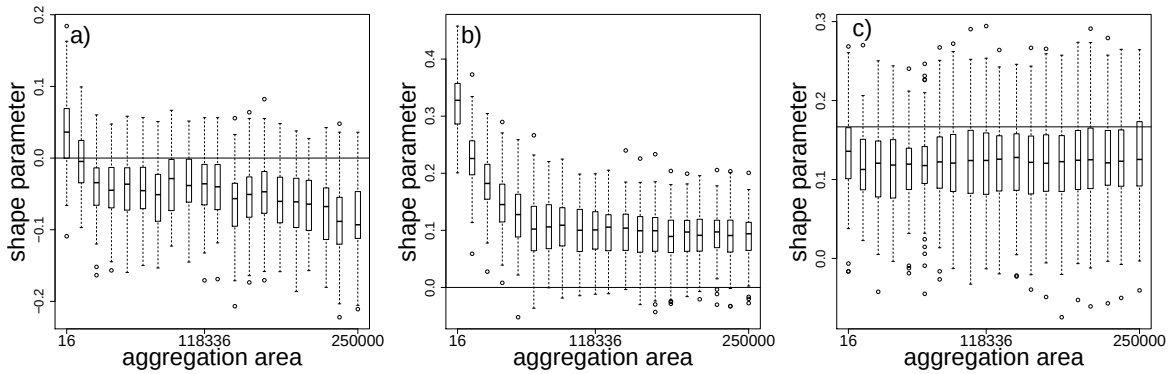

Figure 3.9: Boxplots of shape parameter of a GPD estimated from the upper 5% of a sample of size $n = 10^4$ bootstraped from a sample of length $n = 10^5$. In a) the first box on the left shows the distribution obtained for a sample of the process (29) (GM), while for the other boxes the process has been averaged over a number of grid points indicated by the x-axis. Analogue plots are given for LNM in b) and StM in c).

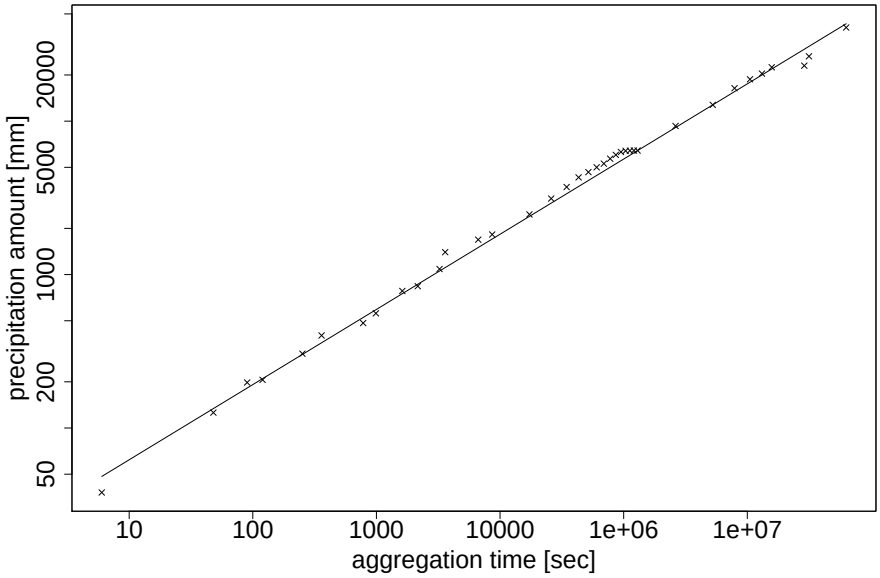

Figure 3.10: Log-log plot of precipitation extremes from a data set of the World Meteorological Organization (WMO, 1994) reproduced from Hense and Friederichs (2006). The x-axis shows the aggregation period and the y-axis the aggregated precipitation amount. The line indicates a least square fit $6.5\tau^{0.49}$.

The StM has a distinctly different behavior. It has a common factor for divergence and the wind field, which is spatially constant. This factor is the main generator of extremes and due to its spatially constant behavior the central limit theorem cannot be applied to such fields. Accordingly, we do not observe a tendency of the shape parameter to reduce with spatial averaging in Figure 3.9 c).

Observational data of precipitation extremes issued by the World Meteorological Society (WMO, 1994) exhibit a strong reduction of precipitation intensities with temporal resolution. Figure 3.10 is a plot reproduced from Hense and Friederichs (2006), where maxima from this data set are shown with respect to their temporal resolution. The maxima are remarkably well approximated by the function $6.5\tau^{0.49}$, where τ is the aggregation duration (Hense and Friederichs, 2006). This behavior suggests that precipitation is a scale-free phenomenon (Hense and Friederichs, 2006). Similar results could be expected from precipitation fields with a correlation range that is smaller than the temporal resolution of the data. For such a time series $(P_n, n \in \mathbb{N})$ of precipitation amounts we have

$$\mathrm{Var}\left(\sum_{i=1}^{n} P_i\right) = \mathcal{O}(n)\,.$$

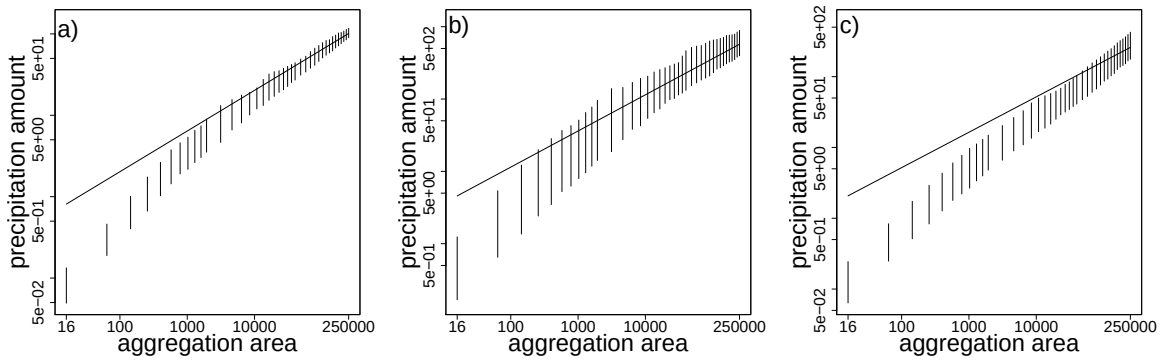

Figure 3.11: Log-log plot of maxima of spatial aggregates of precipitation fields. The x-axis represents the aggregation area and the y-axis the spatial aggregates. The vertical lines show the 95% confidence interval of the maximum over $n = 10^3$ realizations bootstraped from $n = 10^5$ replicates. The line is the $K\tau$, where τ is the aggregation area and $K \in \mathbb{R}$ such that the line coincides with the median of the maxima over aggregation area 250000. A similar function is considered in Figure 3.10. The data have been simulated with a) GM, b) LNM c) StM.

For a distribution that is stable under summation this implies, that the quantiles of aggregated precipitation increases proportional to $n^{0.5}$. The normal distribution is the only summation-stable distribution with finite second moments. Yet, it is certainly no appropriate distribution for precipitation.

In Figure 3.11a) the maxima over 10^3 samples of GM are shown as a function of spatial aggregation. For very large spatial aggregates the variance of the aggregate increases linearly as the precipitation rate of remote grid points are uncorrelated and do not increase the variance of the sum superlinearly. Together with the convergence to the Gaussian limit, this explains why the maxima can be well approximated by a linear function in the limit. In a one-dimensional setting the same consideration would suggest an increase by $n^{0.5}$. For small aggregation areas these approximations are no longer valid and the rate is lower. In Figure 3.11b),c) it is shown that similar results hold for the LNM and the StM. Particularly in the case of StM the linear increase of precipitation extremes with aggregation area is an unsatisfactory approximation.

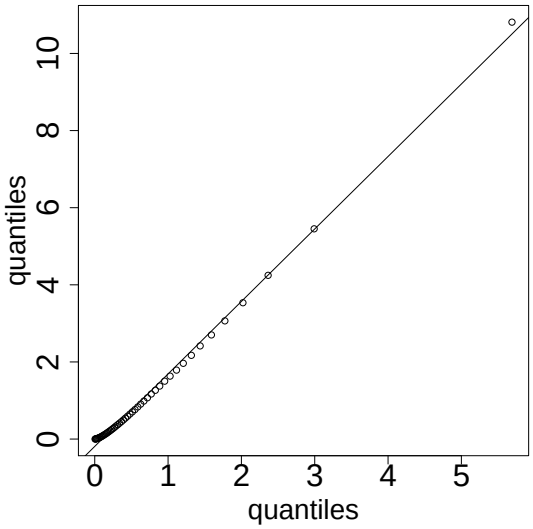

Figure 3.12: Quantiles of χ^2_1 random variable (y-axis) and the absolute value of a product of two standard Gaussian variables (x-Axis). The quantiles $q = 2i/100$ for $i = 1, \ldots, 49$ and the 0.999 quantile estimated from samples of length $n = 10^6$ are shown. The straight line is a regression line.

3.4.6 Max-stable limit of the Gaussian model

In this section we study the convergence of pointwise maxima of GM to a max-stable limit. Max-stable processes are natural stochastic processes to describe the spatial structure of precipitation extremes. The convergence of stochastic processes to their max-stable limit gives insight in the typical size of spatial extreme events relative to their intensity (Kabluchko et al., 2009) and is therefore an important tool to estimate the tails of spatial functionals. Further, max-stable processes provide opportunity to perform conditional simulation of extremes (Oesting et al., 2012) and therefore allow to interpolate extremes fields to non-observed locations.

Section 3.4.4 shows that the precipitation fields of the GM have a distribution very close to the product of two Gaussian variables. Figure 3.12 shows a qq-plot for a χ^2_1 distribution and the absolute value of a product of two Gaussian variables. The almost linear behavior of the quantiles shows that the distributions have a very similar shape. A bootstrap revealed negligible uncertainties of the estimated quantiles (not shown). The two distributions are up to an affine transformation similar. This suggests that the precipitation fields of the GM can be well-approximated by χ^2_1 fields. Such a field is given by the squared of a zero-mean Gaussian random

field. We will investigate the convergence of a χ^2_m to max-stable processes in this section. We need the following definition before introducing the main result.

Definition 10. A measurable function L that is positive in an open set containing 0 is *slowly varying at zero* if

$$\lim_{x\to 0}\frac{L(ax)}{L(x)}=1 \quad \forall a\in\mathbb{R}_+.$$

The following assumption is slightly stronger than an assumption in Kabluchko et al. (2009). We additionally assume the continuity of the following function L in order to prove Theorem 12.

Assumption 11. Let $(X(t), t\in D)$ be a zero-mean, unit-variance Gaussian process defined on an open set $D\subset\mathbb{R}^d$ containing 0 with covariance function $C(s,t)=\mathbb{E}\left(X\left(s\right)X\left(t\right)\right)$. We assume

$$\lim_{\varepsilon\downarrow 0}\frac{1-C\left(\varepsilon s,\varepsilon t\right)}{L\left(\varepsilon\right)\varepsilon^{\alpha}}=\gamma\left(s-t\right)$$

is uniform for bounded s,t, where L is continuous, slowly varying at zero; $\alpha\in(0,2]$ and $\gamma:\mathbb{R}^d\to[0,\infty)$ is a continuous function satisfying $\gamma\left(\lambda t\right)=\lambda^{\alpha}\gamma(t)$, for $\lambda\geq 0, t\in\mathbb{R}^d$.

A zero-mean, unit-variance Gaussian process with differentiable covariance function fulfills Assumption 11 with $\alpha=1$ and $L=1$. We introduce the following sequence, which has been considered in Hashorva et al. (2012)

$$b_{n,m}:=2\ln n+(m-2)\ln\ln n-2\ln\Gamma\left(m/2\right), \tag{37}$$

where Γ is the gamma function. This sequence can be used to change the location of the maximum of n *iid* copies ofχ^2_m, where m is the degree of freedom. If Assumption 11 is fulfilled, we define following Kabluchko et al. (2009) the sequence

$$s_n=\min\left\{s>0\,\middle|\,L(s)s^{\alpha}=\frac{1}{2\ln n}\right\}. \tag{38}$$

Theorem 12. Let $X_{i,j}$ $i,j\in\mathbb{N}$ *iid* processes satisfying condition 11. For $m\in\mathbb{N}$ define

$$\chi^2_{i,m}(t):=\sum_{j=1}^{m}X^2_{i,j}(t).$$

$\chi^2_{i,m}$ is a χ^2 distributed random field with m degrees of freedom. We have the following asymptotic distribution

$$\bigvee_{i=1}^{n}\frac{\chi^2_{i,m}(ts_n)-b_{n,m}}{2}\Rightarrow\eta(t), \tag{39}$$

where η is the Brown-Resnick process associated to the variogram 2γ from Assumption 11. The sequences $b_{n,m}$ and s_n are given in (37) and (38). The convergence denoted by "$\Rightarrow$" holds in the sense that for any compact set K the left hand side converges weakly in the space of continuous functions $\mathcal{C}(K)$ equipped with the infinity-norm $\|\cdot\|_\infty$.

Proof. Idea: Hashorva et al. (2012) showed that in the finite dimensional setting the asymptotic distributions of the componentwise maxima of χ^2_m vectors and Gaussian vectors are identical given the right normalizing sequences. The Kolmogorov extension theorem states that a continuous process is completely characterized by its finite dimensional distribution. Hence, we can extend the result of Kabluchko et al. (2009) that was derived for the maxima of Gaussian fields to maxima of χ^2_m fields.

Assumption 16 of Kabluchko et al. (2009) is slightly weaker than Assumption 11. We have to show that the latter implies the following condition which is the condition of Theorem 1.1 in Hashorva et al. (2012). The condition was introduced by Hüsler and Reiss (1989). Let X_n be a sequence of d-dimensional Gaussian vectors with correlation matrix Σ_n. The condition of Hüsler and Reiss (1989) is

$$\lim_{n\to\infty} 4\ln n(\mathbb{1}\mathbb{1}^T - \Sigma_n) = \Lambda \in [0,\infty)^{d\times d}\,, \tag{40}$$

where $\mathbb{1}$ is the d-dimensional vector consisting of 1 entries. We have to show that the Gaussian vector obtained by projecting a Gaussian field fulfilling Assumption 11 to d points fulfills the condition (40). It is sufficient to do this for $d = 2$. The condition (40) is trivially satisfied for the diagonal entries. For the non-diagonal entries we have

$$\begin{aligned}
&\lim_{n\to\infty} 4\ln n\,(1 - C\,(t_1 s_n, t_2 s_n)) \\
&= \lim_{n\to\infty} \frac{1 - C\,(t_1 s_n, t_2 s_n)}{L(s_n) s_n^\alpha} \frac{4\ln n}{L(s_n) s_n^\alpha} \\
&= \gamma\,(t_1 - t_2) \lim_{n\to\infty} \frac{4\ln n}{2\ln n} \\
&= 2\gamma\,(t_1 - t_2)\,.
\end{aligned}$$

In the second equation the continuity of L implies $L\,(s_n)\, s_n^\alpha = 2\ln n$. Hence (40) is satisfied and the $\Lambda_{i,j}$ is given by $2\gamma(t_i - t_j)$, where $i, j = 1,\ldots,d$ and $t_1,\ldots t_d$ are the locations where η is evaluated. Due to Theorem 1.1 of Hashorva et al. (2012), the finite dimensional distributions of this process converge to the Hüsler-Reiss process M_Λ. A similar consideration for the asymptotic limit of Gaussian fields (Kabluchko et al., 2009) shows that the finite dimensional distributions of

such fields converge to the same limit, namely the Hüsler-Reiss process M_Λ. By the Kolmogorov extension theorem, which shows that stochastic processes are uniquely characterized by the finite dimensional distributions, both processes converge to the same limit. In Kabluchko et al. (2009) it was shown that this is the Brown-Resnick process associated to the variogram $2\gamma(\cdot)$. □

The sequence s_n describes the characteristic scale of precipitation extremes drawn from n independent precipitation fields from the GM. If the covariance function of the fields is differentiable, then $s_n \sim 1/\sqrt{\ln n}$. The sequence s_n can be understood as a zooming sequence which increases the resolution such that a stable dependence structure is obtained when the maximum is taken over an increasing number of fields n. The theorem suggests that a company insuring precipitation risks of different individuals in a neighborhood could assume asymptotic independence for extreme incidents.

Figure 3.13 depicts pointwise maxima of multiple precipitation fields of the GM. A moderate decrease of the characteristic size of the precipitation clusters can be spotted when comparing the maximum over $n = 10$ fields to the maximum over $n = 10^3$.

For StM extreme values are mainly generated by a spatially constant factor. Up to this factor the model is identical to the GM. This suggests that the maximum over n fields of this model could be well-approximated by a univariate extrapolation of the factor. At least for moderate n we conjecture that the spatial structure of the maximum is similar to a random draw from the GM.

3.5 Conclusions

In this chapter we extensively study the stochastic properties of precipitation fields based on the budget equation of humidity (25). We begin by introducing methods from EVT in Section 3.1 and deriving relations for the asymptotic shape of products of random variables. Further, in Section 3.2 we summarize some important aspects discussed in the literature about precipitation extremes. We present a physically motivated statistical model of precipitation extremes (Wilson and Toumi, 2005) in Section 3.3.1, that is an important motivation for this thesis. In Sections 3.3.2 we derive a simplified equation (26) of the budget equation (25), that can be modeled by the methods developed in Chapter 2. In Section 3.3.3 we define three different stochastic models GM, LNM and StM. Both analytic methods and simulation studies are used to describe and understand the stochastic properties of these models.

Some very basic relations of the terms of the simplified budget equation (1) can be seen from the differential relations that hold between the variables. For

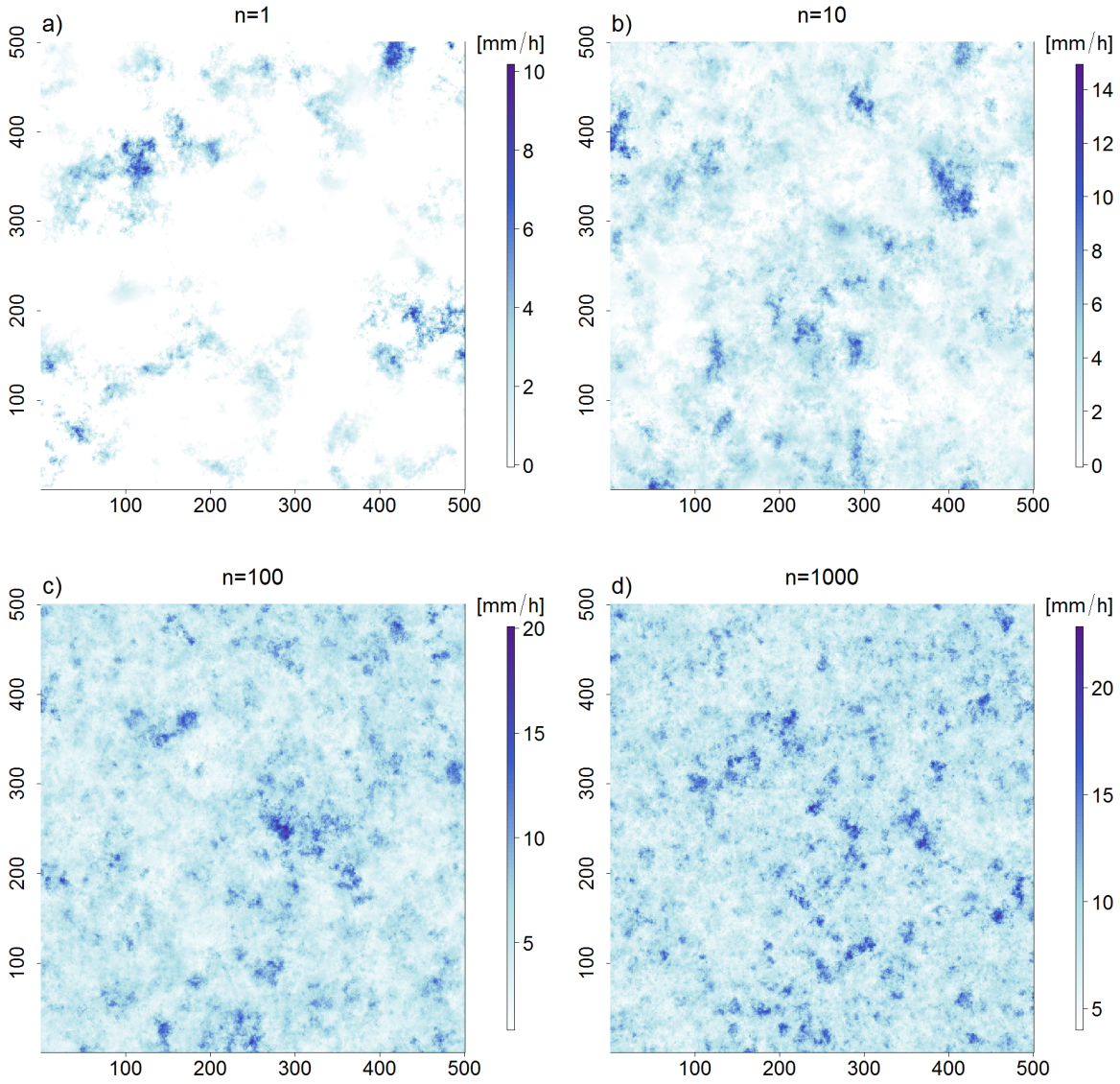

Figure 3.13: Pointwise maxima of n independent realizations of the GM. a) $n = 1$, b) $n = 10$ c) $n = 10^2$, d) $n = 10^3$.

example, due to kinematic properties the advection term and the divergence term are uncorrelated for a stationary and isotropic covariance structure of ψ, χ and q. Importantly, we have derived extremal properties of products of random variables from moment relations for a wide class of random variables. For example we have shown that the product of light-tailed distributions is under weak conditions not heavy-tailed. Hence, the budget equation cannot be used to argue that precipitation has heavy tails, if the humidity and the wind field are light-tailed. Further, we show that for heavy-tailed distributions products of independent variables have no higher

shape parameter than their multiplicands. However, the square of a heavy-tailed distribution has a higher shape parameter if it is in the domain of attraction of an extreme value distribution at all. Based on these results we show that an argument of Koutsoyiannis (2004) is misleading, which claims that seasonality could be a plausible generator of a heavy-tailed distribution of precipitation. Further, we obtain analytic relations for the convergence of the shape parameter to its limit for the precipitation models introduced here. Such relations have been used to improve the convergence rates to limit relations of EVT (Embrechts et al., 1997). These approximations illustrate that finite-sample properties may converge extremely slow to the limit relation.

The results of Section 3.4.3 suggest that a diverse behavior with respect to the correlation parameter can be observed. For finite samples the correlation can have non-negligible influence on the extremal behavior even for light-tailed distributions, opposed to the asymptotic irrelevance of correlation. For heavy-tailed distributions the product of two perfectly correlated random variables has doubled shape parameter when compared to the product of independent variables.

In two physically motivated models of precipitation we do not find influence of the correlation parameter on the preasymptotic extremal behavior. Particularly interesting is the case of LNM, where the kinematic properties of the stochastic process studied in Chapter 2 leads to an irrelevance of the correlation parameter, even though we show that for products of Gaussian and log-normal distribution the correlation is non-negligible in a finite-sample regime.

The preasymptotic extremal behavior of LNM and GM are hardly affected by the transition from purely rotational flow to purely divergent flow. The small reactions of the extremal behavior to this transition are heterogeneous. While the GM shows a reduction of the shape parameter for rotational flow LNM exhibits a mild increase of the shape parameter (see Section 3.4.4).

The models (29)-(31) can be used to generate physically meaningful fields of precipitation with the associated fields of streamfunction, velocity potential, humidity, the gradient of humidity, divergence and vorticity. Due to the implementation in the R packages RandomFields (Schlather et al., 2016) highly efficient algorithms like circulant embedding (Wood and Chan, 1994) can be used to generate fields of size 800×800. Such spatial models are useful to obtain relations of aggregation and precipitation intensity like in Figure 3.7 via Monte Carlo methods. The spatial aggregates of the GM converge relatively fast to a negative shape parameter. The GPD shape parameter fitted to spatial aggreagtes of LNM reduces considerably with the aggregation area, yet the convergence is slower as for GM. A different picture

is obtained for the StM, whose shape parameter is stable under spatial aggregation. This could be an appropriate feature of precipitation models for small scales, where an approximation under the Gumbel limit is inappropriate.

A scale-free behavior of precipitation extremes with respect to temporal resolution presented in Hense and Friederichs (2006) amongst others cannot be reproduced by the three model discussed here.

The wind field process (3) can be used for conditional simulation, such that the models (29)-(31) are able to generate conditional simulation of precipitation fields given certain realizations of the wind and humidity fields, which could be a useful method for downscaling.

The GM has marginals very close to the product of two Gaussian variables. The absolute value of this product in turn is very close to a χ_1^2 variable with one degree of freedom. We prove the convergence to a Brown-Resnick process for pointwise maxima of χ_m^2 processes with arbitrary degrees of freedom. Such results are the natural extension of the convergence of a univariate maximum to an extreme value distribution. They allow insight into the spatial dependence structure and its convergence to the asymptotic limit of spatial independence.

The three models (29)-(31) differ markedly in their extremal behavior. Assuming zero-mean and unit variance a value that has an average return period of 100 years for the GM occurs once every 16 years in the StM and every 5 years in LNM. The differences make clear that careful checking of the appropriateness of the marginal modeling assumptions is necessary to make useful inference about the shape of precipitation distribution. It is presumably difficult to find adequate distributions for wind and humidity that fit for various data sets. With respect to the large influence of these distributions on the marginal distribution of precipitation, it is difficult to use our approach to find a universally valid approximation for the distribution of precipitation. Yet, this sensitivity exhibits a property of the balance equation (25) and therefore cannot be neglected. This sensitivity could be used in future work to solve the problem vice-versa and to find distributions for wind and humidity that result in distributions in accordance with precipitation observations. Similar to Wilson and Toumi (2005) we find that the asymptotic properties of models are of limited practical relevance. For example for finite-sample LNM shows a more extreme shape than the StM with $d = 6$ degree of freedoms, although the former is light-tailed and the latter heavy-tailed, if they are in any domain of attraction.

The precipitation in GM has a distribution largely similar to the product of two independent normal variables. The inclusion of precipitation efficiency fields as a

further multiplicative factor for the precipitation rate would yield more realistic products of three independent Gaussian variables similar to Wilson and Toumi (2005). We agree with Wilson and Toumi (2005) that precipitation efficiency is potentially an essential feature of precipitation. Nevertheless, the sensitivity to the type of marginal distribution suggests that a careful checking of appropriate distributions is necessary. Modeling precipitation efficiency κ as a normal random variable seems inappropriate since it does not fulfill $0 \leq \kappa \leq 1$.

The parametrization of the transition of cloud droplets to precipitation droplets in Seifert and Beheng (2001) suggests a precipitation rate quadratically increasing with the humidity exceeding the Clausius-Clapeyron threshold. For the GM we would then obtain relatively high preasymptotic GPD shape parameter $\gamma \approx 0.3$ for the upper 5% of data. This may be already too high to be consistent with observational data. For LNM we obtain a totally unrealistic high preasymptotic shape parameter $\gamma \approx 0.75$ and for StM estimates close to the shape parameter $\gamma = 0.8$. This suggests that the parametrization of Seifert and Beheng (2001) is unsatisfactory for extreme precipitation events. For such events, Kessler (1969)'s linear parametrization may be more adequate. However, Seifert and Beheng (2001)'s parametrization suggests that precipitation efficiency increases with the density of cloud droplets. This could be a vital feature in modeling precipitation extremes.

For LNM the main generator of extremes is the advection term, while for the GM the advection and convergence term are of comparable importance. This shows that the marginal assumption even have influence on the interplay of the terms of the budget equation. LNM yields a shape parameter $\gamma \approx 0.3$ for finite sample size, which may be too high to be a realistic approximation. In this model the variability of the humidity field is the main generator of precipitation extremes.

The high kurtosis of data described in Section 2.3 suggests that the wind data are well described by distributions with much fatter tails than the normal distribution. This is a motivation of the StM, that is able to describe a diverse extremal behavior of the wind fields. For six degrees of freedom it yields a realistic extremal behavior, which is mainly generated by fluctuations in the wind fields and the divergence of it. In order to have a multivariate-t distribution, we multiply the whole wind field and divergence field by a single constant. This may be a useful approximation for small-scales, that yields stable shape parameter under aggregation. For larger scales a spatially varying scaling parameter could be considered.

Although the multiplication of random variables cannot generate heavy tails from light-tailed distribution, the multiplication of random variables leads to an intensification of the preasymptotic distribution. For example the product of two

Gaussian variables has a slightly positive shape parameter when estimated from the upper 5% of the data. For a single Gaussian variable a shape parameter close to -0.1 would be obtained. We agree with Wilson and Toumi (2005) that the multiplicativity of the budget equation is a very reasonable explanation for the extreme shape of precipitation. The similarity of the distribution of precipitation in the GM and the product of two Gaussian variables, suggests that the simplifications made in Wilson and Toumi (2005) when deriving the budget equation are acceptable.

4 Conclusions and outlook

In this thesis physically motivated stochastic models for wind fields and precipitation extremes have been developed. These models allow for better understanding of stochastic properties of meteorological processes. Further, the methods developed in this thesis have multiple applications for example in data assimilation or risk assessment related to precipitation.

In Chapter 2 we have introduced a stochastic process that models the differential relations, which hold between a two-dimensional wind field and further related variables. Due to its consistency with physical relations and its ability to preserve balances like geostrophy or non-divergence, it has multiple applications in data assimilation. Further applications of our model are kriging and the conditional simulation of physical relations. Our approach extends similar methods that have been used in data assimilation, most notably the work by Daley (1985, 1991). We have reviewed the conditions under which derivative processes like our GRF exist and showed that it is non-trivially transformed by anisotropy. In the introduction we have posed the following questions.

> Is there a stochastic process able to represent the differential relations between the variables of the Helmholtz decomposition, which is sufficiently flexible to be a useful approximation for realistic wind fields? Can such a process model the correlations of streamfunction and velocity potential?

With respect to the first question the answer is affirmative. The process (3) has been shown to be a useful geostatistical model for a mesoscale wind field. Yet, the application to such data also reveals that the assumption of marginal Gaussianity and stationarity may be quite restrictive. To overcome this restriction we have shown that it is possible in some situations to extend the process to non-Gaussian fields by transforming the data. The second question can be answered positively, too. Our model allows for such correlations and we have disproved a theorem of Obukhov (1954), which claims that such models cannot exist, if they are isotropic.

Particularly important for this thesis is the inclusion of divergence in the model introduced in Chapter 2, which allows to model the transport of tracer variables like aerosols or humidity. The transport of humidity is essential to the generation of precipitation extremes. The methods of Chapter 2 allow us to build a stochastic model for precipitation extremes based on the moisture budget, which models the moisture flux convergence. In Chapter 3 we have extensively discussed such models,

their limitations and their ability to explain characteristics of precipitation. We return to the questions posed in the introduction.

> Under which conditions generates the moisture budget (1) a heavy-tailed P? Which terms in (1) are essential for the generation of extremes?

With respect to the first question, we find that the moisture budget (1) generates heavy tails only if the wind or the humidity field is heavy-tailed. Thus, the moisture budget cannot account for the emergence of heavy-tailed distributions from light-tailed ones. Nevertheless we have shown that such asymptotic results may be of very limited practical relevance, as the convergence of sample maxima to their asymptotic distribution may be extremely slow. Instead, preasymptotic approximations give useful information about the extremal behavior. In such a preasymptotic sense our results suggest similar to Wilson and Toumi (2005), that the multiplications in (1) can account for a heavy-tailed behavior.

With respect to the second question, we verify Wilson and Toumi (2005)'s ansatz to reduce the moisture budget to a multiplicative process. Wilson and Toumi (2005) considered a similar yet less justifiable model for precipitation extremes. In our approach we have been able to largely reproduce their results, which suggests that their simplifications are acceptable. On the other hand, we have argued that some of the distributional assumptions made in Wilson and Toumi (2005) are questionable, which is particularly problematic since the precipitation field obtained from the budget equation are highly sensitive to the marginal distributions of the physical quantities in the moisture budget. Additionally, the found sensitivity suggests that we are in a strong need of well-established distributional assumptions for humidity and wind. Particularly the extremal behavior of vertical velocity is of tremendous interest. Due to convection triggered by an unstable atmosphere it is very plausible that it has a quite extreme distribution. Unfortunately, few observational data sets of vertical velocity are available (Chu et al., 1996; Donner et al., 2016). Particularly noteworthy is the insensitivity of precipitation extremes on the correlation of the quantities ψ, χ and q.

Our approach is an extension of Wilson and Toumi (2005) as it is able to generate spatial precipitation fields and therefore allows to study the spatial structure of precipitation extremes. We prove the convergence of maxima of the Gaussian precipitation model (29) to a Brown-Resnick process and show that precipitation extremes are asymptotically independent in this model.

This thesis illustrates the value of linking complex statistical approaches with physical reasoning in a twofold way. First, most of the applications of the GRF in

Chapter 2 are particularly interesting due to their physical consistency. Secondly, the inclusion of the budget equation into a stochastic model has allowed us to assess to which extent it is able to account for precipitation extremes.

We conclude by giving a short outlook on how the models of both chapters could be improved. A promising approach for both Chapter 2 and Chapter 3 is to model streamfunction and velocity potential as the quotient of a Gaussian process and a χ^2-process.

$$\chi_s = \frac{X(s)}{\sqrt{\chi^2_m(s)/m}} \quad s \in \mathbb{R}^2,$$

where $X(s)$ is a Gaussian process with a correlation structure $\rho(h)$ and $\chi^2_m(s)$ is a field obtained by the sum of m independent squared standardized Gaussian processes with common correlation structure $\varphi(h)$. The streamfunction could be modeled as an independent copy of this process. Since the χ^2 process is non-constant in space this process is not identical to the standard multivariate Student-t distribution. If the spatial range of φ is sufficiently large the derived quantities $\nabla\chi(s)$ could be approximated by

$$\nabla\left(\frac{X(s)}{\sqrt{\chi^2_m(s)/m}}\right) \approx \frac{\nabla X(s)}{\sqrt{\chi^2_m(s)/m}},$$

where obviously $\nabla X(s)$ can be modeled as in Chapter 2. Analogously, one could approximate $U, \Delta\chi$ and $\Delta\psi$. The process obtained in this way would be similar to the process in Chapter 2, yet it would have non-constant variability much like the data analysed in Section 2.3. The transformation of the data described in Section 2.3, that reduces its non-Gaussianity would no longer be necessary, as the process is able to model due to the degrees of freedom m a variable tail-behavior. If the wind field model of the StM would be replaced by this model, a very plausible model for precipitation extremes would be obtained. The marginal precipitation distribution is identical to the StM, which yields a realistic shape parameter. If the correlation structure φ is sufficiently large the shape parameter of this distribution would be insensitive subject to spatial averaging on small scales as shown in Section 3.4.5. If $m > 2$ precipitation aggregates over very large areas would tend to a normal distribution.

A Positive definiteness of Daley's (1985) model

Daley (1985) proposed the covariance model (cf. Moreva and Schlather, 2016; Gneiting et al., 2010)

$$C(r) = \begin{pmatrix} \exp\left(-\frac{1}{2}r^2\right) & \lambda \exp\left(-\frac{1}{2}\left(\frac{r}{a}\right)^2\right) \\ \lambda \exp\left(-\frac{1}{2}\left(\frac{r}{a}\right)^2\right) & \exp\left(-\frac{1}{2}\left(\frac{r}{a}\right)^2\right) \end{pmatrix}, \quad r = \|h\|,$$

for streamfunction and velocity potential. The Fourier transform of this covariance matrix is given by

$$\mathfrak{F}(C)(\varphi) = \begin{pmatrix} \exp\left(-\frac{1}{2}\varphi^2\right) & \frac{\lambda}{a} \exp\left(-\frac{1}{2}\left(\frac{\varphi}{a}\right)^2\right) \\ \frac{\lambda}{a} \exp\left(-\frac{1}{2}\left(\frac{\varphi}{a}\right)^2\right) & \frac{1}{a} \exp\left(-\frac{1}{2}\left(\frac{\varphi}{a}\right)^2\right) \end{pmatrix}.$$

By Cramér Theorem (Chiles and Delfiner, 2009) this Fourier-transform needs to be positive definite for almost all frequencies φ. This is equivalent to

$$\det(\mathfrak{F}(C)(\varphi)) \geq 0 \quad \forall \varphi \in \mathbb{R}$$

a condition equivalent to

$$\exp\left(-\frac{1}{2}\varphi^2\left(1 - \frac{1}{a^2}\right)\right) \geq \frac{\lambda^2}{a} \quad \forall \varphi \in \mathbb{R}.$$

If $a > 1$ the model is not positive definite unless $\lambda = 0$. If $0 < a \leq 1$ the model is positive definite if $a \geq \lambda^2$. Daley proposed $a > 1$ such that the model does not allow for a nonzero correlation.

B Obukhov's (1954) independence claims

Obukhov (1954) presents two arguments for an isotropic rotational field having zero correlation with an isotropic scalar field and with an isotropic gradient field. We believe that both arguments are erroneous for the same reason. As the argument for the scalar field is much less involved, we restrict ourselves to this case. Obukhovs claims that the covariance of an isotropic rotational field to an arbitrary scalar isotropic variable is of the form $\mathrm{Cov}(\chi_s, \nabla \times \psi_{s+h}) = P(\|h\|) h/\|h\|$ for some function P. Using the non-divergence of a rotational field Obukhov deduces from his assumption:

$$0 = \mathbb{E}(\chi_s \nabla \cdot \nabla \times \psi_{s+h}) = \nabla \cdot \mathbb{E}(\chi_s \nabla \times \psi_{s+h}) = \nabla \cdot \left(\frac{P(\|h\|)}{\|h\|} \begin{pmatrix} h_1 \\ h_2 \end{pmatrix}\right)$$
$$= \frac{2P(\|h\|)}{\|h\|} + \frac{\partial}{\partial \|h\|}\left(\frac{P(\|h\|)}{\|h\|}\right)\|h\| = \frac{P(\|h\|)}{\|h\|} + P'(\|h\|)$$

This differential equation is solved by the function

$$P(\|h\|) = \frac{c}{\|h\|} \qquad c \in \mathbb{R}.$$

If $c \neq 0$ this function has a pole. This implies that the variance of the corresponding field could not exist. Hence $c = 0$ and this again implies the zero correlation between the scalar field and the rotational field.

We believe that the correct covariance of a scalar field and a rotational field is given by

$$\mathrm{Cov}(\chi_s, \nabla \times \psi_{s+h}) = \frac{P(\|h\|)}{\|h\|} \begin{pmatrix} -h_2 \\ h_1 \end{pmatrix},$$

for some P, as the curl operator derives the first component in direction e_2 and the second in direction e_1. This covariance is consistent with the anisotropic transformation of the field, which has been described in (8). Using this assumption the independence of an isotropic scalar field and an isotropic rotational field cannot be deduced. However,

$$\mathbb{E}(\chi_s \nabla \cdot \nabla \times \psi_{s+h}) = \nabla \cdot \mathbb{E}(\chi_s \nabla \times \psi_{s+h}) = \nabla \cdot \left(\frac{P(\|h\|)}{\|h\|} \begin{pmatrix} -h_2 \\ h_1 \end{pmatrix} \right)$$
$$= \frac{P(\|h\|)}{\|h\|^2} (-h_2 h_1 + h_1 h_2) = 0$$

for any differentiable function P.

C Formulae of the isotropic covariance model

We describe the formula for the covariance function considered in Chapter 2 (equation (3)). For brevity we introduce the following notation

$$X_{1,s} := \psi_s \qquad X_{2,s} := \chi_s$$
$$U_{1,s} := u_s \qquad U_{2,s} := v_s$$
$$\partial_i := \partial_{e_i},$$

and omit the argument of the covariance functions, which is $(t - s)$ in all of the following cases.

$C^{i,j} := \mathrm{Cov}\left(X_{i,s}, X_{j,t}\right)$

$$\mathrm{Cov}\left(U_{i,s}, U_{j,t}\right) = (-1)^{i+j} \frac{\partial^2}{\partial_{3-i}\partial_{3-j}} C^{1,1} + (-1)^{i} \frac{\partial}{\partial_{3-i}\partial_{j}} C^{1,2} + (-1)^{j} \frac{\partial^2}{\partial_{i}\partial_{3-j}} C^{2,1} + \frac{\partial}{\partial_{i}\partial_{j}} C^{2,2}$$

$$\mathrm{Cov}\left(\Delta X_{i,s}, \Delta X_{j,t}\right) = \sum_{(k,l)\in\{1,2\}^2} \frac{\partial^4}{\partial_k^2 \partial_l^2} C^{i,j}$$

$$\mathrm{Cov}\left(U_{i,s}, X_{j,t}\right) = -\mathrm{Cov}\left(X_{j,s}, U_{i,t}\right) = (-1)^{i} \frac{\partial}{\partial e_{3-i}} C^{1,j} + \frac{\partial}{\partial e_i} C^{2,j}$$

$$\mathrm{Cov}\left(X_{i,s}, \Delta X_{j,t}\right) = \mathrm{Cov}\left(\Delta X_{j,s}, X_{i,t}\right) = \frac{\partial^2}{\partial^2 e_1} C^{i,j} + \frac{\partial^2}{\partial^2 e_2} C^{i,j}$$

$$\begin{aligned}\mathrm{Cov}\left(U_{i,s}, \Delta X_{j,t}\right) &= -\mathrm{Cov}\left(\Delta X_{j,s}, U_{i,t}\right) \\ &= (-1)^{i} \frac{\partial^3}{\partial_{3-i}\partial_1^2} C^{1,j} + (-1)^{i} \frac{\partial^3}{\partial_{3-i}\partial_2^2} C^{1,j} + \frac{\partial^3}{\partial_{i}\partial_1^2} C^{2,j} + \frac{\partial^3}{\partial_{i}\partial_2^2} C^{2,j},\end{aligned}$$

where $i, j \in \{1, 2\}$.

D Pareto optimal transformation of the inner-LBC

In this appendix we introduce a Pareto optimal solution to the trade-off in Section 2.3. We apply a kernel smoother to the kinetic energy field associated to the horizontal wind field U_s.

$$\widehat{g}_\theta(s) = \frac{1}{N(s)} \sum_{t\in\mathbb{G}} \left(u_t^2 + v_t^2\right) \exp\left(\frac{-\|t-s\|_2}{\theta}\right) \quad s \in \mathbb{R}^2,$$

where $(u_s, v_s) = U_s$, $\theta > 0$ is a bandwidth parameter, $\mathbb{G}$ is the grid containing all data locations, $\|\cdot\|_2$ is the Euclidean distance and $N(s) = \sum_{t\in\mathbb{G}} \exp\left(-\|t-s\|_2/\theta\right)$. Let χ_s and ψ_s be the velocity potential and streamfunction that solve $\nabla\chi_s + \nabla \times \psi_s = U_s$ on the grid $\mathbb{G}$ with periodic boundary conditions. For a constant $c \in \mathbb{R}_+$ let $\widetilde{U} = U/(c+\widehat{g}_\theta)^{0.5}$. Further let $\widetilde{\chi}$ and $\widetilde{\psi}$ be the velocity potential and streamfunction that solve $\nabla\widetilde{\chi}_s + \nabla \times \widetilde{\psi}_s = \widetilde{U}_s$ on the grid $\mathbb{G}$ with periodic boundary conditions. We search for transformations such that

$$\mathrm{RMSE}\left(\widetilde{\psi}_s, \psi_s/(c+\widehat{g}_\theta)^{0.5}\right) + \mathrm{RMSE}\left(\widetilde{\chi}_s, \chi_s/(c+\widehat{g}_\theta)^{0.5}\right) \tag{41}$$

is small, where

$$\mathrm{RMSE}\left(X_s, Y_s\right) := \frac{\sum_{s\in\mathbb{G}} \left(X_s - Y_s\right)^2}{\sum_{s\in\mathbb{G}} X_s^2}.$$

The second objective of the transformation is to reduce the high kurtosis of the data, which indicates a deviation from marginal Gaussianity. As the high kurtosis is plausibly mainly a result of the non-stationarity of the variance of U_s, in this

case the kurtosis may also be used as measure of non-stationarity. We consider the excess kurtosis of $\widetilde{U}_s$,

$$\mathrm{EK}\left(\widetilde{U}_s\right) := \sum_{s\in\mathbb{G}} \left(u_s^4 + v_s^4\right) \left(\sum_{s\in\mathbb{G}} \left(u_s^2 + v_s^2\right)\right)^{-2} - 3. \tag{42}$$

A Gaussian variable has excess kurotsis 0. Here, we search for Pareto optimal solutions to this trade-off. We define a configuration x' with properties f and g to be Pareto optimal relativ to a set $\mathcal{A}$ if for all $x \in \mathcal{A}$

$$f(x) \leq f(x') \Rightarrow g(x) \geq g(x').$$

In our setting (relative mean square error and excess kurtosis) small values are good, therefore our definition slightly deviates from the more typical positively oriented. For simplicity we choose $\mathcal{A}$ to be a grid containing different values of θ and c. Table 2 shows the excess kurtosis and the relative mean squared error for different values of θ and c. Table 2 suggests that surprisingly low values of $\theta = 0.6, 0.9$ yield good results. This transformations outperform the one of Section 2.3, where $\theta = 6$ and $c = 1/3$ was chosen, yielding a relative mean squared error close to 0.15 and a excess kurtosis of 13. In principle any Pareto optimal choice is reasonable. We restrict the further discussion to $\theta = 0.6$ and $c = 1$, as it has lowest kurtosis given relative mean square error below 0.1.

Figure D.1a) depicts the zonal wind component of $U_s/\sqrt{1 + g_{0.6}(s)}$, where U_s are the inner-LBC anomalies. When comparing with Figure 2.6a) we see that the non-stationarity of the variance is better removed than for the transformed inner-LBC anomalies of Section 2.3. We perform maximum-likelihood estimation as described in Section 2.4. We obtain the following estimates $\nu \approx 1.17$, $\sigma_\chi/\sigma_\psi = \lambda \approx 0.79$, $\rho_{\psi,\chi} \approx -0.02$, $r_1 \approx 0.08$, $r_2 \approx 0.07$, $\theta \approx 0.79$. The estimates are relatively close to the values obtained in Section 2.4 and shown in Figure 2.4, which suggests that the distribution of $U_s/\sqrt{1 + g_{0.6}(s)}$ is similar to the transformed inner-LBC anomalies.

Figure D.2 compares the empirical covariance estimate of the data $U_s/\sqrt{1 + g_{0.6}(s)}$ with the fitted covariance of our model. The results are similar to Figure 2.5. Figure D.1b) shows a simulation of the GRF, scaled by the variance not resolved by the transformation $\widetilde{U}_s = U_s/\sqrt{1 + g_{0.6}(s)}$. Again the results are similar to Figure 2.6, yet the accordance of the fields seems to be improved. The simulated fields exhibit a slightly rougher structure than the transformed data.

Table 2: Relative mean square error (41) & excess kurtosis (42) for different values of θ and c. Bold entries indicate Pareto optimality.

θ \ c	0.4	0.7	1	1.3	1.6	1.9
0.02	0.178 & 9.067	0.127 & 9.807	0.099 & 10.356	0.081 & 10.8	0.069 & 11.178	0.059 & 11.507
0.3	0.178 & 8.577	0.127 & 9.465	0.099 & 10.098	0.081 & 10.599	0.068 & 11.016	0.059 & 11.376
0.6	**0.177 & 8.034**	**0.125 & 9.104**	**0.097 & 9.864**	**0.079 & 10.457**	**0.067 & 10.947**	**0.057 & 11.365**
0.9	**0.174 & 8.169**	**0.123 & 9.313**	**0.095 & 10.118**	**0.078/10.744**	**0.065/11.258**	**0.056/11.692**
1.2	**0.172 & 8.474**	**0.121 & 9.652**	0.094 & 10.474	0.076 & 11.108	0.064 & 11.625	**0.054 & 12.060**

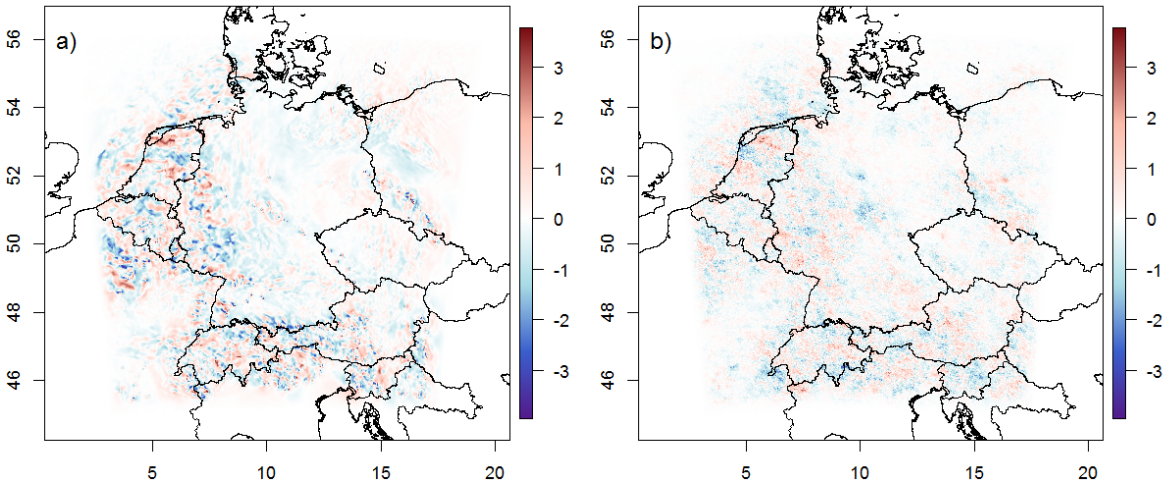

Figure D.1: Zonal wind component at 12 UTC on 5 June 2011. a) Shows $U_s/\sqrt{1+g_{0.6}}$, where U_s are the inner-LBC anomalies, b) a simulation of the fitted GRF with covariance (3). The colors represent wind speed in m/s. The x/y- axis are in longitude and latitude.

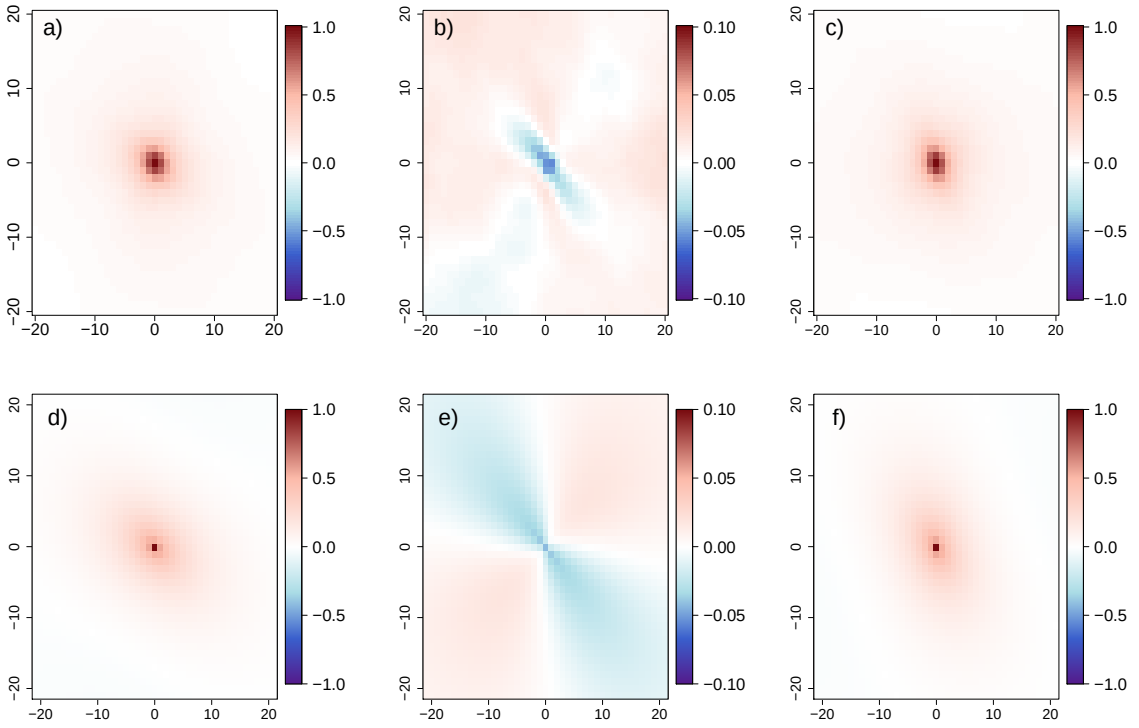

Figure D.2: Empirical correlation (above) and estimated correlation (below) for data set 1. a) (u,u) empirical correlation; b) (u,v) empirical correlation; c) (v,v) empirical correlation; d) (u,u) estimated correlation; e) (u,v) estimated correlation; f) (v,v) estimated correlation.

List of Figures

List of Acronyms

EVT extreme value theory 8

NWP numerical weather prediction 8

GRF Gaussian random field 10

DWD German meteorological service 11

COSMO consortium of Small-scale Modeling 16

LBC lateral boundary conditions 16

CL composite likelihood 18

GEV generalized extreme value distribution 28

GPD generalized Pareto distribution 31

GM Gaussian model 43

LNM log-normal model 44

StM Student-t model 44

References

Adler, R. J., and J. E. Taylor, 2007: *Random Fields and Geometry*, Vol. 17. Springer, 448 pp.

Allen, M. R., and W. J. Ingram, 2002: Constraints on future changes in climate and the hydrologic cycle. *Nature*, **419 (6903)**, 224–232.

Aref, H., 2007: Point vortex dynamics: A classical mathematics playground. *Journal of mathematical Physics*, **48 (6)**.

Baldauf, M., A. Seifert, J. Förstner, D. Majewski, M. Raschendorfer, and T. Reinhardt, 2011: Operational convective-scale numerical weather prediction with the COSMO model: Description and sensitivities. *Monthly weather review*.

Bannister, R. N., 2008: A review of forecast error covariance statistics in atmospheric variational data assimilation. ii: Modelling the forecast error covariance statistics. *Quarterly Journal of the Royal Meteorological Society*, **134 (637)**, 1971–1996.

Bauer, P., A. Thorpe, and G. Brunet, 2015: The quiet revolution of numerical weather prediction. *Nature*, **525 (7567)**, 47–55.

Beirlant, J., Y. Goegebeur, J. Segers, and J. L. Teugels, 2004: *Statistics of extremes: Theory and applications*. John Wiley & Sons, 490 pp.

Bierdel, L., C. Snyder, S.-H. Park, and W. C. Skamarock, 2016: Accuracy of rotational and divergent kinetic energy spectra diagnosed from flight-track winds. *Journal of the Atmospheric Sciences*, **73 (8)**, 3273–3286.

Biondini, R., 1976: Cloud motion and rainfall statistics. *Journal of Applied Meteorology*, **15 (3)**, 205–224.

Bonavita, M., L. Isaksen, and E. Hólm, 2012: On the use of EDA background error variances in the ECMWF 4D-Var. *Quarterly Journal of Royal Meteorological Society*, **138 (667)**, 1540–1559.

Brown, B. M., and S. Resnick, 1977: Extreme values of independent stochastic processes. *Journal of Applied Probability*, **14 (4)**, 732–739.

Bühl, J., R. Leinweber, U. Görsdorf, M. Radenz, A. Ansmann, and V. Lehmann, 2015: Combined vertical-velocity observations with doppler lidar, cloud radar and wind profiler. *Atmospheric Measurement Techniques*, **8 (8)**, 3527–3536.

Bühler, O., J. Callies, and R. Ferrari, 2014: Wave-vortex decomposition of one-dimensional ship-track data. *Journal of Fluid Mechanics*, **756**, 17 033–17 038.

Caracena, F., 1987: Analytic approximation of discrete field samples with weighted sums and the gridless computation of field derivatives. *Journal of the Atmospheric Sciences*, **44 (24)**, 3753–3768.

Chiles, J.-P., and P. Delfiner, 2009: *Geostatistics: Modeling Spatial Uncertainty*, Vol. 497. John Wiley & Sons.

Chu, C. R., M. B. Parlange, G. G. Katul, and J. D. Albertson, 1996: Probability density functions of turbulent velocity and temperature in the atmospheric surface layer. *Water resources research*, **32 (6)**, 1681–1688.

Coles, S., and J. Tawn, 1996: *Journal of the Royal Statistical Society (B)*, **58 (2)**, 329–347.

Cox, D. R., and N. Reid, 2004: A note on pseudolikelihood constructed from marginal densities. *Biometrika*, **91 (3)**, 729–737.

Daley, R., 1985: The analysis of synoptic scale divergence by a statistical interpolation procedure. *Monthly weather review*, **113 (6)**, 1066–1080.

Daley, R., 1991: *Atmospheric Data Analysis*. 2nd ed., Cambridge University Press, 457 pp.

De Haan, L., 1984: A spectral representation for max-stable processes. *The annals of probability*, **12 (4)**, 1194–1204.

De Haan, L., and A. Ferreira, 2006: *Extreme value theory: An introduction*, Vol. 417. Springer Science & Business Media, 225 pp.

Donner, L. J., T. A. O'Brien, D. Rieger, B. Vogel, and W. F. Cooke, 2016: Are atmospheric updrafts a key to unlocking climate forcing and sensitivity? *Atmospheric Chemistry and Physics*, **16 (20)**, 12 983–12 992.

Doswell III, C. A., and F. Caracena, 1988: Derivative estimation from marginally sampled vector point functions. *Journal of the Atmospheric Sciences.*, **45 (2)**, 242–253.

Efron, B., and R. J. Tibshirani, 1994: *An Introduction to the Bootstrap*. Chapman & Hall„ 456 pp.

Elstrodt, J., 1997: *Maß- und Integrationstheorie*. Springer Lehrbuch, 434 pp.

Embrechts, P., C. Klüppelberg, and T. Mikosch, 1997: *Modelling extremal events: for insurance and finance*, Vol. 33. Springer Science & Business Media, 648 pp.

Embrechts, P., S. I. Resnick, and G. Samorodnitsky, 1999: Extreme value theory as a risk management tool. *North American Actuarial Journal*, **3 (2)**, 30–41.

Engle, R. F., 1982: Autoregressive conditional heteroscedasticity with estimates of the variance of United Kingdom inflation. *Econometrica: Journal of the Econometric Society*, **50 (4)**, 987–1007.

Evensen, G., 1994: Sequential data assimilation with a nonlinear quasi-geostrophic model using Monte Carlo methods to forecast error statistics. *Journal of Geophysical Research: Oceans*, **99 (C5)**, 10 143–10 162.

Ferrier, S. B., J. Simpson, and W.-K. Tao, 1996: Factors responsible for precipitation efficiencies in midlatitude and tropical squall simulations. *Monthly weather review*, **124 (10)**, 2100–2125.

Fisher, R. A., and L. H. C. Tippett, 1928: Limiting forms of the frequency distribution of the largest or smallest member of a sample. *Mathematical Proceedings of the Cambridge Philosophical Society*, Cambridge University Press, Vol. 24, 180–190.

Frehlich, R., L. Cornman, and R. Sharman, 2001: Simulation of Three-Dimensional Turbulent Velocity Fields. *Journal of Applied Meteorology*, **40 (2)**, 246–258.

Frisch, U., and D. Sornette, 1997: Extreme deviations and applications. *Journal of Physics I*, **7 (9)**, 1155–1171.

Furrer, E. M., and R. W. Katz, 2008: Improving the simulation of extreme precipitation events by stochastic weather generators. *Water Resources Research*, **44 (12)**.

Gandin, L., 1963: Objective analysis of meteorological fields. Translated by Israel program for scientific translations. *Gidrometeorologicheskoe Izdatel'stv*, 21–121.

Gebhardt, C., S. Theis, M. Paulat, and Z. B. Bouallégue, 2011: Uncertainties in COSMO-DE precipitation forecasts introduced by model perturbations and variation of lateral boundaries. *Atmospheric Research*, **100 (2-3)**, 168 – 177.

Gnedenko, B., 1943: Sur la distribution limite du terme maximum d'une serie aleatoire. *Annals of mathematics*, **44 (3)**, 423–453.

Gneiting, T., W. Kleiber, and M. Schlather, 2010: Matérn cross-covariance functions for multivariate random fields. *Journal of the American Statistical Association*, **105 (April 2014)**, 1167–1177.

Gomes, D. P., M. Neves, and E. Moreira, 2016: An exploratory study of spatial annual maximum of monthly precipitation in the northern region of Portugal. *Physics and Chemistry of the Earth, Parts A/B/C*, **94**, 77–84.

Gomes, M. I., and L. De Haan, 1999: Approximation by penultimate extreme value distributions. *Extremes*, **2 (1)**, 71–85.

Gottwald, G. A., 2014: Controlling balance in an ensemble Kalman filter. *Nonlinear Processes in Geophysics*, **21 (2)**, 417–426.

Goulard, M., and M. Voltz, 1992: Linear coregionalisation model: Tools for estimation and choice of cross-variogram matrix. *Mathematical Geology*, **24 (3)**, 269–286.

Groisman, P. Y., and Coauthors, 1999: Changes in the probability of heavy precipitation: Important indicators of climatic change. *Weather and Climate Extremes*, Springer, 243–283.

Haerter, J. O., P. Berg, and S. Hagemann, 2010: Heavy rain intensity distributions on varying time scales and at different temperatures. *Journal of Geophysical Research Atmospheres*, **115 (17)**, 1–7.

Hashorva, E., Z. Kabluchko, and A. Wübker, 2012: Extremes of independent chi-square random vectors. *Extremes*, **15 (1)**, 35–42.

Hense, A., and P. Friederichs, 2006: Wind and precipitation extremes in the earth's atmosphere. *Extreme Events in Nature and Society*, Springer, 169–187.

Hewer, R., P. Friederichs, A. Hense, and M. Schlather, 2017: A Matérn based multivariate Gaussian random process for a consistent model of the horizontal wind components and related variables. *Journal of the Atmospheric Sciences*, **74 (2017)**.

Hollingsworth, A., and P. Lönnberg, 1986: The statistical structure of short-range forecast errors as determined from radiosonde data. Part I: The wind field. *Tellus A*, **38 A**, 111–136.

Hüsler, J., and R.-D. Reiss, 1989: Maxima of normal random vectors: between independence and complete dependence. *Statistics & Probability Letters*, **7 (4)**, 283–286.

Jackson, J. D., 1962: *Electrodynamics*. John Wiley Sons, 641 pp.

Kabluchko, Z., M. Schlather, and L. De Haan, 2009: Stationary max-stable fields associated to negative definite functions. *The Annals of Probability*, **37 (5)**, 2042–2065.

Kalnay, E., 2003: *Atmospheric Modeling, Data Assimilation and Predictability*. Cambridge University Press, 341 pp.

Katz, R., 1999: Extreme value theory for precipitation: Sensitivity analysis for climate change. *Advances in Water Resources*, **23 (2)**, 133–139.

Kessler, E., 1969: On the distribution and continuity of water substance in atmospheric circulations. *On the Distribution and Continuity of Water Substance in Atmospheric Circulations (sic!)*, Springer, 1–84.

Kesten, H., 1973: Random difference equations and renewal theory for products of random matrices. *Acta Mathematica*, **131 (1)**, 207–248.

Knopoff, L., and Y. Kagan, 1977: Analysis of the theory of extremes as applied to earthquake problems. *Journal of Geophysical Research*, **82 (36)**, 5647–5657.

Kolmogorov, A. N., 1941: The local structure of turbulence in incompressible viscous fluid for very large reynolds numbers. *Proceedings of the Royal Society A*, **434 (1890)**, 9–13.

Koutsoyiannis, D., 2004: Statistics of extremes and estimation of extreme rainfall: I. theoretical investigation. *Hydrological Sciences Journal*, **49 (4)**.

Koutsoyiannis, D., D. Kozonis, and A. Manetas, 1998: A mathematical framework for studying rainfall intensity-duration-frequency relationships. *Journal of Hydrology*, **206 (1-2)**, 118–135.

Laloyaux, P., M. Balmaseda, D. Dee, K. Mogensen, and P. Janssen, 2016: A coupled data assimilation system for climate reanalysis. *Quarterly Journal of the Royal Meteorological Society*, **142 (694)**, 65–78.

Langousis, A., and D. Veneziano, 2007: Intensity-duration-frequency curves from scaling representations of rainfall. *Water Resources Research*, **43 (2)**.

Lenderink, G., and E. Van Meijgaard, 2008: Increase in hourly precipitation extremes beyond expectations from temperature changes. *Nature Geoscience*, **1 (8)**, 511–514.

Li, Y., W. Cai, and E. Campbell, 2005: Statistical modeling of extreme rainfall in southwest Western Australia. *Journal of climate*, **18 (6)**, 852–863.

Lindborg, E., 2015: A Helmholtz decomposition of structure functions and spectra calculated from aircraft data. *Journal of Fluid Mechanics*, **762**, R4–1 –R4–11.

Liu, S. C., C. Fu, C.-J. Shiu, J.-P. Chen, and F. Wu, 2009: Temperature dependence of global precipitation extremes. *Geophysical Research Letters*, **36 (17)**.

Moreva, O., and M. Schlather, 2016: Modeling and simulation of bivariate gaussian random fields. *arXiv preprint arXiv:1609.06561*.

MunichRe, 2017: Topics Geo: Natural catastrophes 2016. URL https://www.munichre.com/topics-online/en/2017/topics-geo/overview-natural-catastrophe-2016#experts.

Obukhov, A., 1954: Statistical description of continuous fields. *Transactions of the Geophysical International Academy*, **24**, 3–42.

Oesting, M., Z. Kabluchko, and M. Schlather, 2012: Simulation of Brown-Resnick processes. *Extremes*, **15 (1)**, 89–107.

Over, T. M., and V. K. Gupta, 1996: A space-time theory of mesoscale rainfall using random cascades. *Journal of Geophysical Research: Atmospheres*, **101 (D21)**, 26 319–26 331.

Pall, P., M. Allen, and D. A. Stone, 2007: Testing the Clausius–Clapeyron constraint on changes in extreme precipitation under CO_2 warming. *Climate Dynamics*, **28 (4)**, 351–363.

Peralta, C., Z. Ben Bouallègue, S. Theis, C. Gebhardt, and M. Buchhold, 2012: Accounting for initial condition uncertainties in COSMO-DE-EPS. *Journal of Geophysical Research: Atmospheres.*, **117 (D7)**.

Pu, Z., S. Zhang, M. Tong, and V. Tallapragada, 2016: Influence of the self-consistent regional ensemble background error covariance on hurricane inner-core data assimilation with the GSI-based hybrid system for HWRF. *Journal of the Atmospheric Sciences*, **(2016)**.

R Core Team, 2015: *R: A Language and Environment for Statistical Computing*. Vienna, Austria, R Foundation for Statistical Computing.

Reed, J. R., and E. E. Recker, 1971: Structure and properties of synoptic-scale wave disturbances in the equatorial western Pacific. *Journal of the Atmospheric Sciences.*, **28**, 1117–1133.

Ritter, K., 2000: *Average-case analysis of numerical problems.* Springer Science & Business Media, 225 pp.

Roeckner, E., and Coauthors, 2003: The atmospheric general circulation model ECHAM 5. PART I: Model description. Tech. rep.

Rosenblatt, M., 1956: A central limit theorem and a strong mixing condition. *Proceedings of the National Academy of Sciences*, **42 (1)**, 43–47.

Royle, J. A., L. M. Berliner, C. K. Wikle, and R. Milliff, 1999: A hierarchical spatial model for constructing wind fields from scatterometer data in the Labrador Sea. *Case Studies in Bayesian Statistics: Volume IV*, C. Gatsonis, R. E. Kass, B. Carlin, A. Carriquiry, A. Gelman, I. Verdinelli, and M. West, Eds., Springer New York, 367–382.

Sardeshmukh, P. D., and P. Sura, 2009: Reconciling non-Gaussian climate statistics with linear dynamics. *Journal of Climate*, **22 (5)**, 1193–1207.

Schaefer, J. T., and C. A. Doswell III, 1979: On the interpolation of a vector field. *Monthly weather review*, **107 (4)**, 458–476.

Scheuerer, M., and M. Schlather, 2012: Covariance models for divergence-free and curl-free random vector fields. *Stochastic Models*, **28 (3)**, 433–451.

Schlather, M., A. Malinowski, and P. J. Menck, 2015: Analysis, simulation and prediction of multivariate random fields with package random fields. *Journal of Statistical Software*, **63 (8)**, 1–25, arXiv:1501.0228.

Schlather, M., and Coauthors, 2016: Randomfields: Simulation and analysis of random fields. *R package version 3.1.16.*

Seifert, A., and K. D. Beheng, 2001: A double-moment parameterization for simulating autoconversion, accretion and selfcollection. *Atmospheric research*, **59**, 265–281.

Serinaldi, F., and C. G. Kilsby, 2014: Rainfall extremes: Toward reconciliation after the battle of distributions. *Water resources research*, **50 (1)**, 336–352.

Sibuya, M., 1960: Bivariate extreme statistics. *Annals of the Institute of Statistical Mathematics*, **11 (2)**, 195–210.

Singleton, A., and R. Toumi, 2013: Super-Clausius-Clapeyron scaling of rainfall in a model squall line. *Quarterly Journal of the Royal Meteorological Society*, **139 (671)**, 334–339.

Stevens, D. E., and R. S. Lindzen, 1978: Tropical wave-cisk with a moisture budget and cumulus friction. *Journal of the Atmospheric Sciences*, **35 (6)**, 940–961.

Tessier, Y., S. Lovejoy, and D. Schertzer, 1993: Universal multifractals: Theory and observations for rain and clouds. *Journal of Applied Meteorology*, **32 (2)**, 223–250.

Thiébaux, H. J., 1977: Extending estimation accuracy with anisotropic interpolation. *Monthly weather review*, **105 (6)**, 691–699.

Trenberth, K. E., 1999: Conceptual framework for changes of extremes of the hydrological cycle with climate change. *Weather and Climate Extremes*, Springer, 327–339.

Trenberth, K. E., A. Dai, R. M. Rasmussen, and D. B. Parsons, 2003: The changing character of precipitation. *Bulletin of the American Meteorological Society*, **84 (9)**, 1205–1217.

Varin, C., N. Reid, and D. Firth, 2011: An overview of composite likelihood methods. *Statistica Sinica*, **21**, 4–42.

Venema, V., and Coauthors, 2012: Detecting and repairing inhomogeneities in datasets, assessing current capabilities. *Bulleting of the American Meteorolological Society*, **93**, 951–954.

Veneziano, D., A. Langousis, and C. Lepore, 2009: New asymptotic and preasymptotic results on rainfall maxima from multifractal theory. *Water resources research*, **45 (11)**.

Wilson, P. S., and R. Toumi, 2005: A fundamental probability distribution for heavy rainfall. *Geophysical Research Letters*, **32 (14)**, 1–4.

WMO, 1994: Guide to hydrological practises. *World Meteorological Sociecy*, **5 (168)**, URL http://www.bom.gov.au/water/designRainfalls/rainfallEvents/worldRecRainfall.shtml.

Wood, A. T. A., and G. Chan, 1994: Simulation of stationary Gaussian processes in $[0, 1]^d$. *Journal of Computational and Graphical Statistics*, **3 (4)**, 409–432.

Woolhiser, D. A., and J. Roldan, 1982: Stochastic daily precipitation models: 2. a comparison of distributions of amounts. *Water resources research*, **18 (5)**, 1461–1468.

BONNER METEOROLOGISCHE ABHANDLUNGEN

Herausgegeben vom Meteorologischen Institut der Universität Bonn durch Prof. Dr. H. FLOHN (Hefte 1-25), Prof. Dr. M. HANTEL (Hefte 26-35), Prof. Dr. H.-D. SCHILLING (Hefte 36-39), Prof. Dr. H. KRAUS (Hefte 40-49), ab Heft 50 durch Prof. Dr. A. HENSE.

Heft 1-63: siehe `http://www.meteo.uni-bonn.de/bibliothek/bma`

64-85: open access, verfügbar unter `https://uni-bn.de/kpSDaQffe1`

Heft 64: ***Michael Weniger***: Stochastic parameterization: a rigorous approach to stochastic three-dimensional primitive equations, 2014, 148 S. + XV.

Heft 65: ***Andreas Röpnack***: Bayesian model verification: predictability of convective conditions based on EPS forecasts and observations, 2014, 152 S. + VI.

Heft 66: ***Thorsten Simon***: Statistical and Dynamical Downscaling of Numerical Climate Simulations: Enhancement and Evaluation for East Asia, 2014, 48 S. + VII. + Anhänge

Heft 67: ***Elham Rahmani***: The Effect of Climate Change on Wheat in Iran, 2014, [erschienen] 2015, 96 S. + XIII.

Heft 68: ***Pablo A. Saavedra Garfias***: Retrieval of Cloud and Rainwater from Ground-Based Passive Microwave Observations with the Multi-frequency Dual-polarized Radiometer ADMIRARI, 2014, [erschienen] 2015, 168 S. + XIII.

Heft 69: ***Christoph Bollmeyer***: A high-resolution regional reanalysis for Europe and Germany - Creation and Verification with a special focus on the moisture budget, 2015, 103 S. + IX.

Heft 70: ***A S M Mostaquimur Rahman***: Influence of subsurface hydrodynamics on the lower atmosphere at the catchment scale, 2015, 98 S. + XVI.

Heft 71: ***Sabrina Wahl***: Uncertainty in mesoscale numerical weather prediction: probabilistic forecasting of precipitation, 2015, 108 S.

Heft 72: ***Markus Übel***: Simulation of mesoscale patterns and diurnal variations of atmospheric CO_2 mixing ratios with the model system TerrSysMP-CO_2, 2015, [erschienen] 2016, 158 S. + II

Heft 73: ***Christian Bernardus Maria Weijenborg***: Characteristics of Potential Vorticity anomalies associated with mesoscale extremes in the extratropical troposphere, 2015, [erschienen] 2016, 151 S. + XI

Heft 74: ***Muhammad Kaleem***: A sensitivity study of decadal climate prediction to aerosol variability using ECHAM6-HAM (GCM), 2016, 98 S. + XII

Heft 75: ***Theresa Bick***: 3D Radar reflectivity assimilation with an ensemble Kalman filter on the convective scale, 2016, [erschienen] 2017, 96 S. + IX

Heft 76: ***Zied Ben Bouallegue***: Verification and post-processing of ensemble weather forecasts for renewable energy applications, 2017, 119 S.

Heft 77: ***Julia Lutz***: Improvements and application of the STatistical Analogue Resampling Scheme STARS, 2016, [erschienen] 2017, 103 S.

Heft 78: ***Benno Michael Thoma***: Palaeoclimate Reconstruction in the Levant and on the Balkans, 2016, [erschienen] 2017, XVI, 266 S.

Heft 79: ***Ieda Pscheidt***: Generating high resolution precipitation conditional on rainfall observations and satellite data, 2017, V, 173 S.

Heft 80: ***Tanja Zerenner***: Atmospheric downscaling using multi-objective genetic programming, 2016, [erschienen] 2017, X, 191 S.

Heft 81: ***Sophie Stolzenberger***: On the probabilistic evaluation of decadal and paleoclimate model predictions, 2017, IV, 122 S.

Heft 82: ***Insa Thiele-Eich***: Flooding in Dhaka, Bangladesh, and the challenge of climate change, 2017, V, 158 S.

Heft 83: ***Liselotte Bach***: Towards a probabilistic regional reanalysis for Europe, 2017 [erschienen] 2018, VI, 114 S.

Heft 84: ***Yen-Sen Lu***: Propagation of land surface model uncertainties in terrestrial system states, 2017, [erschienen] 2018, X, 120 S.

Heft 85: ***Rüdiger Hewer***: Stochastic physical models for wind fields and precipitation extremes, 2018, 99 S.+IV

METEOROLOGISCHES INSTITUT
MATHEMATISCH NATURWISSENSCHAFTLICHE FAKULTÄT
UNIVERSITÄT BONN

Meteorologisches Institut
Universität Bonn